Biol Blood Marrow Transplant xxx (2014) 1–7

Biology of Blood and Marrow Transplantation

journal homepage: www.bbmt.org

ASBMT American Society for Blood and Marrow Transplantation

Choreito Formula for BK Virus–associated Hemorrhagic Cystitis after Allogeneic Hematopoietic Stem Cell Transplantation

Q5 Nozomu Kawashima, Yoshinori Ito, Yuko Sekiya, Atsushi Narita, Yusuke Okuno, Hideki Muramatsu, Masahiro Irie, Asahito Hama, Yoshiyuki Takahashi, Seiji Kojima*

Department of Pediatrics, Nagoya University Graduate School of Medicine, Nagoya, Japan

Article history:
Received 28 August 2014
Accepted 21 October 2014

Key Words:
BK virus
Hemorrhagic cystitis
Pediatric
Choreito
Kampo medicine

A B S T R A C T

Therapy for BK virus (BKV)–associated hemorrhagic cystitis (BKV-HC) is limited after hematopoietic stem cell transplantation (HSCT). We examined whether choreito, a formula from Japanese traditional Kampo medicine, is effective for treating BKV-HC. Among children who underwent allogeneic HSCT between October 2006 and March 2014, 14 were diagnosed with BKV-HC (median, 36 days; range, 14 to 330 days) after HSCT, and 6 consecutive children received pharmaceutical-grade choreito extract granules. The hematuria grade before treatment was significantly higher in the choreito group than in the nonchoreito group ($P = .018$). The duration from therapy to complete resolution was significantly shorter in the choreito group (median, 9 days; range, 4 to 17 days) than in the nonchoreito group (median, 17 days; range, 15 to 66 days; $P = .037$). In 11 children with macroscopic hematuria, the duration from treatment to resolution of macroscopic hematuria was significantly shorter in the choreito group than in the nonchoreito group (median, 2 days versus 11 days; $P = .0043$). The BKV load in urine was significantly decreased 1 month after choreito administration. No adverse effects related to choreito administration were observed. Choreito may be a safe and considerably promising therapy for the hemostasis of BKV-HC after HSCT.

INTRODUCTION

Hemorrhagic cystitis (HC) is a severe complication in patients undergoing hematopoietic stem cell transplantation (HSCT), resulting in significant morbidity, such as nephropathy and renal failure, prolonged hospitalization, and prolonged blood transfusion requirement [1,2]. Effects on mortality have also been reported in children undergoing HSCT [3]. Early-onset HC occurs within 1 week after HSCT and is mostly a symptom of regimen-related toxicity. Late-onset HC usually occurs after engraftment and is associated with viral infections, including those caused by the human polyomavirus BK (BKV), polyomavirus JC, adenovirus (AdV), and cytomegalovirus (CMV) [4]. BKV is the most frequent cause of late-onset HC and affects 5.3% to 21.2% of children undergoing HSCT [5-9]. BKV viruria is detected by real-time quantitative PCR (RT-PCR) in all patients with BKV-HC. A BKV load of more than 10^6 copies/mL in urine may be associated with a high risk of developing HC after HSCT [5]. However, asymptomatic BK viruria is detected in 50% to 100% of patients after HSCT [5,7,10], implicating that the presence of BKV viruria alone does not explain the pathogenesis of HC. High BKV viremia ($\geq 10^3$ copies/mL) is a better predictor of BKV-HC after HSCT, with a reported specificity of 93% [8]. Children with high BKV viremia ($\geq 10^4$ copies/mL) are at a higher risk of developing severe HC [6].

The standard treatment for BKV-HC has not been established [2]. Supportive therapy is provided to patients with mild BKV-HC, including intravenous hydration, bladder irrigation, and symptomatic relief treatment, such as the use of analgesics. Patients with severe BKV-HC require additional therapy. The current first line BKV-oriented therapy is intravenous cidofovir; however, its efficacy remains controversial [2]. Alternative strategies include intravesical instillation of cidofovir [2,7], hyperbaric oxygen therapy [11], leflunomide, and fluoroquinolone [12]; however, their effect is limited [13]. Invasive intervention such as vascular embolization or cystectomy may be necessary in uncontrollable HC.

Choreito is a formula derived from Japanese traditional Kampo medicine. The indication for choreito in the context of

Financial disclosure: See Acknowledgments on page 6.

* Correspondence and reprint requests: Seiji Kojima, MD, PhD, Department of Pediatrics, Nagoya University Graduate School of Medicine, 65 Tsurumai-cho, Showa-ku, Nagoya, Aichi, 466-8550 Japan.
E-mail address: kwnozomu@gmail.com (S. Kojima).

http://dx.doi.org/10.1016/j.bbmt.2014.10.018
1083-8791/

Kampo medicine is "dampness-heat" in the lower abdomen, the characteristic symptoms of which include dysuria, heat in the lower abdomen, and thirst. All these symptoms may be caused by inflammation and blood clots in the bladder. Based on this indication, choreito has been administered to patients with acute simple cystitis and urolithiasis, and its effectiveness has been confirmed [14]. Recently, choreito was successfully used to treat massive gross hematuria with clot retention in the bladder in a child with refractory acute lymphoblastic leukemia [14]. At present, choreito is covered by the national health insurance and is widely used for genitourinary symptoms in Japan.

Symptoms leading to the traditional use of choreito appear to overlap with symptoms associated with BKV-HC; indeed, some children receive choreito for HC. In this study, we retrospectively analyzed BKV-HC in children undergoing HSCT and evaluated the efficacy of choreito treatment.

PATIENTS AND METHODS

Definition

HC was defined as microscopic (blood in urine graded 1+ or more) or macroscopic hematuria combined with dysuria, pollakisuria, urinary urgency, and/or the sensation of residual urine in the absence of bacteria in urine as observed by culture [9]. *BKV-HC* was defined as the association of HC with BKV viruria and/or viremia. HC was graded according to the widely used criteria [15]. Grade I is defined as microscopic hematuria, grade II as macrohematuria, grade III as macroscopic hematuria with clots, and grade IV as macroscopic hematuria with renal or bladder dysfunction. The onset of BKV-HC was defined as the first day when patients presented with urinary symptoms, and *complete resolution* (CR) of HC was defined as blood in urine (− or + for hemoglobin) and disappearance of dysuria, pollakisuria, urinary urgency, and the sensation of residual urine related to HC.

Patient Inclusion Criteria of BKV-HC and Choreito Administration

Among the children (≤18 years old) who received allogeneic HSCT between October 2006 and March 2014 in Nagoya University Hospital, 14 were diagnosed with BKV-HC and included in the study. Their medical records were retrospectively analyzed. Patient characteristics are listed in Table 1. Intravenous fluids corresponding to 2.5 to 3.0 L/m^2/day with forced alkalinized diuresis were administered during conditioning, and patients treated with cyclophosphamide received prophylactic mesna for the prevention of HC. All the patients received acyclovir for herpes prophylaxis and weekly intravenous immunoglobulin for viral prophylaxis. Tacrolimus was intravenously administered for graft-versus-host disease (GVHD) prophylaxis in patients receiving HSCT from an unrelated donor. Cases of engraftment syndrome and GVHD were treated by methylprednisolone, followed by salvage therapies in nonresponding patients. Six children with BKV-HC diagnosed after March 2013 received a pharmaceutical-grade medicine, choreito extract granules (Tsumura & Co., Tokyo, Japan) with a dose of .2 g/kg per os daily in 3 divided doses (maximum, 7.5 g/day). Cidofovir and choreito were administered at the onset of macroscopic hematuria. Because it is not currently approved for clinical use in Japan, cidofovir was administered only to those who provided written informed consent.

Quantification of BKV DNA

Children undergoing HSCT were weekly monitored for plasma CMV, human herpesvirus 6, and Epstein-Barr virus, and those who met the criteria for HC underwent additional viral workup, including analysis for BKV, polyomavirus JC, and AdV. For 2 patients with BKV diagnosed before December 2009, BKV had been detected in urine by qualitative PCR. This qualitative PCR could not detect BKV in patients without HC. After January 2010, viruses were monitored by multiplex RT-PCR for quantification of DNA from BKV, polyomavirus JC, and AdV, as described previously [16]. In April 2010, BKV RT-PCR was used to screen all 30 hospitalized children with various hemato-oncological diseases who had neither HC-related symptoms nor abnormal urinalysis. All patients provided informed consent for viral PCR workup in accordance with the Declaration of Helsinki. This retrospective analysis was approved by the ethics committee of Nagoya University Graduate School of Medicine.

Statistical Analysis

Statistical analysis was performed using the Fisher's exact test for categorical variables and the Mann-Whitney's U test for continuous variables. The Wilcoxon signed-rank test was used for paired samples. Odds ratios with confidence intervals were estimated by the logistic regression. A probability (P) value <.05 was considered to indicate statistical significance. All statistical analyses were conducted using JMP Pro 11.0.0 (SAS Institute Inc., Cary, NC).

RESULTS

BKV Screening in Hemato-oncological Patients without Genitourinary Symptoms

All children with hemato-oncological disorders hospitalized in the same ward were screened for BKV viruria for the purpose of surveillance. BKV viruria was detected in 5 (17%) of 30 hospitalized children with various hemato-oncological diseases who had neither HC-related symptoms nor abnormal urinalysis. The median urine BKV load in children with asymptomatic viruria was 1.3×10^6 copies/mL (range, 3.5×10^3 to 2.0×10^9 copies/mL), which was significantly lower than that in children with BKV-HC (median, 5.4×10^{10} copies/mL; range, 8.3×10^7 to 1.5×10^{11} copies/mL; $P = .0021$).

Patient Characteristics of Cases with BKV-HC after HSCT

Table 1 summarizes the patient characteristics of 14 children who underwent HSCT and later developed BKV-HC. In patients 1 and 2, BKV was detected in urine by qualitative

Table 1
Patient Demographics of BKV-HC after HSCT

UPN	Choreito Treatment	Age, yr	Sex	Diagnosis	Clinical Status	Preconditioning Regimen	Stem Cell Source	GVHD Prophylaxis
1	No	15.3	M	AA	Non CR	CY + ATG + TBI 5 Gy	UR-BM	FK + sMTX
2	No	16.0	M	AA	Non CR	FLU + CY + Campath + TBI 3 Gy	UR-BM	FK + sMTX
3	No	12.3	M	B-ALL	CR1	MEL + TBI 12 Gy	UR-BM	FK + sMTX
4	No	11.8	M	CML	CyCR	FLU + MEL + TBI 3 Gy	UR-BM	FK + sMTX
5	No	7.1	F	T-ALL	CR2	FLU + MEL + ATG + TBI 12 Gy	Haplo	FK + sMTX
6	No	5.7	M	NB	CR1	FLU + MEL + TBI 2 Gy	UR-CB	FK + sMTX
7	No	15.4	M	CMML	Non CR	FLU + MEL + ATG + TBI 5 Gy	Haplo	FK + sMTX
8	No	7.8	M	B-ALL	CR2	MEL + ATG + TBI 12 Gy	UR-BM	FK + sMTX
9	Yes	14.3	M	AA	Non CR	FLU + MEL + ATG + TBI 3 Gy	Haplo	FK + sMTX
10	Yes	5.4	M	MDS	Non CR	FLU + MEL + ATG + TBI 5 Gy	Haplo	FK + sMTX
11	Yes	10.1	F	AA	Non CR	FLU + MEL + ATG + TBI 5 Gy	Haplo	FK + sMTX
12	Yes	12.2	F	CMML	Non CR	FLU + MEL + ATG + TBI 5 Gy	Haplo	FK + sMTX
13	Yes	6.8	M	B-ALL	CR2	MEL + TBI 12 Gy	UR-BM	FK + sMTX
14	Yes	7.5	M	MDS	Non CR	FLU + MEL + ATG + TBI 5 Gy	Haplo	FK + sMTX

UPN indicates unique patient number; M, male; AA, aplastic anemia; Cy, cyclophosphamide; ATG, antithymocyte globulin; TBI, total body irradiation; UR, unrelated; BM, bone marrow; FK, tacrolimus; sMTX, short course of methotrexate; FLU, fludarabine; Campath, alemtuzumab; ALL, acute lymphoblastic leukemia; MEL, melphalan; CML, chronic myelogenous leukemia; CyCR, cytological complete remission; F, female; Haplo, haploidentical transplant; NB, neuroblastoma; CB, cord blood; CMML, chronic myelomonocytic leukemia; MDS, myelodysplastic syndrome.

PCR; therefore, other agents including preconditioning could have contributed to HC. Six of the 14 children received choreito because of BKV-HC. All patients were older than 5 years (median, 11 years; range, 5.4 to 16 years). Antithymoglobulin or alemtuzumab was administered to 10 of 14 children (71%) as a preconditioning. Notably, all the children received total body irradiation with various doses.

Children were diagnosed with BKV-HC at a median 36 days (range, 14 to 330 days) (Table 2) after HSCT. Six of 14 patients (43%) had grade II to IV acute GVHD, and 11 of 14 (79%) received steroids for treatment of engraftment syndrome and/or acute GVHD before being diagnosed with BKV-HC. Three children with acute GVHD grade III or IV received intensified immunosuppressive treatment for steroid-resistant GVHD; 1 received infliximab and the other 2 received infliximab, basiliximab, and mesenchymal stem cells. All 3 responded well to additional therapy for acute GVHD. Concomitant AdV viruria was detected in 2 of 14 children (14%), and 12 of 14 children (86%) developed CMV and/or Epstein-Barr virus infection after HSCT. AdV titers in the urine were 2.6×10^8 copies/mL in patient 3 and 1.8×10^8 copies/mL in patient 7 at the time of diagnosis. CMV viruria was not detected in any of these 14 children when BKV-HC was diagnosed. Six children were receiving gancyclovir and/or foscarnet for CMV reactivation at the time of BKV-HC diagnosis.

Treatment for BKV Cystitis with Choreito

Six of 14 children with BKV-HC diagnosed after October 2013 received choreito (Tables 1 to 3). All 6 fulfilled the Kampo indication for receiving choreito ("lower energizer dampness-heat" in patients 9, 11, 12, 13, and 14, and "heat binding in the lower energizer" in patient 10). Patient characteristics, including age at HSCT, sex, underlying disease, engraftment syndrome, acute GVHD frequency and grade, immunosuppressive treatment, absolute lymphocyte count, antiviral therapy, duration of steroid use before the diagnosis of BKV-HC, and duration from HSCT to the onset of BKV-HC, did not differ significantly between the choreito group and the nonchoreito group (Tables 1 and 2). However, the hematuria grade at the time of diagnosis of BKV-HC was significantly higher in the choreito group than in the nonchoreito group ($P = .018$) (Table 2). Choreito was administered over a median of 5 days after the onset of symptoms related to BKV-HC (range, 2 to 16 days), and this interval was not statistically different from that of other treatments (median, 4 days; range, 1 to 23 days; $P = .43$) (Table 3). The urine BKV load before treatment amounted to a median of 2.6×10^{10} copies/mL (range, 1.3×10^9 to 6.3×10^{10} copies/mL) in children receiving choreito, which was not statistically different from that in those not receiving choreito (median, 3.4×10^{10} copies/mL; range, 8.3×10^7 to 1.3×10^{11} copies/mL; $P = .67$) (Table 3). Similarly, the BKV load in whole blood before treatment was not statistically different between the choreito and nonchoreito groups ($P = .24$, Table 3).

In all 14 children with BKV-HC, the duration from the start of therapy to CR as defined by disappearance of dysuria, pollakisuria, urinary urgency, and the sensation of residual urine was significantly shorter in the choreito group (median, 9 days; range, 4 to 17 days) than in the nonchoreito group (median, 17 days; range, 15 to 66 days; $P = .037$) (Table 3, Figure 1A): the odds ratio of choreito versus nonchoreito was .63 (95% confidence interval, .22 to .93; $P = .0031$). With regard to 11 children with HC graded ≥ II at the beginning of therapy, the administration of choreito

Table 2
Clinical Characteristics of Patients with BKV Cystitis

UPN	Engraftment Syndrome	Acute GVHD		ALC at the Diagnosis of BKV-HC ($\times 10^9$/L)	Steroid Use (d before BKV-HC)	Other Immunosuppressants	Onset of BKV-HC (d from SCT)	Hematuria (Grade)	Viruria (Urine log copy/mL)	CMV (Whole Blood log copy/mL)	Viral Infections	Antiviral Therapy at BKV-HC
		Stage	Grade									
1	+	-	-	4.7	14	-	35	II	BKV	0.0	CMV, EBV	GCV
2	-	skin 3	II	.3	24	-	65	II	BKV	3.1	CMV	PFA
3	+	-	-	.8	10	-	36	III	BKV (9.2), AdV (8.4)	0.0	CMV	PFA
4	+	skin 3	II	1	90	-	330	II	BKV (7.9)	0.0	CMV, EBV	PFA
5	+	skin 2, gut 1	II	.2	-	-	14	II	BKV (10.8)	2.6	CMV	-
6	-	skin 2, gut 3	III	1	10	INX	45	I	BKV (10.9)	0.0	-	-
7	-	skin 3, gut 2	III	.6	67	INX, BSX, MSC	86	I	BKV (11.1), AdV (8.3)	3.0	CMV, EBV	-
8	+	-	-	2	2	-	27	II	BKV (10.0)	3.2	CMV	-
9	-	-	-	.2	-	-	16	III	BKV (9.1)	2.9	EBV	-
10	+	skin 2, liver 4, gut 2	IV	.8	12	INX, BSX, MSC	25	III	BKV (9.2)	0.0	-	-
11	+	-	-	1.8	30	-	48	III	BKV (9.5)	0.0	CMV, EBV	GCV + PFA
12	+	-	-	.2	45	-	67	III	BKV (10.8)	2.7	CMV	GCV
13	-	-	-	1.3	-	-	21	III	BKV (10.7)	0.0	CMV	-
14	+	-	-	.5	6	-	26	I	BKV (10.7)	0.0	EBV	-

ALC indicates absolute lymphocyte count; SCT, stem cell transplanation; EBV, Epstein-Barr virus; GCV, gancyclovir; PFA, foscarnet; INX, infliximab; BSX, basiliximab; MSC, mesenchymal stem cell transplantation.

Table 3
Summary of Treatment for Patients with BKV Cystitis

UPN	Duration from Onset to Tx, d		Primary Tx for BKV	Hematuria Grade at Tx	Hematuria Grade ≤I (d from Tx)	CR (d from Tx)	Urine BKV Load before Tx (log copy/mL)	Plasma BKV Load before Tx (log copy/mL)	Urine BKV Load 1 mo after Tx (log copy/mL)	Plasma BKV Load 1 mo after Tx (log copy/mL)	Possible Complications
1	7		Cidofovir (5 mg/kg qwk ×2), hydration	II	11	17	N/A	N/A	N/A	N/A	None
2	4		Bladder irrigation, hydration	II	16	55	N/A	N/A	N/A	N/A	None
3	14		Cidofovir (1 mg/kg qwk ×2), hydration	III	28	66	9.2	0.0	6.5	3.8	Renal failure
4	4		Hydration	II	10	15	7.9	0.0	N/A	N/A	None
5	2		Hydration	II	5	16	10.8	0.0	N/A	N/A	None
6	1		Hydration	I	N/A	15	10.9	3.0	10.5	3.6	None
7	1		Hydration	I	N/A	15	11.1	0.0	N/A	N/A	None
8	23		Hydration	II	8	23	10.0	0.0	N/A	N/A	None
9	16		Choreito, cidofovir (1 mg/kg qwk ×11), hydration	III	4	6	9.1	4.0	8.7	4.6	None
10	5		Choreito	III	2	4	9.2	3.1	8.3	4.0	None
11	2		Choreito	III	2	16	9.5	0.0	7.8	0.0	None
12	4		Choreito	III	3	17	10.8	0.0	8.2	5.8	None
13	5		Choreito	III	2	7	10.7	5.0	4.4	0.0	None
14	16		Choreito	I	N/A	11	10.7	2.1	10.5	3.2	None

Tx indicates treatment; qwk, every week; N/A, not applicable or available.

significantly shortened the duration from the onset to BKV-HC grade ≤ I (median, 2 days; range, 2 to 4 days) in comparison with that in the nonchoreito group (median, 11 days; range, 5 to 28 days; $P = .0043$) (Table 3, Figure 1B). The duration from start of therapy to CR was also significantly shorter in the choreito group (median, 7 days; range, 4 to 17 days) than in the nonchoreito group (median, 20 days; range, 15 to 66 days; $P = .048$) (Table 3, Figure 1C): here, the odds ratio of choreito versus nonchoreito was .66 (95% confidence interval, .14 to .95; $P = .0058$).

Sequential Analysis of BKV Load after Choreito Treatment

BKV-HC–related symptoms improved significantly earlier in children receiving choreito, and we studied whether these earlier improvements were related to the clearance of BKV. The BKV load in urine and whole blood was monitored after the diagnosis of BKV-HC in children receiving choreito. The urine BKV load generally decreased over time. The median urine BKV load was 1.7×10^8 copies/mL (range, 2.6×10^4 to 3.1×10^{10} copies/mL) 1 month after BKV-HC diagnosis when all children had achieved CR, and they experienced a statistically significant decrease in BKV load since the time of diagnosis ($P = .031$; Wilcoxon signed-rank test for paired samples) (Table 3, Figure 2A). At the time of CR, only 1 of 6 children had a urine BKV load lower than 1.3×10^6 copies/mL, which was the median urine BKV load in children with asymptomatic viruria. The BKV load in whole blood appeared stable during the course of BKV-HC, and no significant decrease was observed a month after diagnosis ($P = .44$) (Table 3, Figure 2B).

All 6 children eventually finished taking choreito, and relapse of HC was not observed, except for in 1 patient who experienced relapse twice (patient 9). This patient was diagnosed with idiopathic aplastic anemia and received a bone marrow transplant from an unrelated donor; however, the graft was rejected and he underwent haplo-identical HSCT as the second HSCT. Because he developed chronic GVHD, he was administered prednisolone, which was increased during the exacerbation of chronic GVHD and which may have contributed to the prolonged elevation of the BKV load. Every time the patient had a relapse of BKV-HC, he was administered choreito, and his genitourinary symptoms resolved within a few days (Supplemental Figure 1).

Safety and Tolerability of Treatment

All children were able to take choreito per os. Notably, there were no adverse effects due to choreito intake, and renal function impairment was not observed in children receiving choreito (Table 3). The reported adverse effects of choreito include drug allergy and mild gastric discomfort [14], which were not observed in any of the children. In the nonchoreito group, 1 patient (patient 3) who received cidofovir for BKV infection developed impaired renal function, possibly resulting from renal toxicity of cidofovir and post-renal acute kidney injury due to clot retention.

DISCUSSION

Unlike its effect in immunocompetent patients, HC is life threatening in immunocompromised patients with hemato-oncological disease, particularly among patients undergoing HSCT [17]. To our knowledge, prospective studies of the treatment for BKV-HC are not available, and there are no standard treatment guidelines for post-HSCT HC. Treatment modalities are limited, particularly in children, partly owing to few reports on children receiving pharmaceutical and

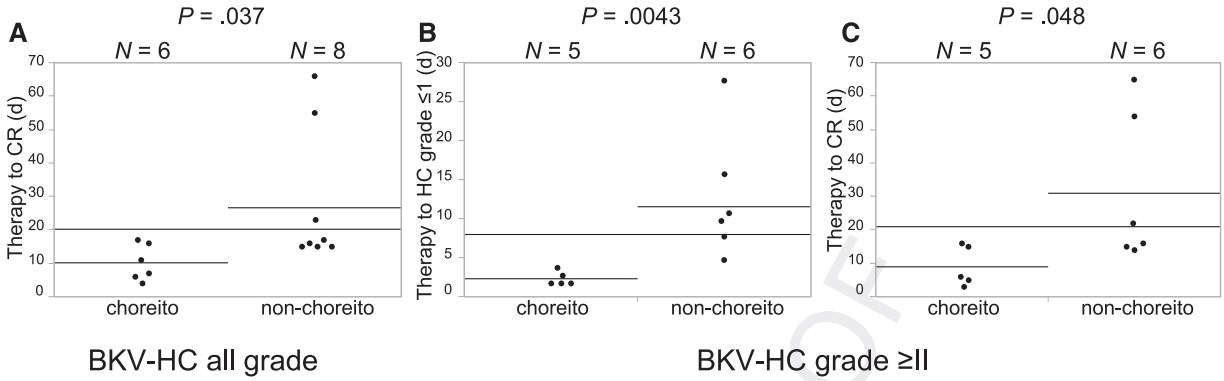

Figure 1. Comparison of choreito and nonchoreito treatment for BK virus-associated hemorrhagic cystitis (BKV-HC). The duration from the beginning of therapy to complete resolution (CR), as defined by the absence of dysuria, pollakisuria, urinary urgency, or the sensation of residual urine, was shorter in the choreito group (median, 9 days; range, 4 to 17 days) than in the nonchoreito group (median, 17 days; range, 15 to 66 days; $P = .037$) (A). When comparing children with HC graded ≥ II, the administration of choreito significantly shortened the duration from the onset to BKV-HC grade ≤ I (median, 2 days; range, 2 to 4 days) in comparison with that in the nonchoreito group (median, 11 days; range, 5 to 28 days) (B). The duration from start of therapy to CR was also significantly shorter in the choreito group (median, 7 days; range, 4 to 17 days) than in the nonchoreito group (median, 20 days; range, 15 to 66 days; $P = .048$) (C).

surgical treatments [4,18-20]. Intravenous hydration with forced diuresis is conducted; however, this is supportive treatment only without reliable efficacy.

At present, cidofovir is the only commercially available antiviral agent against BKV, and its efficacy for BKV-HC has been investigated only in retrospective studies [19-21]. In the report from the European Group for Blood and Marrow Transplantation, intravenous or intravesical cidofovir was administered to 62 patients with BKV-HC [21]. Of the 62 patients, 41 (66%) achieved CR and 8 (13%) had partial response after cidofovir treatment; however, no improvement or deterioration was observed in 12 patients (19%). CR is related to clearance of BK viremia in patients with BK viremia detected at the beginning of treatment, and the median time to clearance is 37 days (range, 7 to 102 days). Of 57 patients receiving intravenous cidofovir, 17 (30%) experienced renal toxicity. In a pediatric cohort, 19 children received cidofovir for BKV-HC grade ≥ II [19]. Macroscopic hematuria resolved in 15 (79%) after a median of 22 days (range, 9 to 63 days). In 1 patient, HC progressed to grade IV during cidofovir treatment. Notably, the baseline creatinine level appeared to be elevated after treatment. Another pediatric cohort included 12 children with BKV-HC treated by intravenous and/or intravesical cidofovir [20]. The median duration of symptoms was 25 days (range, 9 to 73 days) and no persistent nephrotoxicity was observed. Compared with cidofovir treatment, children treated with choreito treatment in our study experienced no impairment of renal function; all patients with BKV-HC achieved CR and BKV-HC resolved earlier.

Hyperbaric oxygen therapy is another alternative treatment for BKV-HC [11,22]. A retrospective study included 16 patients with BKV-HC grade ≥ II (5 patients under 19 years of age), 15 (94%) of whom achieved CR after a median of 17 days (range, 4 to 116 days) [11]. In a pediatric cohort of 10 children with BKV-HC grade ≥ II, 9 (90%) achieved CR after a median of 15 days (range, 10 to 37 days), including spontaneous resolution [22]. Hyperbaric oxygen is generally well tolerated; however, it requires a high-cost facility and adverse effects have been reported, including ruptured tympanum.

Other alternative therapies include leflunomide and fluoroquinolone antibiotics [12]; however, experience is limited, even in adults [13]. Few reports of leflunomide use in the setting of HSCT are available and its safety has not been

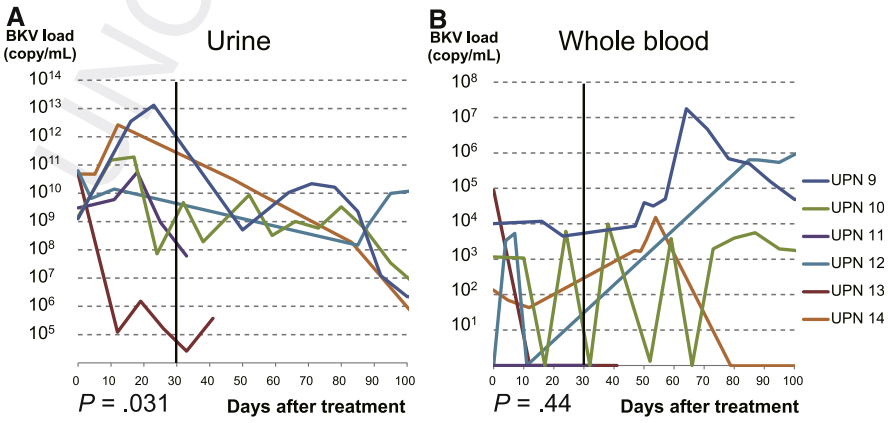

Figure 2. BK virus (BKV) load after choreito treatment. The BKV load before treatment amounted to a median of 2.6×10^{10} copies/mL in urine (range, 1.3×10^{9} to 6.3×10^{10} copies/mL) and a median of 6.5×10^{2} copies/mL in whole blood (range, 0 to 9.0×10^{4} copies/mL). The median urine BKV load was 1.7×10^{8} copies/mL (range, 2.6×10^{4} to 3.1×10^{10} copies/mL) 1 month after BKV-HC diagnosis, and the BKV load had significantly decreased since the time of diagnosis (Wilcoxon signed-rank test, $P = .031$) (A). The BKV load in whole blood appeared stable during the course of BKV-HC, and no significant decrease was observed a month after diagnosis (Wilcoxon signed-rank test, $P = .44$) (B).

confirmed in children. Fluoroquinolones are historically contraindicated in children because they cause arthrotoxicity in juvenile animals and are associated with reversible musculoskeletal events in both children and adults; therefore, they are not recommended in the absence of convincing evidence.

Choreito is a formula stemming from Japanese traditional (Kampo) medicine, originally developed from traditional Chinese medicine; it was the orthodox medicine in Japan until the 19th century, when modern Western medicine took over [14]. Nevertheless, some Kampo formulae are still officially registered in the Japanese Pharmacopoeia. Although Kampo extracts are crude drugs derived from plants, animals, and minerals, their quality is strictly controlled in accordance with the Japanese Pharmacopoeia by quantitative analysis of marker components using high-performance liquid chromatography. Kampo formulae are classified as dietary supplements outside Japan and are approved for marketing by the Food and Drug Administration in the United States.

Choreito is a crude product from *Polyporus umbellatus* sclerotium, *Wolfiporia extensa* sclerotium, *Alisma orientale* rhizome, aluminum silicate hydrate with silicon dioxide, and glue. Ergone isolated from *P. umbellatus* prevented early renal injury in a rat model of nephropathy [23] and may play a central role in the effect exerted by choreito. Pollakisuria was ameliorated in 93% of patients who received choreito for lower urinary tract symptoms in an open-label, single-arm study of 30 patients [24]. Choreito was also administered to patients with urolithiasis for enhancing the evacuation of stones after extracorporeal shock wave lithotripsy [25]. In these studies, no severe adverse effects were observed, suggesting high safety of choreito.

Considering the wide range of indications in genitourinary disorders, choreito may protect epithelial cells irrespective of the type of pathogens and thereby be an effective treatment option for the hemostasis of HC. Although the precise pathogenesis of BKV-HC remains unclear, urothelial cells infected with BKV in vitro detached without causing local cell lysis, which may be associated with the denudation of the damaged mucosa in patients with BKV-HC [26]. Choreito may protect urothelial cells from detaching, which may result in a significant reduction of the BKV load in urine, although the whole blood BKV load appears unchanged and the BKV burden itself is not reduced. Notably, unlike other antiviral agents or surgical interventions, no adverse effects were observed during choreito administration, although the mechanism of action of choreito remains unclear; hence, its safety cannot be easily predicted.

Our study has some limitations. The small number of study subjects in this single-center retrospective analysis may result in bias. Five of 8 subjects in the nonchoreito group had grade II to III GVHD, whereas 1 out of 6 subjects in the choreito group had grade IV GVHD. This difference in GVHD frequency could have been a contributing factor for the difference in HC severity and BKV clearance, although it was not statistically different ($P = .14$) among the 2 groups, possibly because of the small sample size. Children with concomitant AdV viruria were included only in the nonchoreito group, which may explain the longer time before CR in the nonchoreito group. In the present study, HC was significantly more severe in the choreito group than the nonchoreito group. This difference may represent the difference in preconditioning and donor sources: the choreito group included more cases of haplo-identical HSCT, which may have resulted in intensified immunosuppression. More severe HC correlates with a longer duration of HC [2]. Nevertheless, the duration of HC was significantly shorter in the choreito group, which exemplifies its effectiveness. Although the urine BKV load had significantly decreased 1 month after choreito treatment examined by the paired samples, this decrease could not be compared with that of the nonchoreito group because of a lack of paired samples in most of the patients in the nonchoreito group. Thus, the impact of choreito treatment on the urine BV virus load should be investigated in a prospective study where the BKV load is sequentially followed for every study subject.

In conclusion, choreito may be a safe and effective therapy for the hemostasis of late-onset BKV-HC following HSCT, although it may not decrease the BKV burden. Although its precise mechanism of hemostasis remains unclear, choreito may be administered as the first-line treatment for post-HSCT HC. Prospective, randomized studies are warranted to confirm the efficacy of choreito in the treatment of BKV-HC. Fundamental research aiming to identify the active ingredients and mechanisms of action is also essential.

ACKNOWLEDGMENTS

The authors thank Fumiyo Ando, Yoshie Miura, Yinyan Xu, and Xinan Wang for their professional assistance.

Financial disclosure: Dr. Seiji Kojima received a research grant from Sanofi K.K. The other authors have no conflicts of interest to disclose.

SUPPLEMENTARY DATA

Supplementary data related to this article can be found online at http://dx.doi.org/10.1016/j.bbmt.2014.10.018.

REFERENCES

1. Lee YJ, Zheng J, Kolitsopoulos Y, et al. Relationship of BK polyoma virus (BKV) in the urine with hemorrhagic cystitis and renal function in recipients of T cell-depleted peripheral blood and cord blood stem cell transplantations. *Biol Blood Marrow Transplant*. 2014;20:1204-1210.
2. Gilis L, Morisset S, Billaud G, et al. High burden of BK virus-associated hemorrhagic cystitis in patients undergoing allogeneic hematopoietic stem cell transplantation. *Bone Marrow Transplant*. 2014;49:664-670.
3. Haines HL, Laskin BL, Goebel J, et al. Blood, and not urine, BK viral load predicts renal outcome in children with hemorrhagic cystitis following hematopoietic stem cell transplantation. *Biol Blood Marrow Transplant*. 2011;17:1512-1519.
4. Decker DB, Karam JA, Wilcox DT. Pediatric hemorrhagic cystitis. *J Pediatr Urol*. 2009;5:254-264.
5. Megged O, Stein J, Ben-Meir D, et al. BK-virus-associated hemorrhagic cystitis in children after hematopoietic stem cell transplantation. *J Pediatr Hematol Oncol*. 2011;33:190-193.
6. Oshrine B, Bunin N, Li Y, et al. Kidney and bladder outcomes in children with hemorrhagic cystitis and BK virus infection after allogeneic hematopoietic stem cell transplantation. *Biol Blood Marrow Transplant*. 2013;19:1702-1707.
7. Laskin BL, Denburg M, Furth S, et al. BK viremia precedes hemorrhagic cystitis in children undergoing allogeneic hematopoietic stem cell transplantation. *Biol Blood Marrow Transplant*. 2013;19:1175-1182.
8. Cesaro S, Facchin C, Tridello G, et al. A prospective study of BK-virus-associated haemorrhagic cystitis in paediatric patients undergoing allogeneic haematopoietic stem cell transplantation. *Bone Marrow Transplant*. 2008;41:363-370.
9. Kloos RQ, Boelens JJ, de Jong TP, et al. Hemorrhagic cystitis in a cohort of pediatric transplantations: incidence, treatment, outcome, and risk factors. *Biol Blood Marrow Transplant*. 2013;19:1263-1266.
10. Drew RJ, Walsh A, Ní Laoi B, et al. BK virus (BKV) plasma dynamics in patients with BKV-associated hemorrhagic cystitis following allogeneic stem cell transplantation. *Transpl Infect Dis*. 2013;15:276-282.
11. Savva-Bordalo J, Pinho Vaz C, Sousa M, et al. Clinical effectiveness of hyperbaric oxygen therapy for BK-virus-associated hemorrhagic cystitis after allogeneic bone marrow transplantation. *Bone Marrow Transplant*. 2012;47:1095-1098.
12. Zaman RA, Ettenger RB, Cheam H, et al. A novel treatment regimen for BK viremia. *Transplantation*. 2014;97:1166-1171.

13. Harkensee C, Vasdev N, Gennery AR, et al. Prevention and management of BK-virus associated haemorrhagic cystitis in children following haematopoietic stem cell transplantation—a systematic review and evidence-based guidance for clinical management. *Br J Haematol*. 2008;142:717-731.
14. Kawashima N, Deveaux TE, Yoshida N, et al. Choreito, a formula from Japanese traditional medicine (Kampo medicine), for massive hemorrhagic cystitis and clot retention in a pediatric patient with refractory acute lymphoblastic leukemia. *Phytomedicine*. 2012;19:1143-1146.
15. Droller MJ, Gomolka D. Expression of the cellular immune response during tumor development in an animal model of bladder cancer. *J Urol*. 1982;128:1385-1389.
16. Funahashi Y, Iwata S, Ito Y, et al. Multiplex real-time PCR assay for simultaneous quantification of BK polyomavirus, JC polyomavirus, and adenovirus DNA. *J Clin Microbiol*. 2010;48:825-830.
17. Hale GA, Rochester RJ, Heslop HE, et al. Hemorrhagic cystitis after allogeneic bone marrow transplantation in children: clinical characteristics and outcome. *Biol Blood Marrow Transplant*. 2003;9:698-705.
18. Hassan Z. Management of refractory hemorrhagic cystitis following hematopoietic stem cell transplantation in children. *Pediatr Transplant*. 2011;15:348-361.
19. Gorczynska E, Turkiewicz D, Rybka K, et al. Incidence, clinical outcome, and management of virus-induced hemorrhagic cystitis in children and adolescents after allogeneic hematopoietic cell transplantation. *Biol Blood Marrow Transplant*. 2005;11:797-804.
20. Kwon HJ, Kang JH, Lee JW, et al. Treatment of BK virus-associated hemorrhagic cystitis in pediatric hematopoietic stem cell transplant recipients with cidofovir: a single-center experience. *Transpl Infect Dis*. 2013;15:569-574.
21. Cesaro S, Hirsch HH, Faraci M, et al. Cidofovir for BK virus-associated hemorrhagic cystitis: a retrospective study. *Clin Infect Dis*. 2009;49:233-240.
22. Zama D, Masetti R, Vendemini F, et al. Clinical effectiveness of early treatment with hyperbaric oxygen therapy for severe late-onset hemorrhagic cystitis after hematopoietic stem cell transplantation in pediatric patients. *Pediatr Transplant*. 2013;17:86-91. Q4
23. Zhao YY, Zhang L, Mao JR, et al. Ergosta-4,6,8(14),22-tetraen-3-one isolated from Polyporus umbellatus prevents early renal injury in aristolochic acid-induced nephropathy rats. *J Pharm Pharmacol*. 2011;63:1581-1586.
24. Horii A, Maekawa M. Clinical evaluation of chorei-to and chorei-to-go-shimotsu-to in patients with lower urinary tract symptoms [article in Japanese]. *Hinyokika Kiyo*. 1988;34:2237-2241.
25. Wada S, Yoshimura R, Yamamoto K, et al. Effect of herbal drug, choreito, after extracorporeal shock wave lithotripsy on spontaneous stone delivery. *Jpn J Endourol ESWL*. 2001;14:155-158.
26. Li R, Sharma BN, Linder S, et al. Characteristics of polyomavirus BK (BKPyV) infection in primary human urothelial cells. *Virology*. 2013;440:41-50.

bjh research paper

Loss of function mutations in *RPL27* and *RPS27* identified by whole-exome sequencing in Diamond-Blackfan anaemia

RuNan Wang,[1] Kenichi Yoshida,[2,3] Tsutomu Toki,[1] Takafumi Sawada,[4] Tamayo Uechi,[4] Yusuke Okuno,[2,3] Aiko Sato-Otsubo,[2,3] Kazuko Kudo,[5] Isamu Kamimaki,[6] Rika Kanezaki,[1] Yuichi Shiraishi,[7] Kenichi Chiba,[7] Hiroko Tanaka,[8] Kiminori Terui,[1] Tomohiko Sato,[1] Yuji Iribe,[9] Shouichi Ohga,[10] Madoka Kuramitsu,[11] Isao Hamaguchi,[11] Akira Ohara,[12] Junichi Hara,[13] Kumiko Goi,[14] Kousaku Matsubara,[15] Kenichi Koike,[16] Akira Ishiguro,[17] Yasuhiro Okamoto,[18] Kenichiro Watanabe,[19] Hitoshi Kanno,[9] Seiji Kojima,[20] Satoru Miyano,[7,8] Naoya Kenmochi,[4] Seishi Ogawa[2,3] and Etsuro Ito[1]

[1]Department of Paediatrics, Hirosaki University Graduate School of Medicine, Hirosaki, [2]Cancer Genomics Project, Graduate School of Medicine, The University of Tokyo, Tokyo, [3]Department of Pathology and Tumour Biology, Graduate School of Medicine, Kyoto University, Kyoto, [4]Frontier Science Research Centre, University of Miyazaki, Miyazaki, [5]Division of Haematology and Oncology, Shizuoka Children's Hospital, Shizuoka, [6]Department of Paediatrics, Saitama National Hospital, Wako, [7]Laboratory of DNA Information Analysis, Human Genome Centre, Institute of Medical Science, The University of Tokyo, [8]Laboratory of Sequence Analysis, Human Genome Centre, Institute of Medical Science, The University of Tokyo, [9]Department of Transfusion Medicine and Cell Processing, Tokyo Women's Medical University, Tokyo, [10]Department of Perinatal and Paediatric Medicine, Graduate School of Medical Sciences, Kyushu University, Fukuoka, [11]Department of Safety Research on Blood and Biological Products, National Institute of Infectious Diseases, [12]Department of Transfusion, Omori Hospital, Toho University, Tokyo, [13]Department of Haematology and Oncology, Osaka City General Hospital, Osaka, [14]Department of Paediatrics, University of Yamanashi, Kofu, [15]Department of Paediatrics, Nishi-Kobe Medical Centre,Kobe, [16]Department of Paediat-

Summary

Diamond-Blackfan anaemia is a congenital bone marrow failure syndrome that is characterized by red blood cell aplasia. The disease has been associated with mutations or large deletions in 11 ribosomal protein genes including *RPS7*, *RPS10*, *RPS17*, *RPS19*, *RPS24*, *RPS26*, *RPS29*, *RPL5*, *RPL11*, *RPL26* and *RPL35A* as well as *GATA1* in more than 50% of patients. However, the molecular aetiology of many Diamond-Blackfan anaemia cases remains to be uncovered. To identify new mutations responsible for Diamond-Blackfan anaemia, we performed whole-exome sequencing analysis of 48 patients with no documented mutations/deletions involving known Diamond-Blackfan anaemia genes except for *RPS7*, *RPL26*, *RPS29* and *GATA1*. Here, we identified a *de novo* splicing error mutation in *RPL27* and frameshift deletion in *RPS27* in sporadic patients with Diamond-Blackfan anaemia. *In vitro* knockdown of gene expression disturbed pre-ribosomal RNA processing. Zebrafish models of *rpl27 and rps27* mutations showed impairments of erythrocyte production and tail and/or brain development. Additional novel mutations were found in eight patients, including *RPL3L*, *RPL6*, *RPL7L1T*, *RPL8*, *RPL13*, *RPL14*, *RPL18A* and *RPL31*. In conclusion, we identified novel germline mutations of two ribosomal protein genes responsible for Diamond-Blackfan anaemia, further confirming the concept that mutations in ribosomal protein genes lead to Diamond-Blackfan anaemia.

Keywords: bone marrow failure, Diamond-Blackfan, genetic analysis, erythropoiesis, childhood.

  doi: 10.1111/bjh.13229

rics, Shinshu University School of Medicine, Matsumoto, [17]Division of Haematology, National Centre for Child Health and Development, Tokyo, [18]Department of Paediatrics, Kagoshima University, Kagoshima, [19]Department of Paediatrics, Graduate School of Medicine, Kyoto University, Kyoto, and [20]Department of Paediatrics, Nagoya University Graduate School of Medicine, Nagoya, Japan

Received 21 August 2014; accepted for publication 7 October 2014
Correspondence: Professor Etsuro Ito, Department of Paediatrics, Hirosaki University Graduate School of Medicine, 53 Honcho, Hirosaki 036-8562, Japan.
E-mail: eturou@cc.hirosaki-u.ac.jp

Professor Seishi Ogawa, Cancer Genomics Project, Graduate School of Medicine, The University of Tokyo, 7-3-1, Hongo, Bunkyo-ku, Tokyo 113-8654, Japan.
E-mail: sogawa-tky@umin.ac.jp

Diamond-Blackfan anaemia (DBA) is an inherited rare red blood cell aplasia that is characterized by normochromic macrocytic anaemia, reticulocytopenia and selective defects in erythroid progenitor cells in normocellular bone marrow. Patients usually present with anaemia in the first year of life, although there is a non-classical mild phenotype diagnosed later in life. Macrocytic anaemia is a prominent feature of DBA but the disease is also characterized by growth retardation and congenital anomalies, including craniofacial, upper limb/hand, cardiac and genitourinary malformations, that are present in approximately half of the patients. In addition, DBA patients have a predisposition to malignancies including acute myeloid leukaemia, myelodysplastic syndrome, colon carcinoma, osteogenic sarcoma and female genital cancer (Lipton *et al*, 2006; Vlachos *et al*, 2008, 2012; Ito *et al*, 2010).

DBA is associated with single, monoallelic, inactivating mutations in ribosomal protein (RP) genes. Except for rare germline *GATA1* mutations reported in two X-linked DBA families (Sankaran *et al*, 2012), all known causative mutations have involved RP genes. Approximately 20% of DBA patients are familial. However, most cases occur sporadically and have *de novo* mutations. In DBA, mutations in RP genes include *RPS7*, *RPS10*, *RPS17*, *RPS19*, *RPS24*, *RPS26* and *RPS29* (encoding RP for the small subunit) and *RPL5*, *RPL11*, *RPL26* and *RPL35A* (encoding RP for the large subunit). These mutations have been reported in up to 60% of DBA patients (Draptchinskaia *et al*, 1999; Gazda *et al*, 2006, 2008, 2012; Cmejla *et al*, 2007; Farrar *et al*, 2008; Doherty *et al*, 2010; Konno *et al*, 2010; Gerrard *et al*, 2013; Mirabello *et al*, 2014). To date, approximately 40% of patients have no known pathogenic mutation. In this study, we carried out whole-exome sequencing (WES) analysis of 48 patients without known causative mutations or deletions and found loss-of function mutations in the *RPS27* and *RPL27* genes.

Methods

Patient samples

Genomic DNA (gDNA) was extracted from peripheral blood leucocytes with the QIAamp DNA Blood Mini Kit (QIAGEN, Hilden, Germany) according to the manufacturer's protocol. The diagnosis of DBA was based on the criteria developed at an international clinical consensus conference (Vlachos *et al*, 2008). All clinical samples were obtained with informed consent from paediatric and/or haematology departments throughout Japan. The Ethics Committee of Hirosaki University Graduate School of Medicine and the University of Tokyo approved this study.

Whole-exome sequencing analysis

To identify the candidate disease variants including non-RP genes, we performed WES analysis. gDNA from patients was enriched for protein-coding sequences with a SureSelect Human All Exon V3, V4 or V5 kit (Agilent Technologies, Santa Clara, CA, USA). This was followed by massively

parallel sequencing with the HiSeq 2000 platform with 100 bp paired-end reads (Illumina, San Diego, CA, USA). Candidate germline variants were detected through our in-house pipeline for WES analysis with minor modifications for the detection of germline variants (Yoshida *et al*, 2011; Kunishima *et al*, 2013). The resultant sequences were aligned to the University of California Santa Cruz (UCSC) Genome Browser hg19 with the Burrows-Wheeler Aligner (Li & Durbin, 2009). After removal of duplicate artifacts caused by polymerase chain reaction (PCR), the single nucleotide variants with an allele frequency >0·25 and insertion-deletions with an allele frequency >0·1 were called. With a mean depth of coverage of 116·3× (67× − 166×), more than 92% of the 50 Mb target sequences were analysed by more than 10 independent reads.

Target deep sequencing analysis was performed for the RP genes with a low depth of coverage of <10×. Amplification of the genome was accomplished by long PCR reactions using KOD-FX-Neo DNA polymerase (TOYOBO, Osaka, Japan) using the primers described in Data S1. The PCR products were used for library preparation after determination of their quantity by the Qubit dsDNA HS Assay (Life Technologies, Invitrogen division, Darmstadt, Germany). Libraries were prepared using the Nextera XT DNA Sample Preparation Kit (Illumina) according to the manufacturer's recommendation. Sequencing reactions were carried out using the MiSeq v2 (2 × 150 bp) chemistries (Illumina). The MiSeq re-sequencing protocol for amplicon was performed. The sequences were mapped on the human GRCh37/hg19 assembly and quality-checked using the on-board software MiSeq Reporter, and analysed by AVADIS NGS software (Agilent Technologies).

To validate *RPL27* and *RPS27* mutations of patients and their families, we performed direct sequencing analysis using the primers described in Data S1.

Cell lines and transient transfection with small interfering RNA

The human erythroleukaemic cell line K562 was maintained in RPMI 1640 medium (Sigma-Aldrich, St. Louis, MO, USA) supplemented with 10% fetal bovine serum (FBS) (Life Technologies, Carlsbad, CA, USA) at 37°C in a 5% CO_2 atmosphere. To knock down the *RPL27* and *RPS27* genes, cells were transfected by using Amaxa Nucleofector (Amaxa Biosystems, Gaithersburg, MD, USA) (Nucleofector solution V, Nucleofector program T-16) with 5 μl of 40 nmol/l siRNA solutions per 2×10^6 cells. The siRNA purchased from Thermo-Fisher Scientific-Dharmacon (Waltham, MA, USA) were ON-TARGET plus SMART pool human *RPS19, RPL5, RPS27, RPL27* and a non-targeting pool.

Northern blot analysis

Total RNA was extracted from cells using the RNeasy plus kit (QIAGEN), and hybridized at high stringency. The probes used in the present study are described in Data S1.

Functional analysis using zebrafish

Morpholino antisense oligonucleotides (MOs) targeting zebrafish *rpl27* and *rps27*, orthologs of human *RPL27* and *RPS27* respectively, were obtained from Gene Tools, LLC (Philomath, OR, USA). They were injected at a concentration of 5·0 or 20 μg/μl into one-cell-stage embryos. The MO-injected embryos (morphants) were grown at 28·5°C. Haemoglobin staining was performed at 48 h post-fertilization (hpf) using *o*-dianisidine (Uechi *et al*, 2006; Torihara *et al*, 2011).

Full-length *rpl27* was amplified by PCR and cloned into a pCS2+ vector for *in vitro* transcription. Capped mRNAs were synthesized from the linearized template using an mMessage mMachine SP6 kit (Life Technologies) and injected at 250 ng/μl into one-cell-stage embryos.

Total RNA was isolated from wild-types and the morphants. Reverse transcription (RT)-PCR was used to distinguish normal or cryptic sizes of the *rpl27* and *rps27.1* transcripts. This was performed by using primer pairs designed at exons 1 and 5 and exons 1 and 4, respectively. The MO and primer sequences are described in Data S1.

Results

Whole exome-sequencing analysis

A total of 98 Japanese DBA patients were registered and blood genomic DNA samples were collected. All samples were first screened for mutations in eight of 10 known DBA genes (*RPL5*, *RPL11*, *RPL35A*, *RPS10*, *RPS17*, *RPS19*, *RPS24* and *RPS26*) as well as *RPS14*, which had been implicated in the 5q- myelodysplastic syndrome, a subtype of myelodysplastic syndrome characterized by a defect in erythroid differentiation (Ebert *et al*, 2008). Screening was achieved by direct sequence analysis accompanied by high-resolution melt analysis (HRM) (Konno *et al*, 2010). Among these patients, 38% (38/100) had identifiable DBA mutations (Table S1). Some of the patients were described in our previous reports (Konno *et al*, 2010; Kuramitsu *et al*, 2012). Then, we screened for large gene deletions in the remaining 60 patients using synchronized-quantitative-PCR DBA gene copy number assay and/or genome wide single nucleotide polymorphism array analysis (Kuramitsu *et al*, 2012). We found that 20% (12 of 60) of samples had large deletions in previously identified DBA genes (Table S1).

WES was performed on the remaining 48 patients who lacked documented mutations or large deletions involving known DBA genes by screening. We found gene alterations in *RPS7*, *RPS27*, *RPL3L*, *RPL6*, *RPL7L1*, *RPL8*, *RPL13*, *RPL14*, *RPL18A*, *RPL27*, *RPL31* and *RPL35A* in 12 patients, whose WES data have been deposited in the European Genome-phenome Archive (EGA) under accession number EGAS00001000875. WES failed to identify a single *GATA1* mutation (Table I). The substitution mutations observed in

Table I. Characteristics of patients investigated by whole-exome sequencing.

Patient (UPN)	Age at diagnosis	Gender	Inheritance	Abnormalities	Mutation
5	1 year	F	Sporadic	None	*RPL18A* c.481C>T p.Arg161Cys
7	1 month	M	Sporadic	SGA, craniofacial abnormalities, skin pigmentation	ND
13	3 months	F	Sporadic	None	ND
21	1 year	F	Familial	None	*RPS7* c.75+1G>A Splicing error, *RPL13* c.547C>T p.R183C
26	Birth	F	Sporadic	Spastic quadriplegia, congenital hip dislocation, severe myopia, optic nerve hypoplasia, growth retardation	ND
35	18 months	M	Familial	None	*RPL6* c.253_255del p.Lys85del
36 (35 cousin)	Birth	M	Familial	Hypospadias, cryptorchidism	ND (No *RPL6* mutation was detected.)
37	4 years	M	Sporadic	Hypospadias, cryptorchidism, SGA	ND
42	2 months	F	Sporadic	None	*RPS27* c.89delC, p.Tyr31Thrfs*5
48	NA	NA	Sporadic	Fetal hydrops	*RPL3L* c.76C>G p.Arg26Gly
49	2 months	M	Sporadic	SGA, growth retardation	ND
50	2 months	F	Familial	Neutropenia	ND
52 (50 sister)	6 months	F	Familial	Neutropenia	ND
51	7 months	F	Sporadic	None	ND
53	8 months	F	Sporadic	SGA	ND
54	8 years	F	Sporadic	None	ND
61	9 months	M	Sporadic	None	ND
67	3 years	M	Sporadic	None	ND
68	16 months	M	Sporadic	None	*RPL14* c.446CTG(9), c.446CTG(15)
69	1 year	M	Sporadic	Flat thenar	ND
75	Birth	F	Familial	Acetabular dysplasia, total anomalous pulmonary venous connection	ND
76	Birth	M	Sporadic	IgG subclass 2 and 4 deficiency	*RPL35A* c.125A>G:p.Tyr42Cys *RPL7L1* c.G544A:p.V182I (His unaffected parents did not possess the mutation in *RPL35A*.)
77	Birth	M	Familial	None	ND
83	9 months	M	Sporadic	None	*RPL31* c.122G>A p.Arg41His
88	Birth	M	Familial	Cryptorchidism, hypospadias, learning disabilities	ND
89 (88 father)	NA	M	Familial	Skeletal malformation of fingers, growth retardation	ND
90	10 months	M	Sporadic	None	ND
91	Birth	F	Sporadic	None	*RPL8* c.413C>T p.Ser138Phe
93	11 months	M	Sporadic	Leucoderma, syndactyly	ND
95	Birth	F	Sporadic	Atrial septal defect, pulmonary stenosis	*RPL27* c.-2-1G>A Splicing error
96	28 months	F	Sporadic	None	ND
97	4 years	F	Sporadic	Growth retardation	ND
105	Birth	M	Sporadic	Growth retardation	ND
109	9 months	F	Sporadic	None	ND

Table I. (*Continued*)

Patient (UPN)	Age at diagnosis	Gender	Inheritance	Abnormalities	Mutation
112	4 months	F	Sporadic	Pulmonary atresia, tricuspid atresia, ventricular septal defect, hypoplasia of right ventricle, polydactyly of thumb, cerebellar hypoplasia, low-set ear, mandibular retraction, growth retardation	ND
116	4 months	M	Sporadic	Flat thenar	ND
117	NA	F	Sporadic	NA	ND
121	2 months	F	Sporadic	Growth retardation	ND
135	1 year	M	Sporadic	Xanthogranuloma	ND
136	Birth	M	Sporadic	None	ND
140	Birth	F	Sporadic	SGA	ND
144	2 months	F	Sporadic	Neutropenia	*RPL35A* c.125A>G p.Tyr42Cys (Her unaffected parents did not possess the mutation in *RPL35A*.)
151	9 months	M	Unknown	None	*RPL35A* c.113A>G p.Glu38Gly (His unaffected father was also heterozygous for the allele.)
152	NA	NA	Sporadic	None	ND
153	17 months	M	Sporadic	None	ND
154	NA	NA	NA	NA	ND
158	3 months	M	Sporadic	Patent ductus arteriosus	ND
159	8 months	M	Sporadic	None	ND

UPN, unique patient number; NA, not available; M, male; F, female; ND, not detected; SGA, small for gestational age.

RPL35A (Patients 76, 144 and 151) had escaped detection by the HRM analysis in the first step screening but were found by WES analysis. The mutations were confirmed by direct sequencing analysis. We speculated that the sensitivity of the HRM screening was insufficient for detection of these particular mutations because the size of the PCR amplicon containing the mutations was too large for the screening. A single missense mutation (c.125A>G: p.Tyr42Cys) observed in two of the sporadic DBA cases, Patients 76 and 144, was predicted to be causative because the unaffected parents of the two patients did not possess the mutation, suggesting that the mutations were *de novo* (Table I). Furthermore, tyrosine at position 42 is highly conserved among species. On the other hand, the pathological significance of the *RPL35A* mutation (c.113A>G p.Glu38Gly) observed in Patient 151 remains unknown because glutamic acid at position 38 is not well-conserved and the patient's unaffected father was also heterozygous for the allele (Table I).

The two known DBA genes, *RPS7* and *RPL26*, were not included in the first screening. Consequently, WES identified a *RPS7* mutation in Patient 21 and confirmed the mutation by direct sequencing. The mutation was predicted to be causative because it seemed to induce a splicing error in the gene. Mutations identified in the eight patients, including *RPL18A* in Patient 5, *RPL13* in Patient 21, *RPL6* in Patient 35, *RPL3L* in Patient 48, *RPL14* in Patient 68, *RPL7L1T* in Patient 76, *RPL31* in Patient 83 and *RPL8* in Patient 91, were missense mutations or in-frame deletions. Almost all of the causative variants of RP genes observed in DBA are loss-of function mutations (Gazda *et al*, 2012). Whereas analyses by SIFT, PolyPhen-2, Mutation Taster and CONDEL predicted that some of these mutations would probably damage the structure and function of ribosomal proteins, the pathological effects of the above-mentioned mutations were uncertain (Table S2). The substitution mutation of *RPL13* observed in Patient 21 seemed to be non-pathological because the *RPS7* splicing error mutation was also identified in this patient. The missense mutation in *RPL7L1T* found in Patient 76 also seemed to be non-pathological, because the *de novo* *RPL35A* mutation was identified in this patient. The in-frame deletion of *RPL6* observed in Patient 35 with familial DBA also might be non-causative, because the mutation was not identified in his cousin, Patient 36 (Table I).

De novo *mutation in* RPL27 *and* RPS27

Next, we focused on novel loss-of function mutations in *RPL27* and *RPS27*, found in the screening. Almost all RP genes were sequenced with enough coverage for detecting germline mutations except for several RP genes (Table S3). Target deep sequencing analysis was performed for the RP genes with a low depth of coverage of <10× (Table S4 and

S5), and we confirmed that the mutations in *RPL27* and *RPS27* were the only ones found in these patients.

In Patient 95, we identified the substitution of c.-2-1G>A in the *RPL27* gene, a putative splicing error mutation (Fig 1A). To confirm the effect of the mutation, we performed RT-PCR analysis by using primers located on the first and third exons and total RNA derived from the patient's leucocytes. We found two transcripts in Patient 95: the full-length transcript and a shorter transcript lacking exon 2 by alternative splicing, a variant skipping exon 2, in which the translation initiation codon is located (Fig 1B,C). We performed a quantitative assessment of the levels of the full-length transcripts and the short transcripts, using the Experion automated electrophoresis system (Bio-Rad, Hercules, CA, USA). The calculated concentration of each product was 48·31 nmol/μl (7·49 ng/μl) and 31·69 nmol/μl (3·19 ng/μl), respectively. The results indicated that the extent of aberrant splicing accounted for about 40% of total *RPL27* transcripts in this patient. Patient 95 was a 2-year-old girl with no family history of anaemia, diagnosed with DBA at birth. She had an atrial septal defect and pulmonary stenosis. She responded to corticosteroid treatment and has been in remission for 2 years. Her clinical characteristics are presented in Table II. As she was thought to be sporadic type DBA, we examined the genotype of her parents. The direct sequencing analysis showed that the parents were homozygous for wild-type *RPL27* (Fig 1A). These results suggested the mutation observed in the patient was *de novo* and a probable pathogenic mutation of DBA.

In Patient 42, we found a single nucleotide deletion (c.90delC, p.Tyr31Thrfs*5) in the *RPS27* gene generating a premature stop codon by frameshift (Fig 1D). The patient was a 4-year-old girl with no family history of anaemia, diagnosed with DBA at 2 months of age. This patient had no abnormalities except for skin pigmentation, and responded to steroid treatment. Her clinical characteristics are presented in Table II. Her unaffected parents did not have the gene alteration observed in the patients (Fig 1D), indicating the mutation was *de novo*.

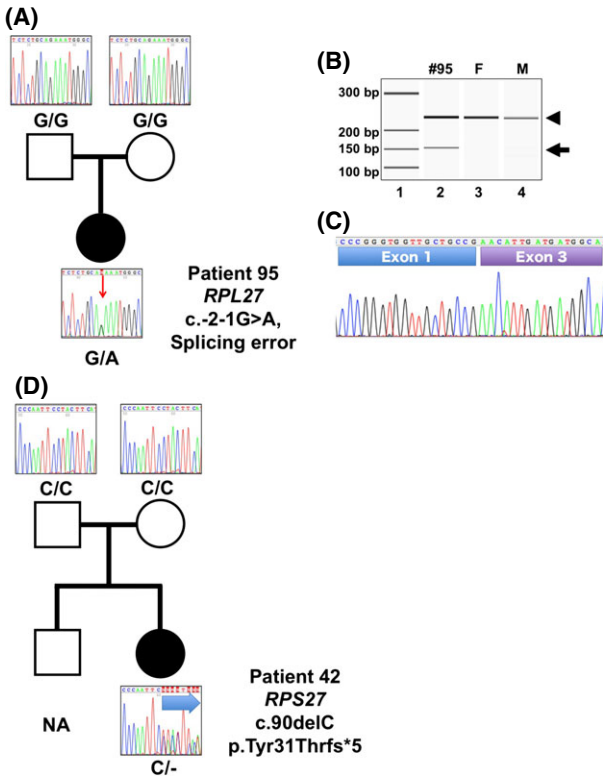

Fig 1. *De novo* mutations in *RPL27* and *RPS27*. (A) Family tree of Patient 95. Electropherograms indicate the gDNA sequence including the boundary between IVS-1 and the first exon of the *RPL27* gene. The red arrow indicates the position of the nucleotide substitution −2-1G>A observed in Patient 95. (B) RT-PCR analysis using the primer set located on the first and third exons of the *RPL27* gene. Arrowhead and arrow indicate PCR products for the full-length variant and the alternative splicing lacking the second exon, respectively. Molecular marker (lane 1), Patient 95 (lane 2), her father (F, lane 3) and mother (M, lane 4) are shown. (C) Sequence analysis of the short PCR product of Patient 95 showing the alternative splicing variants lacking the second exon. (D) Family tree of Patient 42. Electropherograms indicate gDNA sequence including a portion of the second exon of the *RPS27* gene. Blue arrow indicates the frameshift signals caused by single nucleotide deletion of c.90delC.

Defective pre-ribosomal RNA processing due to repression of RPL27 *or* RPS27

A single pre-ribosomal RNA (pre-rRNA), called 45S is processed into mature 28S, 18S and 5.8S rRNAs (Hadjiolova *et al*, 1993; Rouquette *et al*, 2005). Among the mature rRNAs, the 28S and 5.8S rRNAs associate with the large ribosomal subunit (60S) and the 18S rRNA associates with the small subunits (40S) of the ribosome. It has been reported that the mutations in RP genes observed in DBA cause defects in pre-rRNA processing. For example, the loss-of-function of the small subunit of RP affects maturation of 18S rRNA (Gazda *et al*, 2006, 2012; Choesmel *et al*, 2007; Flygare *et al*, 2007; Idol *et al*, 2007; Doherty *et al*, 2010). To validate the effects of the knockdown of *RPS27* or *RPL27* on erythroid lineage cells, we introduced siRNA into the human erythroid cell line K562 cells and analysed pre-rRNA processing by Northern blotting analysis.

Consistent with previous reports, decreased expression of *RPS19* was associated with a defect in rRNA processing characterized by a decrease in 18S-E rRNA with accumulation of a 21S rRNA precursor, and decreased expression of *RPS26* resulted in accumulation of a 26S rRNA precursor. Reduction of *RPS27* led to the accumulation of 30S rRNA and a decrease in the 21S rRNA and 18S-E rRNA (Fig 2). These findings suggest that RPS27 is also essential for 18S rRNA processing, although RPS27 involves rRNA processing associated with the small subunit at different stages from RPS19 and RPS26. In contrast, knockdown of *RPL27* caused accumulation of 32S rRNA, which is very similar to the effects by *RPL5* siRNA, suggesting that RPL27 is important for the

Table II. Clinical characteristics of DBA patients with *RPS27* or *RPL27* mutation.

UPN	42	95
Mutated gene	*RPS27*	*RPL27*
Age (years)	4	2
Gender	Female	Female
Family history of anaemia	No	No
Onset	2 months of age	At birth
Malformation	Skin pigmentation	Atrial septal defect pulmonary stenosis
Clinical data at onset		
RBC ($\times 10^{12}$/l)	1·38	2·17
Hb (g/l)	49	71
MCV (fl)	105	92·3
Reticulocytes (%)	0·17	0·1
WBC ($\times 10^{9}$/l)	11·68	5·5
Platelets ($\times 10^{9}$/l)	373	446
Bone marrow	Hyper cellularity, erythroid 1%	Normo-cellularity, erythroid 7·4%
Response to first steroid therapy	Yes	Yes
Present therapy	NA	NA

UPN, unique patient number; RBC, red blood cell count; WBC, white blood cell count; NA, not available.

maturation of 28S and 5.8S rRNAs (Fig 2). These findings showed that decreased expression of *RPS27* and *RPL27* perturbed pre-rRNA processing associated with the small and large subunits, respectively.

To accurately model the degree of ribosomal haploinsufficiency, we titrated the dose of the siRNA to obtain approximately 50% of the expression compared with wild-type cells (Figure S1A). For this experiment, we used 50% *RPS19*, *RPS26* and *RPL5* knocked-down cells as positive controls. However, the rRNA processing defects were not clearly observed under these conditions even in the positive controls (Figure S1B). These results suggested that a more accurate functional assay was necessary to investigate the pathological significance of these mutations. For that reason, we turned to the zebrafish model.

Impairment of erythroid development in rpl27 *and* rps27*-deficient zebrafish*

To investigate the effects of *RPL27* mutations in DBA, we knocked down the zebrafish ortholog (*rpl27*) using MOs and analysed the morphology and erythropoietic status during embryonic development. The coding region of *rpl27* shares 84% nucleotide and 96% amino acid identities with its human ortholog. Although gene duplication is common in zebrafish, available information from public databases suggests that *rpl27* exists as a single copy in the genome. We inhibited expression of this gene using an MO designed to target the 3′-splice site of the first intron that corresponded

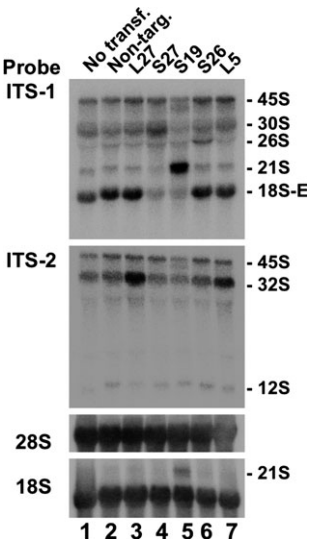

Fig 2. Perturbation of pre-rRNA processing by knockdown of the *RPL27* or *RPS27* gene. Northern blot analysis using K562 cells knocked down by siRNAs. The 5′ extremities of the internal transcribed spacer 1 (ITS-1) and internal transcribed spacer 2 (ITS-2) were used as probes to detect the precursors to the 18S rRNA associated with the small subunit and 28S rRNA and 5.8S rRNA associated with the large subunit of the ribosome, respectively. *RPS19, RPS26* and *RPL5* knocked-down cells were used as positive controls for the detection of defects in rRNA processing. ITS-1 and ITS-2 probes revealed the accumulation of 30S pre-rRNA in *RPS27* knocked-down cells and 32S pre-rRNA in *RPL27* knocked-down cells, respectively. Decrease of 18S-E pre-rRNA was also detected by the ITS-1 probe in *RPS27* knockdown cells. The mature 18S and 28S rRNAs were detected with specific probes.

to the position at which the mutation was identified in the patient (Fig 3A). Injection of this MO into the one-cell stage embryos perturbed the splicing and resulted in exclusion of exon 2 as observed in the patient (Fig 3B). When injected with 5 μg/μl MO targeted against *rpl27,* the expression level of a smaller transcript lacking exon 2 was comparable to that seen in Patient 1 (Figs 1B and 3B). Therefore, all of the following experiments were performed using 5 μg/μl MO.

We compared the morphological features of the morphants with wild-type embryos and found that the morphants showed abnormal phenotypes, such as a thin yolk sac extension and a bent tail at 25 hpf (Fig 3C). We also performed haemoglobin staining at 48 hpf and found a marked reduction of erythrocyte production in the cardial vein of the morphants (Fig 3D). All these abnormalities were rescued by the simultaneous injection of *rpl27* mRNA into the embryos, indicating that the morphological defects and decreased erythropoiesis observed in the morphants were caused by the aberrant splicing of *rpl27* in zebrafish (Fig 3B,D). These results suggested that the splice site mutation identified in human *RPL27* could be responsible for the pathogenesis of DBA.

We next investigated the effects of *RPS27* mutations in DBA. Public databases suggest that there are three copies of the zebrafish *rps27* gene, *rps27.1*, *rps27.2* and *rps27.3*, whereas

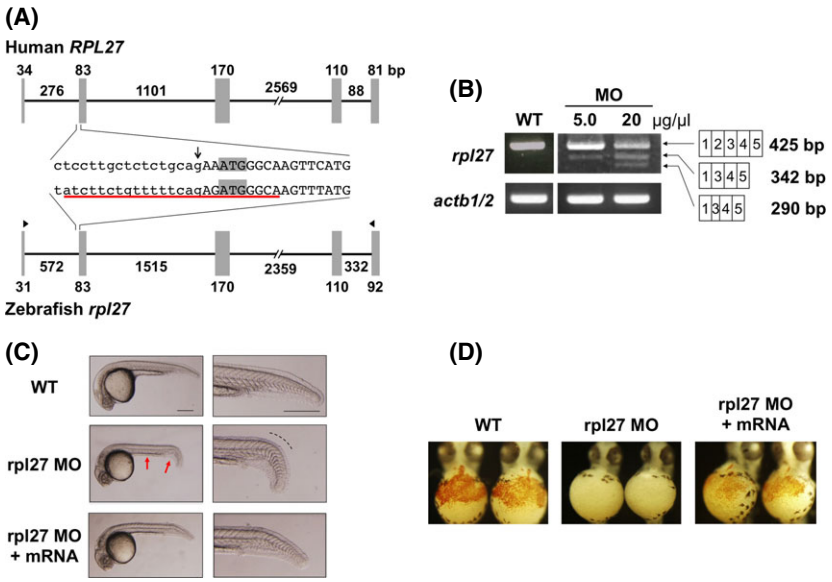

Fig 3. Morphological defects and decreased erythropoiesis in *rpl27* morphants. (A) The gene structures of human *RPL27* and zebrafish *rpl27*. The sequences of intron 1/exon 2 boundary regions are indicated. Uppercase and lowercase letters show the exon and intron sequences, respectively. The MO target site is underlined and the translation initiation codons (ATG) are shaded. The arrow indicates the position of the mutated nucleotide in the patient. Arrowheads show the primer positions for the RT-PCR. (B) The results of RT-PCR of *rpl27* and *actb* (control) in wild type and MO injected embryos. A smaller transcript without exon 2 was observed in the morphants as seen in the patient at a comparable level, when 5 μg/μl MO was injected into the one-cell-stage embryos. Injection with higher concentrations of MO (20 μg/μl) also produced a truncated exon 3. (C) Morphological features of wild-type and MO-injected embryos. A thin yolk sac extension and a bent tail are prominent in the morphants injected with 5 μg/μl MO (arrows), whereas these features are rescued in the embryos injected with *rpl27* mRNA. Scale bars: 250 μm. (D) The haemoglobin staining of cardial veins at 48 hpf. Compared to wild-type embryos, *rpl27* morphants injected with 5 μg/μl MO showed a drastic reduction in the number of haemoglobin-stained blood cells. Morphants co-injected with *rpl27* mRNA show recovery of the stained cells.

the human genome contains two copies, *RPS27* and *RPS27L*. We inhibited expression of the zebrafish *rps27.1*, which shares 96% amino acid identity with the human *RPS27*, using an MO designed to target the 5′-splice site of the second intron (Fig 4A). Injection of this MO into the embryos perturbed the splicing and resulted in exclusion of exon 2 (Fig 4B) that consequently introduced a stop codon in exon 3. The morphants showed abnormal phenotypes, such as a thin yolk sac extension, a bent tail and a malformed brain region at 26 hpf (Fig 4C). We also observed reduced erythrocyte production in about 60% of the morphants (Fig 4D). These results suggested that the frameshift mutation identified in human *RPS27* is a strong candidate for a causative mutation for DBA.

Discussion

WES analysis identified loss-of-function mutations in two RP genes. Each of the patients carrying one of these mutations was a sporadic case, and the mutations were *de novo*. Knockdown of *RPL27* and *RPS27* disturbed pre-rRNA processing for the large and small subunits, respectively. Although the zebrafish models cannot reproduce the exact features of DBA, such as macrocytic anaemia appearing after birth and skeletal abnormalities, the models of *RPL27* and *RPS27* mutations showed impairment of erythrocyte production. These results suggested that *RPL27* and *RPS27* play important roles in erythropoiesis, and that haploinsufficiency of either RP could lead to pure red cell aplasia. However, these findings only represent a single patient in relation to each gene. The identification of new DBA cases in the future with mutations in these genes will be important to confidently label *RPS27* and *RPL27* as DBA disease genes.

Interestingly, RPS27 binds to MDM2 through its N-terminal region, and overexpression of RPS27 stabilizes TP53 by inhibiting MDM2-induced TP53 ubiquitination (Xiong *et al*, 2011). Although the exact mechanism by which ribosome disruptions leads to DBA is unclear, a widely accepted hypothesis is that imbalances in expression of individual RPs trigger a TP53-mediated checkpoint, leading to cell cycle arrest and apoptosis of erythroid precursors (Narla & Ebert, 2010). Several animal models have demonstrated the role of TP53 in the pathophysiology of DBA (McGowan & Mason, 2011). In support of this conclusion, it was observed that certain RPs, such as RPL5, RPL11, RPL23, RPL26 and RPS7, bind to and inhibit the TP53 regulator MDM2, thereby inhibiting its ability to promote TP53 degradation (Zhang & Lu, 2009). Notably, like *RPL27*, many of the RP genes, including *RPL5*, *RPL11*, *RPL26* and *RPS7*, are mutated in DBA.

Here, we report the results of RP gene mutations observed in 98 Japanese DBA patients. The frequency of the patients harbouring probable causative mutations/large

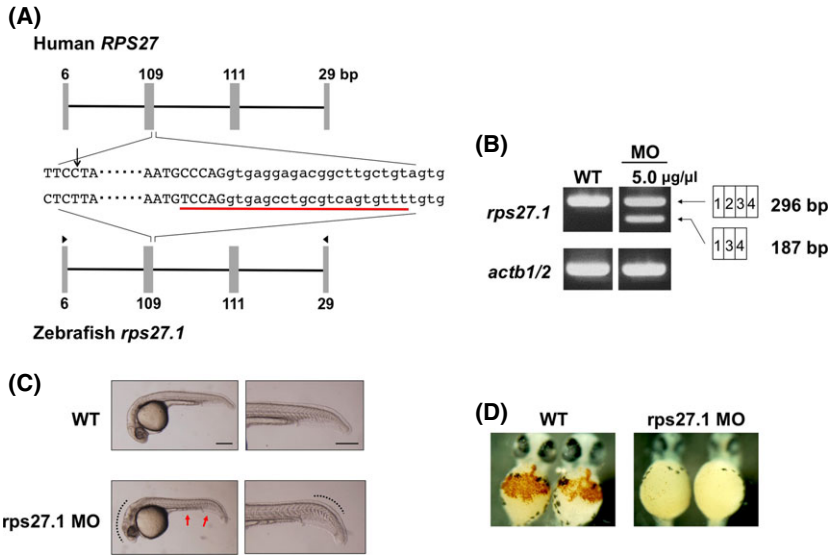

Fig 4. Morphological defects and decreased erythropoiesis in *rps27* morphants. (A) The gene structures of human *RPS27* and zebrafish *rps27.1*. The sequences of exon 2/intron 2 boundary regions are indicated. Uppercase and lowercase letters show the exon and intron sequences, respectively. The MO target site is underlined. The arrow indicates the position of the mutated nucleotide in the patient. Arrowheads show the primer positions for RT-PCR. (B) The results of RT-PCR of *rps27.1* and *actb* (control) in wild-type and MO-injected embryos. A smaller transcript without exon 2 was observed in the morphants. (C) Morphological features of wild-type and MO-injected embryos at 26 hpf. A thin yolk sac extension and a bent tail are prominent in the morphants (arrows). An abnormal development in the brain region was also observed. Scale bars: 250 μm. (D) Haemoglobin staining of cardial veins at 48 hpf.

deletions in RP genes was 55% (56/98), including *RPS19* 16% (16), *RPL5* 12% (12), *RPL11* 5% (5), *RPS17* 7% (7), *RPL35A* 7% (7), *RPS26* 4% (4), *RPS10* 1% (1), *RPS7* 1% (1), *RPL27* 1% (1) and *RPS27* 1% (1). No mutation of *RPS24*, *RPS29* or *RPL26* was identified in this study. In addition to above mutations, we found a missense mutation of *RPL35A* in a sporadic case (Patient 151). Mutations in RP genes are characterized by a wide variability of phenotypic expression. Even family members with the same mutation in the RP gene can present with clinical differences (Willig *et al*, 1999). For example, *RPS19* mutations are found in some first-degree relatives presenting only with isolated high erythrocyte adenosine deaminase activity and/or macrocytosis. Therefore, there is still the possibility that this *RPL35A* mutation is disease-causing, although the patients' father had the same heterozygous mutation without anaemia. To confirm the pathological effect of the substitution, a functional analysis is necessary. The zebrafish model might be very useful for this assay.

Recently, Gerrard *et al* (2013) found inactivating mutations in 15/17 patients by targeted sequencing of 80 RP genes. All mutations were in genes previously found to be DBA genes. The differences between these results and those in our study might be due to differences between human populations. In our cohort, all patients were Asian, whereas 80% were Caucasian in the cohort reported by Gerrard *et al* (2013). The frequency of RP gene mutaitons may vary between ethnic groups. However, the data from both cohorts are based on a relatively low number of patients and values showing significant differences between cohorts are missing. Interestingly, Gazda *et al* (2012) reported large-scale sequencing of 79 RP genes in a cohort of 96 DBA probands, none of whom had previously been found to have a pathogenic mutation. The study showed *c.* 53·9% of DBA patients had mutations in one of 10 known DBA-associated RP genes, including a novel causative *RPL26* gene. The results were very similar to ours, although their data did not contain large deletions of RP genes, which would escape regular sequencing analysis.

An additional five missense single nucleotide variants affecting single cases were identified in six patients, including *RPL3L*, *RPL7L1*, *RPL8*, *RPL13*, *RPL18A* and *RPL31* together with two in-frame deletions of *RPL6* and *RPL14* in two patients, which cause deletion of a single amino-acid (Table I). However, the pathological significance in these seven cases is uncertain. In the remaining 36 patients, no mutations were detected in *RP* genes. In conclusion, we identified novel germline mutations of two RP genes that could be responsible for DBA, further confirming the concept that RP genes are common targets of germline mutations in DBA patients and also suggesting the presence of non-RP gene targets for DBA. To identify the candidate disease variants in non-RP genes, we are now pursuing WES of their parents and planning to perform functional assays of these variants.

Acknowledgements

We thank T. Kudo and A. Mikami for their technical assistance. This work was supported by the Research on Measures for Intractable Diseases Project and Health and Labor

Sciences Research grants (Research on Intractable Diseases) from the Ministry of Health, Labour and Welfare, by Grants-in-Aid from the Ministry of Health, Labour and Welfare of Japan and by grants-in-aid for scientific research from the Ministry of Education, Culture, Sports, Science and Technology of Japan (KAKENHI: 25291003).

Authorship and Disclosure

Y.O., Y. S., A.S.-O., K.C., H.T. and S.M. performed bioinformatics analyses of the resequencing data. R.W., K.Y., T.T. and R.K. processed and analysed genetic material, prepared the library and performed sequencing. R.W., K.Y., T.T. and R.K. performed the Northern blot analyses and RT-PCR analyses. M.K and I.H. performed DBA copy number analysis. T. S., T. U. and N.K. performed zebrafish experiments. K. K., I.K., S. Ohga, A.O., J.H., K.S., K.M., K. K., A.I., Y. K., S.K., K.T., T. S. and E.I. collected specimens and were involved in planning the project. Y.I. and H.K. analysed data and designed the study. E.I. and S.O led the entire project. T.T., R.W., N.K. and I.E. wrote the manuscript. All authors participated in discussions and interpretation of the data and results.

Supporting Information

Additional Supporting Information may be found in the online version of this article:

Fig S1. Perturbation of pre-rRNA processing by knockdown of the *RPL27* or *RPS27* gene when the extent of the knockdown was approximately 50%.

Data S1. Methods.

Table S1. Mutations identified in *RPS19*, *RPL5*, *RPL11*, *RPL35A*, *RPS17* and *RPS26* in Japanese DBA patients.

Table S2. Prediction of functional effects of mutations in ribosomal protein genes.

Table S3. Mean coverage of whole-exome sequencing of RP genes in Patients #42 and #95.

Table S4. Average coverage of target deep sequencing of RP genes in Patient #95.

Table S5. Average coverage of target deep sequencing of RP genes in Patient #42.

References

Choesmel, V., Bacqueville, D., Rouquette, J., Noaillac-Depeyre, J., Fribourg, S., Crétien, A., Leblanc, T., Tchernia, G., Da Costa, L. & Gleizes, P.E. (2007) Impaired ribosome biogenesis in Diamond-Blackfan anemia. *Blood*, **109**, 1275–1283.

Cmejla, R., Cmejlova, J., Handrkova, H., Petrak, J. & Pospisilova, D. (2007) Ribosomal protein S17 gene (RPS17) is mutated in Diamond-Blackfan anemia. *Human Mutation*, **28**, 1178–1182.

Doherty, L., Sheen, M.R., Vlachos, A., Choesmel, V., O'Donohue, M.F., Clinton, C., Schneider, H.E., Sieff, C.A., Newburger, P.E., Ball, S.E., Niewiadomska, E., Matysiakm M, Glader., B., Arceci., R.J., Farrar., J.E., Atsidaftosm.E., Liptonm J, M., Gleizes, P.E. & Gazda, H.T. (2010) Ribosomal protein genes RPS10 and RPS26 are commonly mutated in Diamond-Blackfan anemia. *The American Journal of Human Genetics*, **86**, 222–228.

Draptchinskaia, N., Gustavsson, P., Andersson, B., Pettersson, M., Willig, T.N., Dianzani, I., Ball, S., Tchernia, G., Klar, J., Matsson, H., Tentler, D., Mohandas, N., Carlsson, B. & Dahl, N. (1999) The gene encoding ribosomal protein S19 is mutated in Diamond-Blackfan anaemia. *Nature Genetics*, **21**, 169–175.

Ebert, B.L., Pretz, J., Bosco, J., Chang, C.Y., Tamayo, P., Galili, N., Raza, A., Root, D.E., Attar, E., Ellis, S.R. & Golub, T.R. (2008) Identification of RPS14 as a 5q- syndrome gene by RNA interference screen. *Nature*, **451**, 335–339.

Farrar, J.E., Nater, M., Caywood, E., McDevitt, M.A., Kowalski, J., Takemoto, C.M., Talbot, C.C. Jr, Meltzer, P., Esposito, D., Beggs, A.H., Schneider, H.E., Grabowska, A., Ball, S.E., Niewiadomska, E., Sieff, C.A., Vlachos, A., Atsidaftos, E., Ellis, S.R., Lipton, J.M., Gazda, H.T. & Arceci, R.J. (2008) Abnormalities of the large ribosomal subunit protein, Rpl35a, in Diamond-Blackfan anemia. *Blood*, **112**, 1582–1592.

Flygare, J., Aspesi, A., Bailey, J.C., Miyake, K., Caffrey, J.M., Karlsson, S. & Ellis, S.R. (2007) Human RPS19, the gene mutated in Diamond-Blackfan anemia, encodes a ribosomal protein required for the maturation of 40S ribosomal subunits. *Blood*, **109**, 980–986.

Gazda, H.T., Grabowska, A., Merida-Long, L.B., Latawiec, E., Schneider, H.E., Lipton, J.M., Vlachos, A., Atsidaftos, E., Ball, S.E., Orfali, K.A., Niewiadomska, E., Da Costa, L., Tchernia, G., Niemeyer, C., Meerpohl, J.J., Stahl, J., Schratt, G., Glader, B., Backer, K., Wong, C., Nathan, D.G., Beggs, A.H. & Sieff, C.A. (2006) Ribosomal protein S24 gene is mutated in Diamond-Blackfan anemia. *The American Journal of Human Genetics*, **2006**, 1110–1118.

Gazda, H.T., Sheen, M.R., Vlachos, A., Choesmel, V., O'Donohue, M.F., Schneider, H., Darras, N., Hasman, C., Sieff, C.A., Newburger, P.E., Ball, S.E., Niewiadomska, E., Matysiak, M., Zaucha, J.M., Glader, B., Niemeyer, C., Meerpohl, J.J., Atsidaftos, E., Lipton, J.M., Gleizes, P.E. & Beggs, A.H. (2008) Ribosomal protein L5 and L11 mutations are associated with cleft palate and abnormal thumbs in Diamond-Blackfan anemia patients. *The American Journal of Human Genetics*, **83**, 769–780.

Gazda, H.T., Preti, M., Sheen, M.R., O'Donohue, M.F., Vlachos, A., Davies, S.M., Kattamis, A., Doherty, L., Landowski, M., Buros, C., Ghazvinian, R., Sieff, C.A., Newburger, P.E., Niewiadomska, E., Matysiak, M., Glader, B., Atsidaftos, E., Lipton, J.M., Gleizes, P.E. & Beggs, A.H. (2012) Frameshift mutation in p53 regulator RPL26 is associated with multiple physical abnormalities and a specific pre-ribosomal RNA processing defect in diamond-blackfan anemia. *Human Mutation*, **33**, 1037–1044.

Gerrard, G., Valgañón, M., Foong, H.E., Kasperaviciute, D., Iskander, D., Game, L., Müller, M., Aitman, T.J., Roberts, I., de la Fuente, J., Foroni, L. & Karadimitris, A. (2013) Target enrichment and high-throughput sequencing of 80 ribosomal protein genes to identify mutations associated with Diamond-Blackfan anaemia. *British Journal of Haematology*, **162**, 530–536.

Hadjiolova, K.V., Nicoloso, M., Mazan, S., Hadjiolov, A.A. & Bachellerie, J.P. (1993) Alternative pre-rRNA processing pathways in human cells and their alteration by cycloheximide inhibition of protein synthesis. *European Journal of Biochemistry*, **212**, 211–215.

Idol, R.A., Robledo, S., Du, H.Y., Crimmins, D.L., Wilson, D.B. & Ladenson, J.H. (2007) Cells depleted for RPS19, a protein associated with Diamond Blackfan anemia, show defects in 18S ribosomal RNA synthesis and small ribosomal subunit production. *Blood Cells Molecules and Diseases*, **39**, 35–43.

Ito, E., Konno, Y., Toki, T. & Terui, K. (2010) Molecular pathogenesis in Diamond-Blackfan anemia. *International Journal of Hematology*, **92**, 413–418.

Konno, Y., Toki, T., Tandai, S., Xu, G., Wang, R.N., Terui, K., Ohga, S., Hara, T., Hama, A., Kojima, S., Hasegawa, D., Kosaka, Y., Yanagisawa, R., Koike, K., Kanai, R., Imai, T., Hongo, T., Park, M.J., Sugita, K. & Ito, E. (2010) Mutations in the ribosomal protein genes in Japanese patients with Diamond-Blackfan anemia. *Haematologica*, **95**, 1293–1299.

Kunishima, S., Okuno, Y., Yoshida, K., Shiraishi, Y., Sandada, M., Muramatsu, H., Chiba, K., Tanaka, H., Miyazaki, K., Sakai, M., Ohtake, M., Kobayashi, R., Iguchi, A., Niimi, G., Otsu, M., Takahashi, Y., Miyano, S., Saito, H., Kojima, S. & Ogawa, S. (2013) ACTN1 mutations cause congenital macrothrombocytopenia. *The American Journal of Human Genetics*, **92**, 431–438.

Kuramitsu, M., Sato-Otsubo, A., Morio, T., Takagi, M., Toki, T., Terui, K., Wang, R., Kanno, H., Ohga, S., Ohara, A., Kojima, S., Kitoh, T., Goi, K., Kudo, K., Matsubayashi, T., Mizue, N., Ozeki, M., Masumi, A., Momose, H., Takizawa, K., Mizukami, T., Yamaguchi, K., Ogawa, S., Ito, E. & Hamaguchi, I. (2012) Extensive gene deletions in Japanese patients with Diamond-Blackfan anemia. *Blood*, **119**, 2376–2384.

Li, H. & Durbin, R. (2009) Fast and accurate short read alignment with Burrows-Wheeler transform. *Bioinformatics*, **25**, 1754–1760.

Lipton, J.M., Atsidaftos, E., Zyskind, I. & Vlachos, A. (2006) Improving clinical care and elucidating the pathophysiology of Diamond Blackfan anemia: an update from the Diamond Blackfan Anemia Registry. *Pediatric Blood & Cancer*, **46**, 558–564.

McGowan, K.A. & Mason, P.J. (2011) Animal models of Diamond Blackfan anemia. *Seminars in Hematology*, **48**, 106–116.

Mirabello, L., Macari, E.R., Jessop, L., Ellis, S.R., Myers, T., Giri, N., Taylor, A.M., McGrath, K.E., Humphries, J.M., Ballew, B.J., Yeager, M., Boland, J.F., He, J., Hicks, B.D., Burdett, L., Alter, B.P., Zon, L. & Savage, S.A. (2014) Whole-exome sequencing and functional studies identify RPS29 as a novel gene mutated in multi-case Diamond-Blackfan anemia families. *Blood*, **124**, 24–32.

Narla, A. & Ebert, B.J. (2010) Ribosomepathies: human disorders of ribosome dysfunction. *Blood*, **115**, 3196–3205.

Rouquette, J., Choesmel, V. & Gleizes, P.E. (2005) Nuclear export and cytoplasmic processing of precursors to the 40S ribosomal subunits in mammalian cells. *EMBO Journal*, **24**, 2862–2872.

Sankaran, V.G., Ghazvinian, R., Do, R., Thiru, P., Vergilio, J.A., Beggs, A.H., Sieff, C.A., Orkin, S.H., Nathan, D.G., Lander, E.S. & Gazda, H.T. (2012) Exome sequencing identifies *GATA1* mutations resulting Diamond-Blackfan anemia. *The Journal of Clinical Investigation*, **122**, 2439–2443.

Torihara, H., Uechi, T., Chakraborty, A., Shinya, M., Sakai, N. & Kenmochi, N. (2011) Erythropoiesis failure due to RPS19 deficiency is independent of an activated Tp53 response in a zebrafish model of Diamond-Blackfan anaemia. *British Journal of Haematology*, **152**, 648–654.

Uechi, T., Nakajima, Y., Nakao, A., Torihara, H., Chakraborty, A., Inoue, K. & Kenmochi, N. (2006) Ribosomal protein gene knockdown causes developmental defects in zebrafish. *PLoS ONE*, **1**, e37.

Vlachos, A., Ball, S., Dahl, N., Alter, B.P., Sheth, S., Ramenghi, U., Meerpohl, J., Karlsson, S., Liu, J.M., Leblanc, T., Paley, C., Kang, E.M., Leder, E.J., Atsidaftos, E., Shimamura, A., Bessler, M., Glader, B. & Lipton, J.M. (2008) Diagnosing and treating Diamond Blackfan anaemia: results of an international clinical consensus conference. *British Journal of Haematology*, **142**, 859–876.

Vlachos, A., Rosenberg, P.S., Atsidaftos, E., Alter, B.P. & Lipton, J.M. (2012) Incidence of neoplasia in Diamond Blackfan anemia: a report from the Diamond Blackfan Anemia Registry. *Blood*, **119**, 3815–3819.

Willig, T.N., Draptchinskaia, N., Dianzani, I., Ball, S., Niemeyer, C., Ramenghi, U., Orfali, K., Gustavsson, P., Garelli, E., Brusco, A., Tiemann, C., Pérignon, J.L., Bouchier, C., Cicchiello, L., Dahl, N., Mohandas, N. & Tchernia, G. (1999) Mutations in ribosomal protein S19 gene and diamond blackfan anemia: wide variations in phenotypic expression. *Blood*, **94**, 4294–4306.

Xiong, X., Zhao, Y., He, H. & Sun, Y. (2011) Ribosomal protein S27-like and S27 interplay with p53-MDM2 axis as a target, a substrate and a regulator. *Oncogene*, **30**, 1798–1811.

Yoshida, K., Sanada, M., Shiraishi, Y., Nowak, D., Nagata, Y., Yamamoto, R., Sato, Y., Sato-Otsubo, A., Kon, A., Nagasaki, M., Chalkidis, G., Suzuki, Y., Shiosaka, M., Kawahata, R., Yamaguchi, T., Otsu, M., Obara, N., Sakata-Yanagimoto, M., Ishiyama, K., Mori, H., Nolte, F., Hofmann, W.K., Miyawaki, S., Sugano, S., Haferlach, C., Koeffler, H.P., Shih, L.Y., Haferlach, T., Chiba, S., Nakauchi, H., Miyano, S. & Ogawa, S. (2011) Frequent pathway mutations of splicing machinery in myelodysplasia. *Nature*, **478**, 64–69.

Zhang, Y. & Lu, H. (2009) Signaling to p53: ribosomal proteins find their way. *Cancer Cell*, **16**, 369–377.

Simple and Efficient Generation of Virus-specific T Cells for Adoptive Therapy Using Anti-4-1BB Antibody

Nobuhiko Imahashi,† Tetsuya Nishida,* Tatsunori Goto,*
Seitaro Terakura,* Keisuke Watanabe,* Ryo Hanajiri,* Reona Sakemura,*
Misa Imai,* Hitoshi Kiyoi,* Tomoki Naoe,* and Makoto Murata**

Summary: Although recent studies of virus-specific T-cell (VST) therapy for viral infections after allogeneic hematopoietic stem cell transplantation have shown promising results, simple and less time-intensive and labor-intensive methods are required to generate VSTs for the wider application of VST therapy. We investigated the efficacy of anti-CD28 and anti-4-1BB antibodies, which can provide T cells with costimulatory signals similar in strength to those of antigen-presenting cells, in generating VSTs. When peripheral blood mononuclear cells were stimulated with viral peptides together with isotype control, anti-CD28, or anti-4-1BB antibodies, anti-4-1BB antibodies yielded the highest numbers of VSTs, which were on an average 7.9 times higher than those generated with isotype control antibody. The combination of anti-CD28 and anti-4-1BB antibodies did not result in increased numbers of VSTs compared with anti-4-1BB antibody alone. Importantly, the positive effect of anti-4-1BB antibody was observed regardless of the epitopes of the VSTs. In contrast, the capacity of dendritic cells (DCs) to generate VSTs differed considerably depending on the epitopes of the VSTs. Furthermore, the numbers of VSTs generated with DCs were at most similar to those generated with the anti-4-1BB antibody. Generation of VSTs with anti-4-1BB antibody did not result in excessive differentiation or deteriorated function of the generated VSTs compared with those generated with control antibody or DCs. In conclusion, VSTs can be generated rapidly and efficiently by simply stimulating peripheral blood mononuclear cells with viral peptide and anti-4-1BB antibody without using antigen-presenting cells. We propose using anti-4-1BB antibody as a novel strategy to generate VSTs for adoptive therapy.

Key Words: virus-specific T-cell therapy, anti-4-1BB antibody, costimulatory signals, antigen-presenting cells

(*J Immunother* 2015;38:62–70)

Allogeneic hematopoietic stem cell transplantation (HSCT) is a potentially curative therapy for patients with various hematologic diseases who are otherwise incurable with conventional therapies, albeit at the expense of high treatment–related mortality. Viral infections such as cytomegalovirus (CMV), Epstein-Barr virus (EBV), and adenovirus (AdV) infections are one of the major contributors to this high mortality.[1] Although antiviral agents are effective against some of the viruses, their efficacy is often limited by weak intrinsic activity against viruses and by their toxicity.[1] Furthermore, reconstitution of virus-specific T cells (VSTs) is important for the control of viral infections.[2] These observations have led to the development of adoptive T-cell therapy for the management of viral infections after allogeneic HSCT. Although the results of recent clinical studies that evaluated the safety and efficacy of VST therapy for viral infections after HSCT are promising,[3,4] several issues remain to be resolved. One of these issues is that generation of VSTs is complex and requires a large amount of time and effort.

Optimal activation of T cells requires not only engagement of the T-cell receptor (TCR) complex, but also a secondary signal that is provided by costimulatory molecules. A number of studies that analyzed the effect of costimulatory signals on T cells using artificial antigen-presenting cells (APCs) expressing costimulatory molecules have shown that costimulatory signals, especially signals through CD28 and 4-1BB, enhance the expansion of VSTs ex vivo.[5–7] Therefore, APCs that express costimulatory molecules are used to generate VSTs for adoptive therapy. Dendritic cells (DCs) are traditional APCs and are widely used to generate antigen-specific T cells for adoptive immunotherapy.[8,9] However, the preparation of DCs requires additional time (approximately 1 wk), effort, and peripheral blood mononuclear cells (PBMCs). Another type of APC that is commonly used is an artificial APC, which is genetically modified to express costimulatory molecules and human leukocyte antigen (HLA) molecules.[10] Although artificial APCs are easy to prepare, once they are generated they can only generate antigen-specific T cells that recognize peptides presented on the same HLA as that expressed on the artificial APC. Thus, artificial APCs cannot be universally used. In addition, virus vectors are required to generate artificial APCs. These issues associated with APCs account for, at least in part, the complexity and the time-intensive and labor-intensive nature of VST therapy. As B cells and monocytes contained in PBMCs have the capacity to present antigen to T cells, one possible solution to the previous limitations to VST generation may be to directly stimulate PBMCs with viral peptides.[11] However, as freshly isolated B cells and monocytes only express low levels of costimulatory molecules,[12,13] the costimulatory signals delivered to T cells when using this method may not be sufficient. Therefore, a simple and less time-intensive and labor-intensive method that provides T cells with sufficient costimulatory signals needs to be developed for the wider application of VST therapy.

Recent advances in the understanding of T-cell biology and in technology have led to the development of immunostimulatory antibodies such as anti-CD28 and

Received for publication October 21, 2014; accepted November 14, 2014.
From the *Department of Hematology and Oncology, Nagoya University Graduate School of Medicine, Nagoya; and †Japan Society for the Promotion of Science (JSPS), Japan.
Reprints: Tetsuya Nishida, Department of Hematology and Oncology, Nagoya University Graduate School of Medicine, 65 Tsurumai-cho, Showa-ku, Nagoya, Aichi 466-8550, Japan (e-mail: tnishida@med.nagoya-u.ac.jp).

TABLE 1. Viral Peptides Used to Generate Virus-specific CD8+ T Cells

Virus	Protein	Epitope	Sequence	Restriction	Donors
CMV	pp65	341-349	QYDPVAALF	HLA-A*24:02	1, 2, 3, 4, 5
CMV	pp65	495-503	NLVPMVATV	HLA-A*02:01	1, 2, 6
CMV	pp65	417-426	TPRVTGGGAM	HLA-B*07:02	7
CMV	pp65	123-131	IPSINVHHY	HLA-B*35:01	1
EBV	EBNA3A	246-254	RYSIFFDYM	HLA-A*24:02	1, 2, 5, 8, 9
AdV	Hexon	37-45	TYFSLNNKF	HLA-A*24:02	1, 3, 4

AdV indicates adenovirus; CMV, cytomegalovirus; EBV, Epstein-Barr virus.

anti-4-1BB antibodies.[14] Although extensive clinical studies have been conducted using these antibodies,[14,15] their efficacy in generating VSTs for adoptive therapy has not been investigated. The potential benefits of using immunostimulatory antibodies are: (1) substitution of antibodies for APCs, which would save the time and effort that are required to prepare APCs, (2) universal applicability irrespective of the patients' HLA types, (3) easy applicability to clinical settings due to the lack of requirements for virus vectors, (4) more uniform quality of the antibodies compared with APCs, and (5) capability of providing sufficient costimulatory signals to T cells, which might not be possible when PBMCs are stimulated with viral peptides alone. In the current study, we investigated the efficacy of anti-CD28 and anti-4-1BB antibodies for the generation of VSTs for adoptive therapy. We found that anti-4-1BB antibody significantly increases the expansion of VSTs ex vivo without causing excessive differentiation or functional deterioration of the generated T cells. The use of this anti-4-1BB antibody may pave the way for a novel strategy to generate VSTs for adoptive therapy.

MATERIALS AND METHODS

Donor Cells and Cell Lines

PBMCs from 9 healthy volunteer donors were obtained after informed consent. The donors were tested for immunity to the target virus.

EBV-transformed B-lymphoblastoid cell lines were generated by infection of PBMCs from healthy donors with concentrated EBV-containing supernatants of cultured B95-8 cells.[16] K562 cells were transduced with retroviruses that encode CD80 and CD86 and were selected to >90% purity by cell sorting for expression of these costimulatory ligands. CD80+ and CD86+ K562 were then transduced with retroviruses that encode a full-length HLA-A*24:02 or HLA-A*02:01 (Phoenix-Ampho System, Orbigen) and were sorted twice to obtain cells of >95% purity that expressed transduced HLA (named K562/A*24:02 and K562/A*02:01).[17] Cell lines were cultured in RPMI-1640 medium (Sigma, St Louis, MO) containing 10% fetal bovine serum.

Preparation of Autologous DCs

Autologous DCs were generated as previously described with some modifications.[18,19] PBMCs obtained from healthy volunteers were placed at a concentration of $5–10 \times 10^6$ cells per well in a 6-well plate with 2 mL of RPMI-1640 medium containing 10% human serum (referred to as culture medium) and were incubated for 90 minutes at 37°C in a humidified CO_2 incubator. After incubation, the nonadherent cells were removed by gentle washing, and the adherent cells were cultured in culture medium with 80 ng/mL granulocyte-macrophage colony-stimulating factor and 17 ng/mL interleukin (IL)-4 (MiltenyiBiotec, Auburn, CA). Fresh cytokines were added on days 3 and 5. On day 6, 10 ng/mL tumor necrosis factor-α, 2 ng/mL IL-1β (R&D Systems, Minneapolis, MN), 10 ng/mL IL-6 (MiltenyiBiotec, Auburn, CA), and 1000 ng/mL prostaglandin E2 (Cayman Chemical, Ann Arbor, MI) were added for maturation of the DCs. Autologous DCs were harvested on day 8 or 9 and were used for stimulation of PBMCs.

Viral Peptides

Minimal peptides corresponding to previously identified virus-specific CD8+ T-cell epitopes were synthesized by Medical & Biological Laboratories (Nagoya, Japan) (Table 1).

Preparation of Peptide-pulsed APCs

For preparation of peptide-pulsed APCs, the cells were washed once, resuspended in RPMI-1640 medium, and pulsed with the corresponding synthetic peptide at 5 μg/mL at room temperature for 2 hours. The cells were then washed and used for the generation of VSTs and for stimulation assays. Where indicated, peptide-pulsed APCs were irradiated before use.

Generation of Virus-specific CD8+ T Cells

PBMCs obtained from healthy volunteers were placed at a concentration of 1×10^6 cells per well in a 48-well plate with 1 mL of culture medium and were directly stimulated with peptides at a concentration of 1 μg/mL and with either the indicated concentration of agonistic antibody to costimulatory receptors (anti-CD28 antibody; MiltenyiBiotec, Auburn, CA) and/or anti-4-1BB antibody; R&D Systems, Minneapolis, MN) or isotype control antibody. As initial experiments showed that adding anti-4-1BB antibody 24 hours after peptide stimulation yielded maximum numbers of virus-specific CD8+ T cells (Fig. 1C), anti-4-1BB antibody was added to the culture at this time point unless otherwise specified. In some experiments, PBMCs were stimulated with 25 Gy-irradiated DCs that were loaded with peptides at a ratio of 10:1. A total of 25 IU/mL of recombinant human IL-2 (ProSpec-Tany Technogene, Rehovot, Israel) were added to the cultures on day 3 and every 3 or 4 days thereafter. VSTs were harvested on days 13 or 14, were counted and were used for phenotypic and functional analyses.

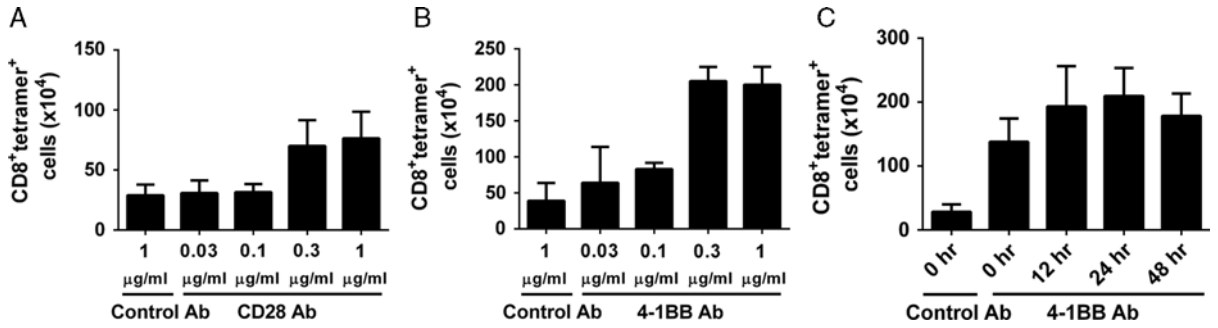

FIGURE 1. Optimization of culture conditions for the generation of virus-specific T cells using anti-CD28 or anti-4-1BB antibodies. A and B, PBMCs from healthy volunteers were stimulated with viral peptides and the indicated concentration of anti-CD28 (A) or anti-4-1BB (B) antibodies. The cells were collected on day 13, and absolute numbers of $CD8^+$ $tetramer^+$ cells were calculated by the formula: (the absolute number of viable cells × percentage of $CD8^+$ $tetramer^+$ cells among viable cells)/100. Data are representative of 8 independent experiments with 4 different virus-specific $CD8^+$ T-cell responses. C, PBMCs were stimulated with viral peptides, and 0.3 μg/mL of anti-4-1BB antibody were added to the culture at the indicated time points after peptide stimulation. The cells were collected on day 13, and absolute numbers of $CD8^+$ $tetramer^+$ cells were determined. Data are representative of 6 independent experiments with 3 different virus-specific $CD8^+$ T-cell responses. PBMCs indicates peripheral blood mononuclear cells.

Flow Cytometric Analysis

All antibodies were purchased from BD Biosciences (San Jose, CA) unless otherwise noted. The cultured T cells were analyzed for CD8, CD62L, CD45RA, CD27, CD28, and virus-specific TCRs. For the staining of virus-specific TCRs, the following phycoerythrin (PE)-conjugated HLA class I tetramers were used.

HLA-A*24:02-CMV-pp65-QYDPVAALF (QYD), HLA-A*02:01-CMV-pp65-NLVPMVATV (NLV), HLA-B*07:02-CMV-pp65-TPRVTGGGAM (TPR), HLA-B*35:01-CMV-pp65-IPSINVHHY (IPS), HLA-A*24:02-EBV-EBNA3A-RYSIFFDYM (RYS), and HLA-A*24:02-AdV-serotype 5-hexon-TYFSLNNKF (TYF) tetramers (Medical & Biological Laboratories). Data acquisition were performed with a FACSAria or FACSCanto flow cytometer (BD Biosciences), and data were analyzed using FlowJo software (TreeStar Inc., Ashland, OR).

Intracellular Cytokine Staining

Intracellular staining assays for the cytokines interferon (IFN)-γ and IL-2 were performed as previously described with some modifications.[20] In brief, cells were cocultured with peptide-pulsed or peptide-unpulsed stimulator cells and were incubated at 37°C for 6 hours. K562/A*24:02, K562/A*02:01, or autologous lymphoblastoid cell lines were used as stimulator cells for the analysis of CMV-specific and AdV-specific T cells, whereas K562/A*24:02 or K562/A*02:01 were used for the analysis of EBV-specific T cells. Brefeldin A (Golgiplug, BD Biosciences) was added during the last 4.5 hours of incubation to block the secretion of cytokines. Subsequently, the cells were fixed, permeabilized, and stained with anti-IFN-γ, anti-IL-2, and CD8 antibodies, using FIX/PERM and PERM/Wash solution (BD Biosciences). The frequency of cytokine-producing cells among $CD8^+$ $tetramer^+$ cells was calculated as follows: (frequency of cytokine-producing cells among $CD8^+$ cells)/(frequency of $tetramer^+$ cells among $CD8^+$ cells) × 100.

CD107a Mobilization Assay

T-cell degranulation was evaluated by a CD107a mobilization assay using the IMMUNOCYTO CD107a Detection Kit (Medical & Biological Laboratories) according to the manufacturer's instructions. In brief, T cells were cocultured with peptide-pulsed or peptide-unpulsed K562/A*24:02 or K562/A*02:01 at an effector-to-target ratio of 1:1, 2 μL of anti-CD107a antibody and 2 μL of monensin in 200 μL of culture medium. After incubation for 4 hours at 37°C, the cells were stained with anti-CD8 antibody and PE-conjugated HLA class I tetramer. The frequency of $CD107a^+$ cells among virus-specific $CD8^+$ T cells was calculated by subtracting the background observed with the no peptide control

Carboxyfluorescein Succinimidyl Ester (CFSE) Proliferation Assay

The CFSE proliferation assay was performed as previously described with some modifications.[17] Briefly, T cells were labeled with 0.2 μM CFSE (Invitrogen, Carlsbad, CA), washed, and cocultured with peptide-pulsed or peptide-unpulsed, 25 Gy-irradiated autologous PBMCs at a ratio of 1:1 in culture medium with 5 IU/mL of recombinant human IL-2. After 120-hour incubation, the cells were stained with anti-CD8 antibody and PE-conjugated HLA class I tetramer. Division of $CD8^+$ $tetramer^+$ cells was assessed by CFSE dye dilution using flow cytometry.

Statistics

Differences between groups were evaluated by a 1-way analysis of variance followed by the Tukey multiple comparison tests, where appropriate. Differences were considered significant when $P < 0.05$.

RESULTS

Optimization of Culture Conditions for Generating Virus-specific $CD8^+$ T Cells Using Anti-CD28 and Anti-4-1BB Antibodies

In the first set of experiments of VST generation, the effects of different concentrations of anti-CD28 and anti-4-1BB antibodies that were added at the time of culture initiation were examined. Addition of increasing concentrations of antibodies to PBMCs from healthy volunteers that were stimulated with viral peptides generally resulted

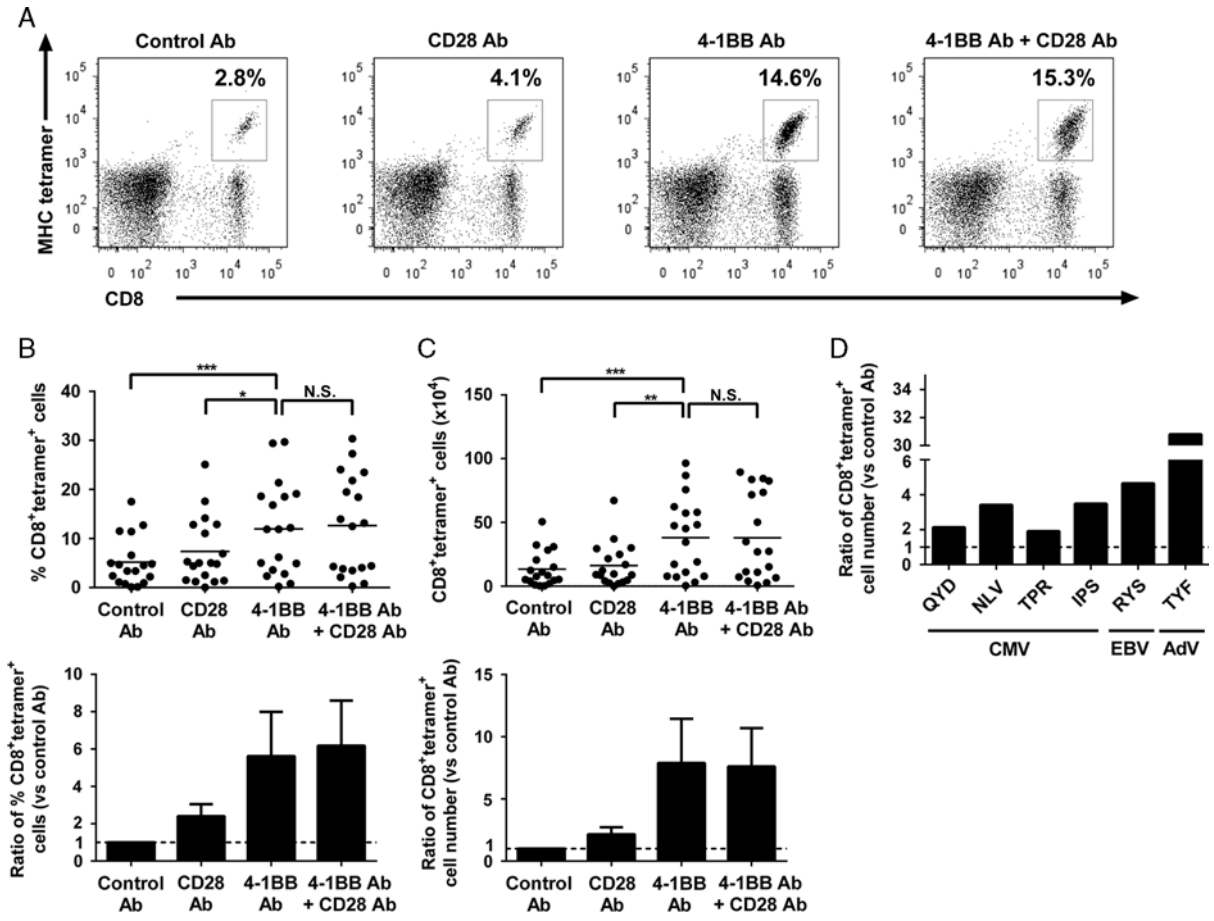

FIGURE 2. Frequencies and absolute numbers of virus-specific CD8$^+$ T cells generated with control, anti-CD28, anti-4-1BB, or a combination of anti-CD28 and anti-4-1BB antibodies. CD8$^+$ T cells specific for cytomegalovirus (CMV, n = 10), Epstein-Barr virus (EBV, n = 5), or adenovirus (AdV, n = 3) were generated with control, anti-CD28, anti-4-1BB, or a combination of anti-CD28 and anti-4-1BB antibodies. The concentrations of all antibodies were 0.3 μg/mL, and anti-4-1BB antibody was added 24 hours after culture initiation, as previously determined. After 13 days of culture, the cells were collected, counted, and analyzed using flow cytometry. A, Representative flow plots of the postculture cells showing the frequency of CD8$^+$ tetramer$^+$ cells among viable cells. Frequencies (B) and absolute numbers (C) of CD8$^+$ tetramer$^+$ cells. Actual values (upper panel) and the ratio of the actual values for the indicated culture conditions to those for control (lower panel) are shown for each measure. Horizontal lines in the upper panels mark the mean values. Means and SEMs are shown in the lower panels (*P < 0.05, **P < 0.01, ***P < 0.001, NS, not significant, repeated measures 1-way analysis of variance followed by the Tukey multiple comparison tests). D, Ratios of absolute numbers of CD8$^+$ tetramer$^+$ cells generated with anti-4-1BB antibody to those generated with control antibody according to the epitopes of virus-specific T cells. Means are shown. B–D shows data pooled from more than 18 independent experiments with 18 different virus-specific CD8$^+$ T-cell responses to CMV-pp65-QYDPVAALF (QYD), CMV-pp65-NLVPMVATV (NLV), TPRVTGGGAM (TPR), CMV-pp65-IPSINVHHY (IPS), EBV-EBNA3A-RYSIFFDYM (RYS), and AdV-serotype 5-hexon-TYFSLNNKF (TYF).

in an increased frequency and number of virus-specific CD8$^+$ T cells, with the maximal response observed at concentrations of 0.3–1 μg/mL for both antibodies (Figs. 1A, B and data not shown). Next, as the surface expression of 4-1BB on activated T cells reaches its peak at about 24–48 hours poststimulation and has declined by 4–5 days,[21,22] we investigated the optimal time of addition of anti-4-1BB antibody to the culture. Addition of anti-4-1BB antibody 24 hours after culture initiation yielded the highest frequency and number of virus-specific CD8$^+$ T cells (Fig. 1C and data not shown). Therefore, for subsequent experiments, anti-4-1BB antibody was added at a concentration of 0.3 μg/mL 24 hours after culture initiation, whereas anti-CD28 antibody was added at a concentration of 0.3 μg/mL at the time of culture initiation.

Effect of Anti-CD28 and Anti-4-1BB Antibodies on the Number of Virus-specific CD8$^+$ T Cells Generated

To evaluate and compare the effects of anti-CD28 and anti-4-1BB antibodies, CD8$^+$ T cells specific for CMV-pp65-QYD (n = 5), CMV-pp65-NLV (n = 3), CMV-pp65-TPR (n = 1), CMV-pp65-IPS (n = 1), EBV-EBNA3A-RYS (n = 5), or AdV-hexon-TYF (n = 3) epitopes were generated by stimulating PBMCs with viral peptides and with either control, anti-CD28, anti-4-1BB, or

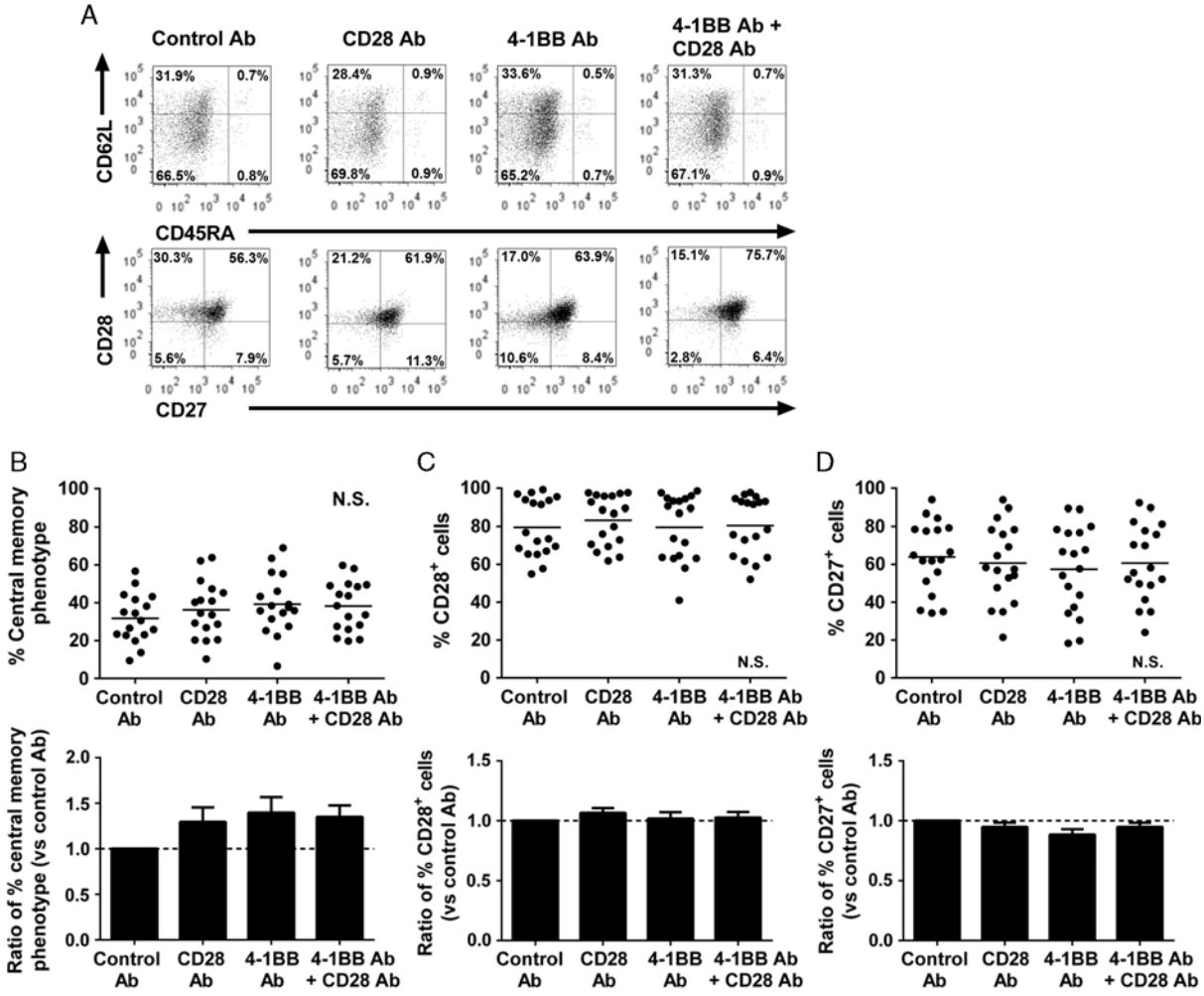

FIGURE 3. Phenotypes of virus-specific CD8+ T cells generated with control, anti-CD28, anti-4-1BB, or a combination of anti-CD28 and anti-4-1BB antibodies. CD8+ T cells specific for CMV (n = 10), EBV (n = 5), or AdV (n = 3) were generated with control, anti-CD28, anti-4-1BB, or a combination of anti-CD28 and anti-4-1BB antibodies. After 13 days of culture, the cells were collected, counted, and analyzed using flow cytometry. A, Representative flow plots of the postculture cells showing the phenotypes of the CD8+ tetramer+ cells. B–D, Frequencies of central memory phenotype (B), CD28+ (C), and CD27+ (D) cells among CD8+ tetramer+ cells. Actual values (upper panel) and the ratio of actual values for the indicated culture conditions to those for control (lower panel) are shown for each measure. Horizontal lines in the upper panels mark the mean values. Means and SEMs are shown in the lower panels (NS, not significant, repeated measures 1-way analysis of variance). B–D, Show data pooled from at least 18 independent experiments with 17 (B) or 18 (C, D) different virus-specific CD8+ T-cell responses.

a combination of anti-CD28 and anti-4-1BB antibodies. The frequencies and numbers of CD8+ tetramer+ cells that were generated with anti-4-1BB antibody were significantly higher than those generated with control or anti-CD28 antibody (Figs. 2A–C). The number of CD8+ tetramer+ cells generated with anti-4-1BB antibody was on an average 7.9 times higher than that generated with control antibody ($P < 0.001$) (Fig. 2C). In contrast, the combination of anti-CD28 and anti-4-1BB antibodies did not result in an increased frequency or number of CD8+ tetramer+ cells compared with anti-4-1BB antibody alone (Figs. 2B, C). Importantly, the positive effect of anti-4-1BB antibody was observed regardless of the epitopes of the VSTs (Fig. 2D).

Effect of Anti-CD28 and Anti-4-1BB Antibodies on the Phenotype of the Generated Virus-specific CD8+ T Cells

Previous studies have shown that extensive ex vivo expansion of T cells may reduce the in vivo activity of adoptively transferred T cells.[23,24] We therefore evaluated the effect of anti-CD28 and anti-4-1BB antibodies on the phenotype of the generated VSTs. Most of the generated CD8+ tetramer+ cells exhibited either a central memory (CM) ($CD62L^+CD45RA^-$) or effector memory ($CD62L^-CD45RA^-$) phenotype (Fig. 3A). The proportion of cells with a CM phenotype, which persist longer and are more effective in vivo after adoptive transfer,[25] among the CD8+ tetramer+ cells did not differ with the type of

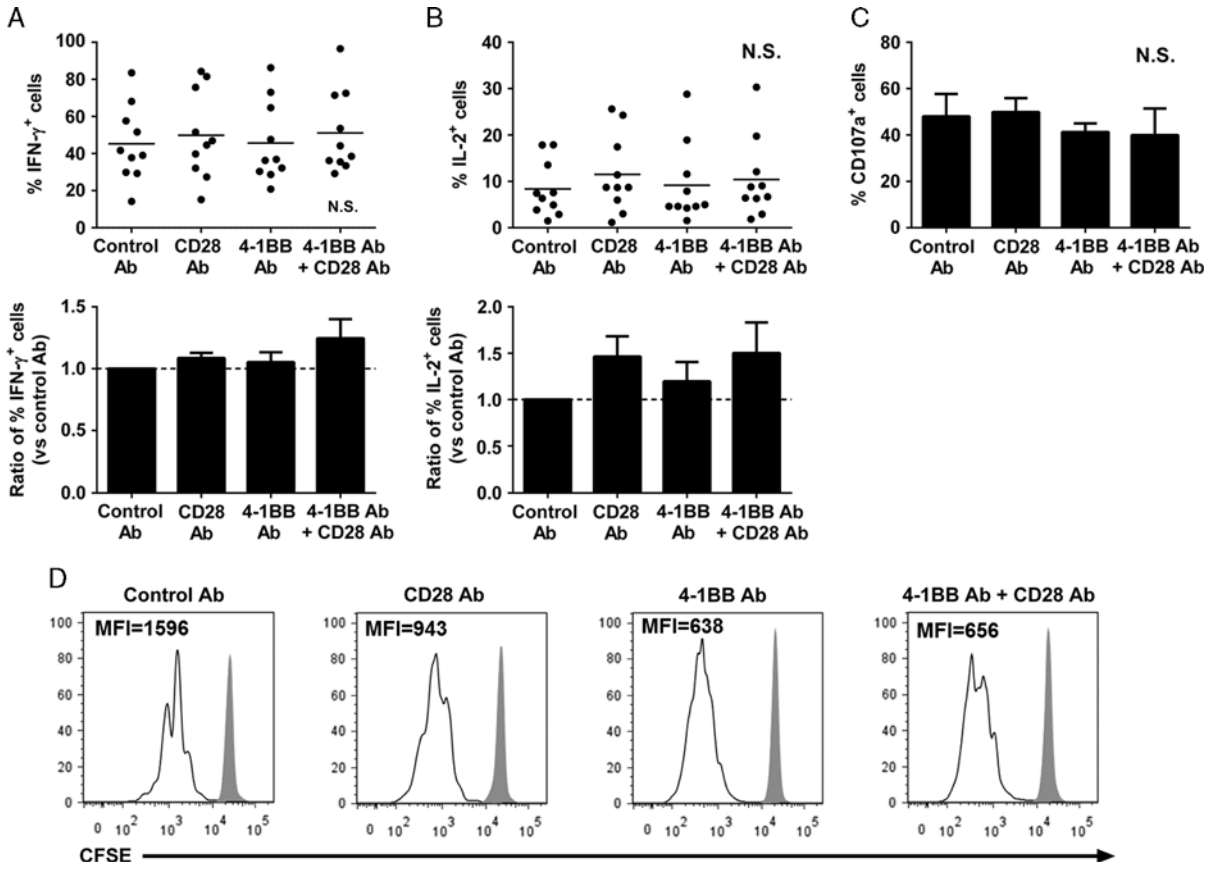

FIGURE 4. Function of virus-specific CD8+ T cells generated with control, anti-CD28, anti-4-1BB, or a combination of anti-CD28 and anti-4-1BB antibodies. A–C, Virus-specific CD8+ T cells generated with control, anti-CD28, anti-4-1BB, or a combination of anti-CD28 and anti-4-1BB antibodies were restimulated with APCs loaded with or without the corresponding peptides. After incubation, the cells were collected and analyzed for cytokine production and CD107a degranulation, as described in the Materials and methods section. Frequencies of interferon (IFN)-γ+ (A), interleukin (IL)-2+ (B), and CD107a+ (C) cells among CD8+ tetramer+ cells are shown. A and B show data pooled from at least 10 independent experiments with 10 different virus-specific CD8+ T-cell responses. Actual values (upper panel) and the ratio of actual values for the indicated culture conditions to those for control (lower panel) are shown for each measure. Horizontal lines in the upper panels mark the mean values. Means and SEMs are shown in the lower panels [NS, not significant, repeated measures 1-way analysis of variance (ANOVA)]. C, Representative data from 6 independent experiments with 3 different virus-specific CD8+ T-cell responses. Mean ± SD of triplicate wells are shown (NS, not significant, ordinary 1-way ANOVA). D, Generated virus-specific CD8+ T cells were labeled with carboxyfluorescein succinimidyl ester (CFSE), restimulated with irradiated autologous peripheral blood mononuclear cells loaded with the corresponding peptides, and analyzed for CFSE dilution using flow cytometry 120 hours after restimulation. Representative flow plots gated on CD8+ tetramer+ cells are shown. The numbers in the histograms indicate the CFSE mean fluorescence intensities (MFIs) of CD8+ tetramer+ cells. Gray shaded histograms indicate CD8+ tetramer+ cells cultured with medium alone. Data are representative of 6 independent experiments with 6 different virus-specific CD8+ T-cell responses.

antibody used. The mean percentage of cells with a CM phenotype was approximately 35% irrespective of the antibody used (Fig. 3B). Similarly, the proportion of CD28+ and CD27+ cells, which are also associated with superior in vivo efficacy after adoptive transfer,[26,27] among the CD8+ tetramer+ cells did not differ with the type of antibody used. The mean percentage of CD28+ and CD27+ cells was approximately 80% and 60%, respectively, irrespective of the antibody used (Figs. 3C, D).

Effect of Anti-CD28 and Anti-4-1BB Antibodies on the Generated Virus-specific CD8+ T-cell Function

To compare the effector functions of the generated virus-specific CD8+ T cells, cytokine production and cytotoxic activity[28] in response to the viral peptide-pulsed target cells were assessed. Virus-specific CD8+ T cells that were generated in the presence of control, anti-CD28, anti-4-1BB, or a combination of anti-CD28 and anti-4-1BB antibodies showed similar levels of IFN-γ production, IL-2 production, and CD107a expression in response to the peptide stimulation (Figs. 4A–C). In addition, the proliferative capacity of the generated virus-specific CD8+ T cells in response to the viral peptide-pulsed target cells was assessed. Of note, proliferation of the anti-4-1BB Ab-treated cells was greater than that of the control antibody treated cells, as indicated by the lower mean fluorescence intensity value in CFSE proliferation assays (Fig. 4D). The combined results indicate that anti-4-1BB antibody promotes the expansion of VSTs without causing excessive differentiation or functional deterioration of the generated T cells.

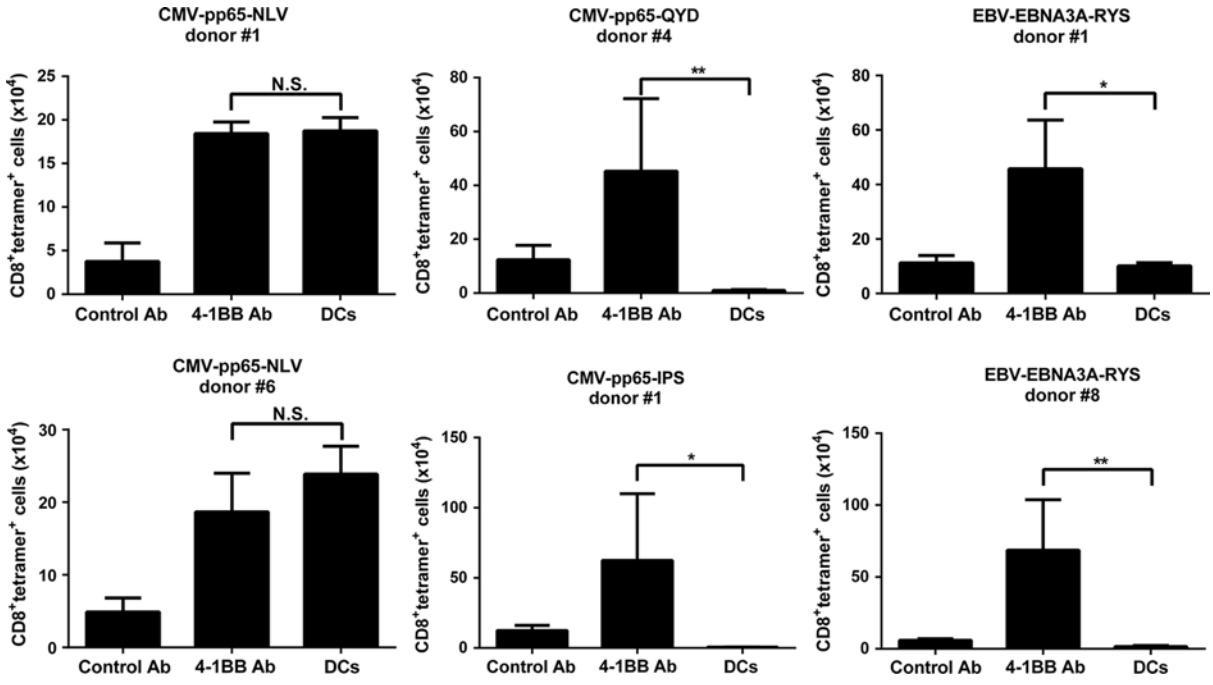

FIGURE 5. Absolute numbers of virus-specific CD8$^+$ T cells generated with control antibody, anti-4-1BB antibody, or autologous dendritic cells (DCs). CD8$^+$ T cells specific for CMV-pp65-QYD (n = 3), CMV-pp65-NLV (n = 2), CMV-pp65-IPS (n = 1), or EBV-EBNA3A-RYS (n = 2) epitopes were generated either with control antibody, anti-4-1BB antibody, or irradiated autologous DCs. After 13 days of culture, absolute numbers of CD8$^+$ tetramer$^+$ cells were determined. The means ± SD of at least triplicate wells are shown (*P < 0.05, **P < 0.01, NS, not significant, ordinary 1-way analysis of variance followed by the Tukey multiple comparison tests. Differences are shown only between anti-4-1BB antibody and DCs). Data are representative of at least 8 independent experiments with 8 different virus-specific CD8$^+$ T-cell responses.

Comparison of Anti-4-1BB Antibody and DCs for Virus-specific CD8$^+$ T-cell Generation

DCs are the most powerful APCs[29] and are widely used for the generation of antigen-specific T cells for adoptive immunotherapy.[9,11] To compare anti-4-1BB antibody and DCs in terms of their capacity to generate virus-specific CD8$^+$ T cells, CD8$^+$ T cells specific for CMV-pp65-QYD (n = 3), CMV-pp65-NLV (n = 2), CMV-pp65-IPS (n = 1), or EBV-EBNA3A-RYS (n = 2) epitopes were generated either with control antibody, anti-4-1BB antibody, or irradiated autologous DCs. The generated DCs consistently exhibited a mature phenotype (data not shown). Of note, the capacity of the DCs to generate VSTs differed considerably depending on the epitopes of the VSTs. The number of CMV-pp65-NLV-specific CD8$^+$ T cells generated with anti-4-1BB antibody was similar to that generated with DCs. In contrast, the number of CMV-pp65-QYD-specific, CMV-pp65-IPS-specific, or EBV-EBNA3A-RYS-specific CD8$^+$ T cells that was generated with anti-4-1BB antibody was significantly higher than that generated with DCs (Fig. 5). The phenotypes and functions of CD8$^+$ tetramer$^+$ cells generated with anti-4-1BB antibody were similar or superior to those generated with DCs (data not shown). These results indicate that anti-4-1BB antibody generated comparable or higher numbers of VSTs compared with DCs without causing excessive differentiation or functional deterioration of the generated T cells.

DISCUSSION

We demonstrated that VSTs can be generated rapidly and efficiently by simply stimulating PBMCs with peptide and anti-4-1BB antibody without using APCs. As there are 2 clinical grade anti-4-1BB antibodies (BMS-663513 and PF-05082566),[15,30] this method can be readily tested in clinical trials. We propose using anti-4-1BB antibody as a novel strategy to generate VSTs for adoptive therapy.

It has been reported that DCs (cytokine-activated monocytes) have only a limited capacity for generation of cytotoxic T-cell responses to subdominant epitopes.[10,31] In line with these studies, in the present study the number of VSTs generated with DCs was similar to the number generated with anti-4-1BB antibody for CMV-pp65-NLV-specific CD8$^+$ T cells, whose epitope is generally regarded as an immunodominant epitope,[10] but the number of DC-generated VSTs specific for other epitopes was lower (Fig. 5). These results suggest that DCs may be suboptimal for the generation of VSTs that are specific for subdominant epitopes. In contrast, anti-4-1BB antibody promoted the generation of VSTs irrespective of the epitope of the VST (Fig. 2D). Therefore, anti-4-1BB antibody may be used to promote the generation of VSTs for both dominant and subdominant epitopes.

Previous studies that compared the functions of purified T cells that received TCR stimulation alone and those that received TCR and 4-1BB stimulation showed that 4-1BB stimulation improved the effector function of T cells.[5,32,33] In contrast, we did not find significant differences between the effector function of VSTs generated with anti-4-1BB antibody and those generated with control antibody. As PBMCs contain B cells and monocytes, which have the capacity to function as APCs, these cells might have provided some costimulatory signals to VSTs, resulting in similar effector functions to the control cells.

Although VSTs generated with the anti-4-1BB antibody showed similar phenotypes and effector functions to those generated with control antibody, the former had improved proliferative capacity (Fig. 4D). Thus, the results of the current study suggest that anti-4-1BB antibody, at the least, does not lead to deterioration of the function of the generated VSTs.

In the current study, anti-4-1BB antibody was more potent than anti-CD28 antibody in expanding VSTs, which was in accordance with the results of previous studies that evaluated the effect of costimulatory signals on T-cell expansion using artificial APCs expressing costimulatory molecules.[7,32] This result could be explained by the fact that CD28 costimulation preferentially expands naive T cells, whereas 4-1BB costimulation preferentially expands memory T cells.[32] In addition, the combination of anti-4-1BB and anti-CD28 antibodies did not show additive or synergistic effects compared with anti-4-1BB antibody alone. A previous study reported that additive effects of 4-1BB and CD28 dual costimulation on T-cell expansion were observed only when IFN-γ in the culture medium was neutralized.[6] Therefore, an antibody cocktail consisting of anti-4-1BB, anti-CD28, and IFN-γ neutralizing antibodies may further enhance the expansion of VSTs. Alternatively, a combination of anti-4-1BB and anti-OX40 antibodies may further promote the generation of VSTs.[7] The optimal combination of antibodies for the generation of VSTs remains to be determined.

Overlapping peptide pools that span the complete sequence of viral proteins are becoming more widely used to generate VSTs because VSTs specific for both known and unknown epitopes can be generated.[11,34] Another advantage of overlapping peptide pools is that both $CD4^+$ and $CD8^+$ VSTs can be generated,[11] which may promote the survival and persistence of the generated T cells after adoptive transfer.[35] As in the current study we stimulated PBMCs with viral-specific $CD8^+$ T-cell epitope peptides, the effect of anti-4-1BB antibody on the generation of viral-specific $CD4^+$ T cells was not examined. In this regard, some studies have shown that 4-1BB stimulation activates $CD4^+$ T cells and $CD8^+$ T cells to a similar extent,[22,36] whereas others have suggested that 4-1BB stimulation preferentially activates $CD8^+$ T cells over $CD4^+$ T cells.[33,37] Whether anti-4-1BB antibody can improve the generation of not only $CD8^+$ VSTs but also of $CD4^+$ VSTs from PBMCs stimulated with overlapping peptide pools needs to be investigated in future studies.

In conclusion, we have clearly demonstrated that VSTs can be generated rapidly and efficiently by simply stimulating PBMCs with viral peptide and anti-4-1BB antibody without using APCs. We propose using anti-4-1BB antibody as a novel strategy to generate VSTs for adoptive therapy.

CONFLICTS OF INTEREST/ FINANCIAL DISCLOSURES

This work was supported by the Japan Society for the Promotion of Science (JSPS) (25-3298 to N.I.), the Hori Sciences and Arts Foundation (N.I.), and JSPS KAKENHI (Grant-in-Aid for Scientific Research (C) 25461446 to T.N.). H.K.: Research funding from Bristol-Myers Squibb, Chugai Pharmaceutical Co. Ltd, Kyowa Hakko Kirin Co. Ltd, Dainippon Sumitomo Pharma, Zenyaku Kogyo, and FUJIFILM Corporation. T.N.: Research funding was from Bristol-Myers Squibb, Chugai Pharmaceutical Co. Ltd, Kyowa Hakko Kirin Co. Ltd, Dainippon Sumitomo Pharma, Zenyaku Kogyo, FUJIFILM Corporation, Nippon Boehringer-Ingelheim Co. Ltd, Otsuka Pharmaceutical Co. Ltd, and Toyama Chemical Co. Ltd.

The remaining authors have declared there are no financial conflicts of interest with regard to this work.

REFERENCES

1. Anderson EJ. Viral diagnostics and antiviral therapy in hematopoietic stem cell transplantation. *Curr Pharm Des*. 2008;14:1997–2010.
2. Tormo N, Solano C, Benet I, et al. Lack of prompt expansion of cytomegalovirus pp65 and IE-1-specific IFNgamma CD8 + and CD4 + T cells is associated with rising levels of pp65 antigenemia and DNAemia during pre-emptive therapy in allogeneic hematopoietic stem cell transplant recipients. *Bone Marrow Transplant*. 2010;45:543–549.
3. Leen AM, Bollard CM, Mendizabal AM, et al. Multicenter study of banked third-party virus-specific T cells to treat severe viral infections after hematopoietic stem cell transplantation. *Blood*. 2013;121:5113–5123.
4. Barker JN, Doubrovina E, Sauter C, et al. Successful treatment of EBV-associated posttransplantation lymphoma after cord blood transplantation using third-party EBV-specific cytotoxic T lymphocytes. *Blood*. 2010;116:5045–5049.
5. Bukczynski J, Wen T, Ellefsen K, et al. Costimulatory ligand 4-1BBL (CD137L) as an efficient adjuvant for human antiviral cytotoxic T cell responses. *Proc Natl Acad Sci USA*. 2004; 101:1291–1296.
6. Bukczynski J, Wen T, Wang C, et al. Enhancement of HIV-specific CD8 T cell responses by dual costimulation with CD80 and CD137L. *J Immunol*. 2005;175:6378–6389.
7. Serghides L, Bukczynski J, Wen T, et al. Evaluation of OX40 ligand as a costimulator of human antiviral memory CD8 T cell responses: comparison with B7.1 and 4-1BBL. *J Immunol*. 2005;175:6368–6377.
8. Gerdemann U, Christin AS, Vera JF, et al. Nucleofection of DCs to generate Multivirus-specific T cells for prevention or treatment of viral infections in the immunocompromised host. *Mol Ther*. 2009;17:1616–1625.
9. Micklethwaite KP, Savoldo B, Hanley PJ, et al. Derivation of human T lymphocytes from cord blood and peripheral blood with antiviral and antileukemic specificity from a single culture as protection against infection and relapse after stem cell transplantation. *Blood*. 2010;115:2695–2703.
10. Hasan AN, Kollen WJ, Trivedi D, et al. A panel of artificial APCs expressing prevalent HLA alleles permits generation of cytotoxic T cells specific for both dominant and subdominant viral epitopes for adoptive therapy. *J Immunol*. 2009;183:2837–2850.
11. Gerdemann U, Keirnan JM, Katari UL, et al. Rapidly generated multivirus-specific cytotoxic T lymphocytes for the prophylaxis and treatment of viral infections. *Mol Ther*. 2012;20:1622–1632.
12. Fleischer J, Soeth E, Reiling N, et al. Differential expression and function of CD80 (B7-1) and CD86 (B7-2) on human peripheral blood monocytes. *Immunology*. 1996;89:592–598.
13. Kinnear G, Jones ND, Wood KJ. Costimulation blockade: current perspectives and implications for therapy. *Transplantation*. 2013;95:527–535.
14. Melero I, Hervas-Stubbs S, Glennie M, et al. Immunostimulatory monoclonal antibodies for cancer therapy. *Nat Rev Cancer*. 2007;7:95–106.
15. Li SY, Liu Y. Immunotherapy of melanoma with the immune costimulatory monoclonal antibodies targeting CD137. *Clin Pharmacol*. 2013;5:47–53.
16. Leen AM, Sili U, Vanin EF, et al. Conserved CTL epitopes on the adenovirus hexon protein expand subgroup cross-reactive and subgroup-specific CD8 + T cells. *Blood*. 2004;104:2432–2440.
17. Terakura S, Yamamoto TN, Gardner RA, et al. Generation of CD19-chimeric antigen receptor modified CD8 + T cells

derived from virus-specific central memory T cells. *Blood*. 2012;119:72–82.
18. Bohnenkamp HR, Noll T. Development of a standardized protocol for reproducible generation of matured monocyte-derived dendritic cells suitable for clinical application. *Cytotechnology*. 2003;42:121–131.
19. Lim JB, Provenzano M, Kwon OH, et al. Identification of HLA-A33-restricted CMV pp65 epitopes as common targets for CD8(+) CMV-specific cytotoxic T lymphocytes. *Exp Hematol*. 2006;34:296–307.
20. Imahashi N, Nishida T, Ito Y, et al. Identification of a novel HLA-A*24:02-restricted adenovirus serotype 11-specific CD8 + T-cell epitope for adoptive immunotherapy. *Mol Immunol*. 2013;56:399–405.
21. Wolfl M, Kuball J, Ho WY, et al. Activation-induced expression of CD137 permits detection, isolation, and expansion of the full repertoire of CD8 + T cells responding to antigen without requiring knowledge of epitope specificities. *Blood*. 2007;110:201–210.
22. Wen T, Bukczynski J, Watts TH. 4-1BB ligand-mediated costimulation of human T cells induces CD4 and CD8 T cell expansion, cytokine production, and the development of cytolytic effector function. *J Immunol*. 2002;168:4897–4906.
23. Tran KQ, Zhou J, Durflinger KH, et al. Minimally cultured tumor-infiltrating lymphocytes display optimal characteristics for adoptive cell therapy. *J Immunother*. 2008;31:742–751.
24. Itzhaki O, Hovav E, Ziporen Y, et al. Establishment and large-scale expansion of minimally cultured "young" tumor infiltrating lymphocytes for adoptive transfer therapy. *J Immunother*. 2011;34:212–220.
25. Berger C, Jensen MC, Lansdorp PM, et al. Adoptive transfer of effector CD8 + T cells derived from central memory cells establishes persistent T cell memory in primates. *J Clin Invest*. 2008;118:294–305.
26. Zhou J, Shen X, Huang J, et al. Telomere length of transferred lymphocytes correlates with in vivo persistence and tumor regression in melanoma patients receiving cell transfer therapy. *J Immunol*. 2005;175:7046–7052.
27. Huang J, Kerstann KW, Ahmadzadeh M, et al. Modulation by IL-2 of CD70 and CD27 expression on CD8 + T cells: importance for the therapeutic effectiveness of cell transfer immunotherapy. *J Immunol*. 2006;176:7726–7735.
28. Rubio V, Stuge TB, Singh N, et al. Ex vivo identification, isolation and analysis of tumor-cytolytic T cells. *Nat Med*. 2003;9:1377–1382.
29. Banchereau J, Steinman RM. Dendritic cells and the control of immunity. *Nature*. 1998;392:245–252.
30. Fisher TS, Kamperschroer C, Oliphant T, et al. Targeting of 4-1BB by monoclonal antibody PF-05082566 enhances T-cell function and promotes anti-tumor activity. *Cancer Immunol Immunother*. 2012;61:1721–1733.
31. Trivedi D, Williams RY, O'Reilly RJ, et al. Generation of CMV-specific T lymphocytes using protein-spanning pools of pp65-derived overlapping pentadecapeptides for adoptive immunotherapy. *Blood*. 2005;105:2793–2801.
32. Zhang H, Snyder KM, Suhoski MM, et al. 4-1BB is superior to CD28 costimulation for generating CD8 + cytotoxic lymphocytes for adoptive immunotherapy. *J Immunol*. 2007;179:4910–4918.
33. Chacon JA, Wu RC, Sukhumalchandra P, et al. Co-stimulation through 4-1BB/CD137 improves the expansion and function of CD8(+) melanoma tumor-infiltrating lymphocytes for adoptive T-cell therapy. *PLoS One*. 2013;8:e60031.
34. Lugthart G, Albon SJ, Ricciardelli I, et al. Simultaneous generation of multivirus-specific and regulatory T cells for adoptive immunotherapy. *J Immunother*. 2012;35:42–53.
35. Walter EA, Greenberg PD, Gilbert MJ, et al. Reconstitution of cellular immunity against cytomegalovirus in recipients of allogeneic bone marrow by transfer of T-cell clones from the donor. *N Engl J Med*. 1995;333:1038–1044.
36. Cannons JL, Lau P, Ghumman B, et al. 4-1BB ligand induces cell division, sustains survival, and enhances effector function of CD4 and CD8 T cells with similar efficacy. *J Immunol*. 2001;167:1313–1324.
37. Shuford WW, Klussman K, Tritchler DD, et al. 4-1BB costimulatory signals preferentially induce CD8 + T cell proliferation and lead to the amplification in vivo of cytotoxic T cell responses. *J Exp Med*. 1997;186:47–55.

Published December 17, 2014, doi:10.4049/jimmunol.1402346

Target Antigen Density Governs the Efficacy of Anti–CD20-CD28-CD3 ζ Chimeric Antigen Receptor–Modified Effector CD8$^+$ T Cells

Keisuke Watanabe,*[,1] Seitaro Terakura,*[,1] Anton C. Martens,[†,‡] Tom van Meerten,[§] Susumu Uchiyama,[¶] Misa Imai,[‖] Reona Sakemura,* Tatsunori Goto,* Ryo Hanajiri,* Nobuhiko Imahashi,* Kazuyuki Shimada,*[,#] Akihiro Tomita,* Hitoshi Kiyoi,* Tetsuya Nishida,* Tomoki Naoe,*[,] and Makoto Murata***

The effectiveness of chimeric Ag receptor (CAR)–transduced T (CAR-T) cells has been attributed to supraphysiological signaling through CARs. Second- and later-generation CARs simultaneously transmit costimulatory signals with CD3ζ signals upon ligation, but may lead to severe adverse effects owing to the recognition of minimal Ag expression outside the target tumor. Currently, the threshold target Ag density for CAR-T cell lysis and further activation, including cytokine production, has not yet been investigated in detail. Therefore, we determined the threshold target Ag density required to induce CAR-T cell responses using novel anti-CD20 CAR-T cells with a CD28 intracellular domain and a CD20-transduced CEM cell model. The newly developed CD20CAR–T cells demonstrated Ag-specific lysis and cytokine secretion, which was a reasonable level as a second-generation CAR. For lytic activity, the threshold Ag density was determined to be ∼200 molecules per target cell, whereas the Ag density required for cytokine production of CAR-T cells was ∼10-fold higher, at a few thousand per target cell. CD20CAR–T cells responded efficiently to CD20-downregulated lymphoma and leukemia targets, including rituximab- or ofatumumab-refractory primary chronic lymphocytic leukemia cells. Despite the potential influence of the structure, localization, and binding affinity of the CAR/Ag, the threshold determined may be used for target Ag selection. An Ag density below the threshold may not result in adverse effects, whereas that above the threshold may be sufficient for practical effectiveness. CD20CAR–T cells also demonstrated significant lytic activity against CD20-downregulated tumor cells and may exhibit effectiveness for CD20-positive lymphoid malignancies. ***The Journal of Immunology*****, 2015, 194: 000–000.**

Chimeric Ag receptor (CAR)–transduced T (CAR-T) cell therapy is an emerging therapeutic strategy for refractory acute lymphoblastic leukemia (ALL) and chronic lymphocytic leukemia (CLL) (1, 2). Second- and later-generation CARs generally consist of a single-chain variable fragment (scFv) from a mAb fused to the signaling domain of CD3ζ, and contain one or two costimulatory endodomains, respectively (3–5). This technology has two main potential benefits over TCR gene insertion. One is that Ag recognition by CAR is independent of HLA, meaning that CAR therapy can be used to treat all Ag-positive patients regardless of their HLA. The other is that once CARs ligate to target molecules, full activation signals, including costimuli such as CD28 or 4-1BB, are transmitted to CAR-T cells (3–5). A superior effector function and proliferation following activation have been reported in second- and third-generation CAR-T cells (6–9).

In contrast, CAR-T cells may induce adverse effects by recognizing low expression levels of the target Ag in an off-target organ. This activity has been referred to as the "on-target/off-tumor effect." A serious adverse event induced by CAR-T cells, which recognize very low expression levels of ERBB2 on lung epithelial cells, was reported with CAR therapy targeting ERBB2 based on trastuzumab (Herceptin) (10). Although ERBB2 is expressed at low levels in various normal tissues, including lung, the anti-ERBB2 humanized mAb trastuzumab has been used safely in clinical settings (11), indicating that ERBB2 expression levels on lung cells are negligible in terms of trastuzumab therapy (12). However, ERBB2–CAR-T cells induce significant Ag-specific responses against this low expression of ERBB2 (10, 11). Therefore, selection of a target Ag is critical for both efficacy and avoiding adverse effects. TCRs recognize very low numbers of peptide/HLA complexes, whereas a relatively high number of target molecules are required for mAbs to induce cytotoxic activity (13, 14). However, the range of Ag density in which CAR-T

*Department of Hematology and Oncology, Nagoya University Graduate School of Medicine, Nagoya 466-8560, Japan; [†]Department of Hematology, VU University Medical Center Amsterdam, 1007 MB Amsterdam, the Netherlands; [‡]Department of Immunology, University Medical Center Utrecht, 3508 GA Utrecht, the Netherlands; [§]Department of Hematology, University Medical Center Groningen, 9700 RB Groningen, the Netherlands; [¶]Division of Advanced Science and Biotechnology, Graduate School of Engineering, Osaka University, Osaka 565-0871, Japan; [‖]Faculty of Pharmacy, Meijo University, Nagoya 468-8503, Japan; [#]Institute for Advanced Research, Nagoya University, Nagoya 464-8601, Japan; and **National Hospital Organization Nagoya Medical Center, Nagoya 460-0001, Japan

[1]K.W. and S.T. contributed equally to this work.

Received for publication September 12, 2014. Accepted for publication November 21, 2014.

This work was supported by grants from the Foundation for Promotion of Cancer Research (Tokyo, Japan; to S.T.), the Japan Society for the Promotion of Science KAKENHI (24790969 to S.T.), the Program to Disseminate Tenure Tracking System (MEXT, Japan; to K.S.), a Grant-in-Aid for Challenging Exploratory Research (23659487 to T. Naoe), and a Health Labor Science Research Grant (H25-Immunology-104 to M.M.).

The online version of this article contains supplemental material.

Address correspondence and reprint requests to Dr. Seitaro Terakura, Department of Hematology and Oncology, Nagoya University Graduate School of Medicine, 65 Tsurumai, Showa-ku, Nagoya, Aichi 466-8560, Japan. E-mail address: tseit@med.nagoya-u.ac.jp

Abbreviations used in this article: ABC, Ab-binding capacity; ADCC, Ab-dependent cellular cytotoxicity; ALL, acute lymphoblastic leukemia; CAR, chimeric Ag receptor; CAR-T, CAR-transduced T (cell); CDC, complement-dependent cytotoxicity; CLL, chronic lymphocytic leukemia; DLBCL, diffuse large B cell lymphoma; FCM, flow cytometry; LCL, EBV-transformed lymphoblastoid cell line; MFI, mean fluorescence intensity; ofa, ofatumumab; sABC, specific Ab binding capacity; scFv, single-chain variable fragment; tEGFR, truncated version of the epidermal growth factor receptor.

cells can recognize and induce cytotoxicity has not been investigated in detail. Furthermore, research has not yet clarified the number of Ag molecules expressed that could be candidates for targets when expressed at low levels or that should be avoided owing to the on-target/off-tumor effect (15).

CD20 is an activated glycosylated phosphoprotein that is expressed on the surface of B lymphocytes. An anti-CD20 mAb is an effective therapeutic option for various B cell malignancies such as ALL (16), CLL (17), and malignant lymphoma (18, 19). Although combination chemotherapies with rituximab have achieved favorable results in CD20-positive B cell lymphoma patients, acquired resistance to rituximab has become a problem, with a suggested mechanism of reduced expression of CD20 (20–24). Accordingly, a therapeutic option that efficiently eradicates target cells expressing low levels of CD20 that survive rituximab or ofatumumab (ofa) therapy needs to be developed. Therefore, we developed a novel CD20-CAR and investigated the minimum threshold Ag expression level required for lysis of target cells and activation of CAR-T cells. To avoid possible immunological rejection against anti-mouse Abs, we used a humanized anti-CD20 mAb to construct CD20CAR (25). We also assessed its effects against tumor cell lines and primary cells isolated from mAb therapy-refractory, CD20-downregulated B cell tumors (24, 26, 27).

Materials and Methods

Cell lines

K562, CCRF-CEM, SU-DHL-4, SU-DHL-6, SU-DHL-10, Raji, RRBL1, and WILL2 cells were cultured in RPMI 1640 medium. OCI-Ly3 and OCI-Ly10 cells were kind gifts from Dr. K. Takeyama (Dana-Farber Cancer Institute, Boston, MA) and were cultured in IMDM (Sigma-Aldrich, St. Louis, MO). Each type of medium contained 10% FBS, 0.8 mM L-glutamine, and 1% penicillin-streptomycin. RRBL1 and WILL2 cells are cell lines established from a B cell lymphoma patient who exhibited CD20-negative phenotypic changes after repeated chemotherapy with rituximab (26, 27). CD20-transduced CCRF-CEM cell lines (CD20-CEMs) expressing various levels of CD20 were described elsewhere (28). CD20-transduced K562 (CD20-K562) cells were generated by retroviral transduction with the full-length CD20 molecule, as described (29).

Primary B cell tumor cells

Primary B cell tumor cells were obtained from PBMCs (CLL patient) or pleural effusion (lymphoma patient) according to protocols approved by the Institutional Review Board of Nagoya University School of Medicine, and written informed consent was obtained from each patient in accordance with the Declaration of Helsinki.

Quantification of CD20 molecules

CD20 molecules expressed on the surface of CD20-CEMs or other cell lines were quantified using quantitative immunofluorescence indirect assay (QIFIKIT; Dako, Glostrup, Denmark). Briefly, cells were stained with unlabeled anti-CD20 mouse mAb (BD Bioscience, San Jose, CA) or purified mouse IgG-κ (BioLegend, San Diego, CA) as an isotype control. The cells of interest and calibration beads from the kit were then simultaneously labeled with primary mAb, followed by FITC-conjugated goat anti-mouse secondary Ab staining. Labeled cells and calibration beads were analyzed on a flow cytometer, and a standard regression line between fluorescence intensity and Ag density that was expressed as Ab-binding capacity (ABC) in molecules per cell was calculated. Finally, the specific ABC (sABC) was determined by subtracting the background Ab equivalent of the isotype control from ABC (30).

Retroviral vector construction

CD20-binding scFv was constructed based on the reported sequences of the humanized anti-CD20 mAb (OUBM mAb) (25). OUBM mAb exhibits high CD20 binding affinity (K_D, 10.09 nM). H chain and L chain V region segments were linked with an 18-aa linker. scFv was then fused to a human IgG_4 hinge, a CD3-ζ chain, a CD28 costimulatory domain, and a truncated version of the epidermal growth factor receptor (tEGFR) that lacked epidermal growth factor binding and intracellular signaling domains downstream of the self-cleaving T2A sequence (31–33). By inserting the T2A sequence between CD20CAR and tEGFR, the two proteins were coexpressed at equimolar levels from a single transcript. Cell-surface tEGFR was detected using the biotinylated anti-EGFR mAb Erbitux (Bristol-Myers Squibb, New York, NY). The CD20CAR transgene was assembled by overlap extension PCR (34). CD20CAR was inserted into LZRS-pBMN-Z, using HindIII and NotI sites, and the CD20CAR-encoding retrovirus was produced using the Phoenix-Ampho system (Orbigen, San Diego, CA) and concentrated with Retro-X Concentrator (Clontech Laboratories, Mountain View, CA).

Generation, expansion, and selection of CD20CAR-transduced T cells

The PBMCs of a normal donor were isolated by centrifugation of whole blood using Ficoll-Paque (GE Healthcare, Wauwatosa, WI). $CD8^+$ lymphocytes were then purified with immunomagnetic beads (Miltenyi Biotec, Bergisch Gladbach, Germany), activated with anti-CD3/CD28 beads (Invitrogen, Carlsbad, CA), and transduced on day 3 after activation with the recombinant human fibronectin fragment (RetroNectin, Takara Bio, Otsu, Japan) by centrifugation at 2100 rpm for 45 min at 32°C with the retroviral supernatant (multiplicity of infection = 3). T cells were expanded in RPMI 1640 medium containing 10% human serum, 0.8 mM L-glutamine, 1% penicillin-streptomycin, and 0.5 μM 2-ME and supplemented with recombinant human IL-2 to a final concentration of 50 IU/ml. CAR-positive cells were enriched using immunomagnetic selection with biotin-conjugated anti-EGFR mAb and streptavidin beads (Miltenyi Biotec). The transduced T cells were expanded in culture by plating with γ-irradiated EBV-transformed lymphoblastoid cell line (LCL) at a T cell to LCL ratio of 1:7 and supplemented with IL-2 to 50 IU/ml (29).

Flow cytometry

All samples were analyzed with flow cytometry (FCM) on the FACSAria instrument (BD Biosciences), and data were analyzed using FlowJo software (Tree Star, Ashland, OR). Biotinylated Erbitux and streptavidin-PE were used to identify T cells that expressed tEGFR.

[^{51}Cr] release assay and coculture assay

For the [^{51}Cr] release assay, target cells were labeled for 2 h with [^{51}Cr] (PerkinElmer, Waltham, MA), washed twice, dispensed at 2×10^3 cells per well into triplicate cultures in 96-well round-bottom plates, and incubated for 4 h at 37°C with CD20CAR–T cells at various E:T ratios. Percent of specific lysis was calculated using a standard formula [(experimental − spontaneous release)/(maximum load − spontaneous release) × 100 (%)] and expressed as the mean of triplicate samples. Regarding the coculture assay, CEMs were labeled with 0.1 μM CFSE (Invitrogen), washed, and plated with CD20 CAR-T cells at a ratio of 1:1 without IL-2 supplementation. After a 72-h incubation, cells were stained with anti-CD8 mAb and analyzed with FCM. The percentages of CAR-T cells and CEMs within the live cell gates were assessed.

Intracellular cytokine staining and cytokine secretion assay

CD20CAR–T cells and K562 or CCRF-CEM cells that expressed CD20 were mixed at a 1:1 ratio in the presence of brefeldin A (Sigma-Aldrich) and then fixed and permeabilized with Cell Fixation/Permeabilization Kits (BD Biosciences) for intracellular cytokine assay. After fixation, T cells were stained with anti–IFN-γ and anti–CD8-allophycocyanin mAb (BD Biosciences). As a positive control for cytokine production, cells were stimulated with 10 ng/ml PMA and 1 μg/ml ionomycin (Sigma-Aldrich). CD20CAR–T cells and CEMs for the cytokine secretion assay were plated at an E:T ratio of 1:1, and IFN-γ, TNF-α, and IL-2 in the supernatant were measured with ELISA (BD Biosciences) after 16 h of incubation.

CFSE proliferation assay

CD20CAR–T cells were labeled with 0.2 μM CFSE, washed, and then plated with stimulator cells at a ratio of 1:1 without IL-2 supplementation. After a 72- or 96-h incubation, cells were stained with the anti-CD8 mAb, samples were analyzed with FCM, and the division of live $CD8^+$ T cells was assessed with CFSE dye dilution.

Intracellular phospho-flow analysis

CD20CAR–T cells and CD20-CEM cells expressing various levels of CD20 were mixed at a 1:5 ratio, centrifuged briefly, and incubated for various times at 37°C. Cells were then fixed by the addition of BD Cytofix Fixation Buffer at 37°C for 10 min, permeabilized in ice-cold BD Phosflow Perm Buffer III, and incubated on ice for 30 min (BD Biosciences). P-p44/42 MAPK (T202/Y204) or P-Zap-70 (Y319)/SyK(Y532) Rabbit Ab (Cell

Signaling Technology, Danvers, MA) and bovine anti-rabbit IgG-FITC as a secondary Ab (Santa Cruz Biotechnology, Dallas, TX) were used for phospho-specific staining.

Statistical analysis

Differences among results were evaluated with one-way or two-way ANOVA analysis and the Bonferroni test, as appropriate. Differences were considered significant when $p < 0.05$. Statistical analysis was performed using GraphPad Prism Version 5 software.

Results

Generation and functional analysis of CD20CAR-transduced T cells

To develop functional CD20CAR, we constructed CD20CAR consisting of anti–CD20-scFv linked to CD3ζ, a CD28 costimulatory domain, and a tEGFR; $CD8^+$ T cells were then retrovirally transduced with CD20CAR (Fig. 1A). After one course of stimulation and transduction, the expression of CD20CAR generally reached 40–80%. To determine transduction efficiency, CD20CAR and tEGFR were labeled with an anti-Fc Ab and biotinylated Erbitux, respectively. The expression of tEGFR reflected that of CAR on the transduced T cells, and we verified that the expression of CAR and tEGFR was similar after each transduction experiment (Fig. 1B) (32). Transduction efficiency could be monitored with tEGFR with high reproducibility (Fig. 1B, *right panel*). Using intracellular staining, we assessed the ability of CAR-T cells to produce IFN-γ in response to CD20. Stimulation with CD20-K562 cells induced robust production of IFN-γ, whereas mock-transduced K562 cells did not (Fig. 1C). These results demonstrated that CD20CAR–T cells recognized CD20 in an Ag-specific manner. After the transduction culture, CD20CAR-positive cells were enriched to a purity of >95% with biotinylated Erbitux and anti-biotin immunomagnetic beads (32), expanded by stimulating with a γ-irradiated LCL, and then used for subsequent experiments. The expression of CAR/tEGFR before and after LCL stimulation was sufficiently maintained (Fig. 1D). The ability of CD20CAR–T cells to lyse $CD20^+$ target cells was assessed after one course of transduction and expansion. CD20CAR–T cells specifically lysed CD20-K562 cells (Fig. 1E) in a highly reproducible manner (Fig. 1E, *right panel*). To examine background cytotoxicity, CD19CAR (non–target-specific CAR)–transduced T cells were examined for cytotoxicity against K562 or CD20-K562. Both experiments demonstrated almost the same range of cytotoxicity by the CD20CAR–T cells against K562 as in Fig. 1E. The range of cytotoxicity was 7–11% at an E:T ratio of 10:1 ($n = 4$). Two repeated LCL stimulations caused a log-scale expansion that resulted in 10,000-fold expansion of CD20CAR–T cells (Supplemental Fig. 1). The CD20CAR–T cells almost uniformly demonstrated effector phenotype ($CD28^-$, $CD62L^-$, $CD45RO^+$) after LCL stimulation (data not shown). In all subsequent experiments, $CD20CAR^-$ T cells were selected with tEGFR and expanded with one course of LCL stimulation; thus the transduction level of CD20CAR was uniformly >95% (Fig. 1D).

Quantification of CD20 molecules on the surface of CD20-CEMs and cell lines

Although CAR-T cells very efficiently recognize targets, the range of target molecule expression to which CAR-T cells can respond

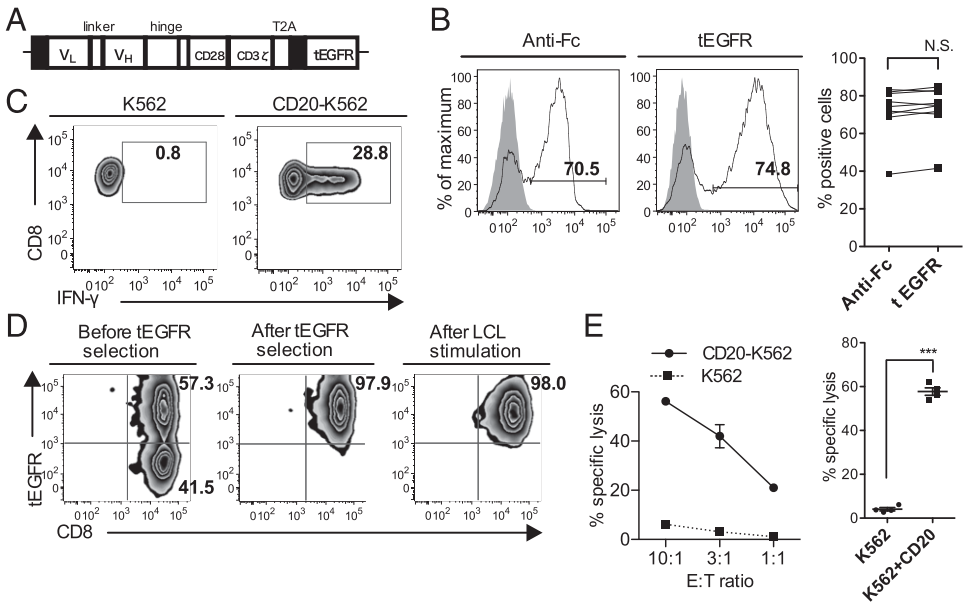

FIGURE 1. Construction, surface expression, and functional analysis of CD20CAR. (**A**) Schematic representation of the CD20CAR construct. CD20CAR consisted of anti-CD20 scFvs linked to CD3ζ, a CD28 costimulatory domain, and tEGFR as a transduction or selection marker via the T2A sequence. Solid black boxes denote the GM-CSF receptor leader sequence. Hinge, a human IgG4 hinge; linker, an 18-aa-long GGGS linker; V_H, H chain variable fragment; V_L, L chain variable fragment. (**B**) Surface expression of CD20CAR and tEGFR after transduction. $CD8^+$ cells were selected and transduced with the CD20CAR-encoding retrovirus supernatant. CD20CAR was stained with the anti-Fc Ab or biotinylated Erbitux, which reflects CAR expression. The surface expression of Fc/tEGFR was assessed on day 8 after one course of retroviral transduction. Gray-shaded histograms show staining of untransduced T cells. Representative flow plots are shown. *Right panel*, Data were pooled from nine independent experiments with T cells from eight donors (NS, paired *t* test). (**C**) Functional analysis of CD20CAR–T cells. On day 9 after transduction, CD20CAR–T cells were stimulated with either CD20-transduced K562 (CD20-K562) or mock-transduced K562 (K562) cells for 4 h at a 1:1 ratio, permeabilized, and then stained for IFN-γ. (**D**) Purity of CD20CAR–T cells before and after tEGFR selection and LCL stimulation. CD20CAR-positive cells were enriched by tEGFR selection and expanded by stimulation with γ-irradiated LCLs at a 1:7 ratio. Representative flow plots of three independent experiments from three donors are shown. (**E**) Cytotoxicity of CD20CAR–T cells. *Left panel*, After one course of expansion, cytotoxicity against either CD20-K562 or K562 cells was assessed at the indicated E:T ratio in the [^{51}Cr] release assay. The means ± SD of triplicate wells are shown. *Right panel*, Data were pooled from four independent experiments with CD20CAR–T cells from four donors (mean and SEM, ***$p < 0.0001$, the Student *t* test).

remains unknown (3–5). To assess this range more precisely, the number of CD20 molecules expressed on the cell surface of various cell lines was quantified as the CD20-specific Ab-binding capacity (CD20-sABC) on a per cell basis. We obtained 30 clones of CD20-CEMs expressing various levels of CD20 for use as target cells or stimulators (28). Of these, expression of CD20 by four representative clones was depicted, and the cells were used for several subsequent experiments as stimulators [CD20–very low CEM (VL-CEM) (CD20-mean fluorescence intensity [MFI]: 126/sABC: 240 molecules); CD20–low CEM (L-CEM) (CD20-MFI: 576/sABC: 5320 molecules); CD20–medium CEM (M-CEM) (CD20-MFI: 2396/sABC: 26,900 molecules); and CD20–high CEM (H-CEM) (CD20-MFI: 11,388/sABC: 142,722 molecules)] (Fig. 2A, Table I). The CD20-sABC values were 500,000 molecules for the germinal center B cell–type diffuse large B cell lymphoma (DLBCL)–derived cell lines; SU-DHL-4, -6, and -10, and 100,000 molecules for the non–germinal center B cell–type DLBCL-derived cell lines Ly-3 and -10 (Fig. 2B, Table I). RRBL1 and WILL2 are cell lines established from patients who experienced a relapse in B cell lymphoma with very weak expression of CD20 and who became resistant to rituximab (26, 27). The expression levels of CD20 by RRBL1 and WILL2 cells were 15,632

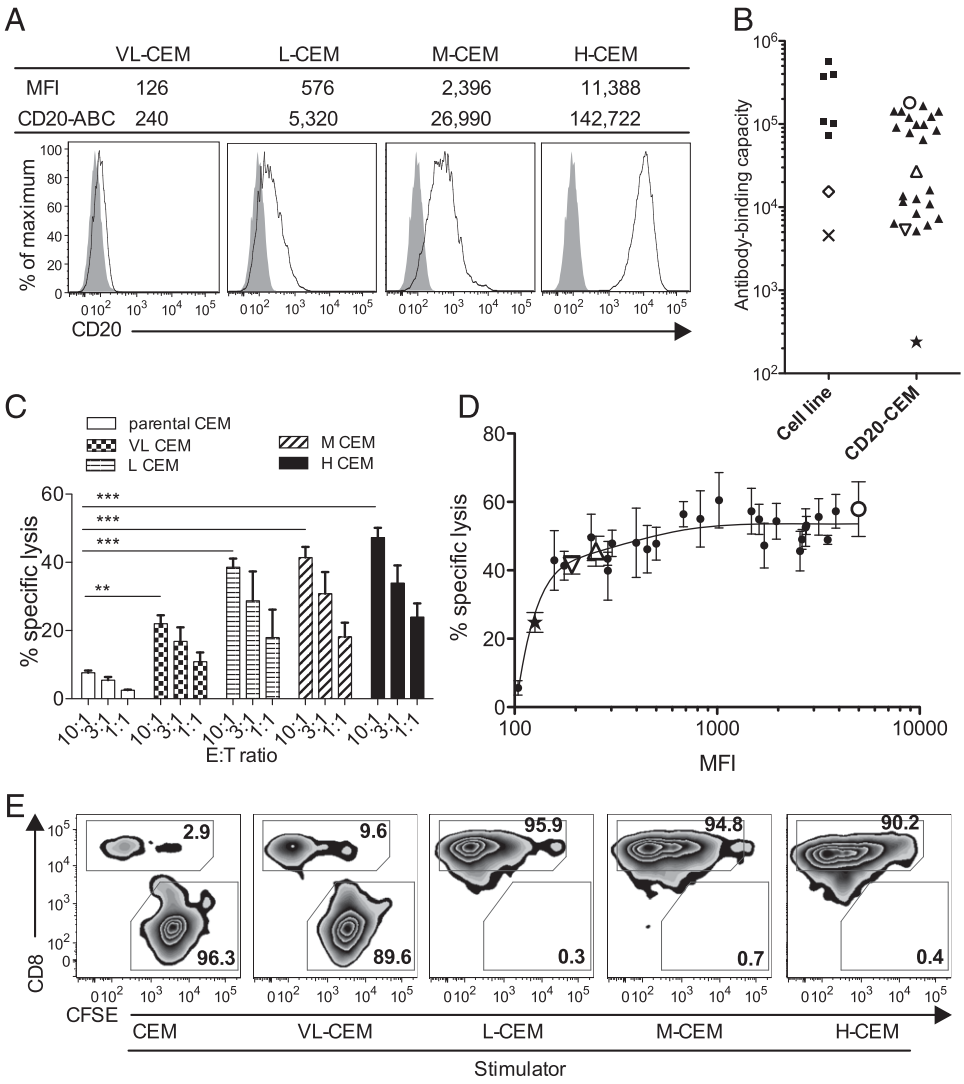

FIGURE 2. Quantification of CD20 molecules on the target cell surface and titration of the CD20 Ag expression level for CD20CAR–T cell cytotoxicity. (**A**) CD20 expression levels of the four representative CD20-CEM cell clones. The table above the histograms shows CD20-MFI and the quantification of CD20 molecules on each cell line as the Ab-binding capacity (CD20-ABC). Gray histograms show CD20 staining of untransduced CEM cells. VL-CEM, CD20-very low CEMs; L-CEM, CD20-low CEMs; M-CEM, CD20-medium CEMs; H-CEM, CD20-high CEMs. (**B**) Quantification of CD20 molecules on the surface of various cell lines. The number of CD20 molecules expressed on the surface of tumor cell lines was plotted in the left column (×, WILL2 cells; ◇, RRBL1 cells; ■, other cell lines). The number on CD20-CEMs is shown in the right column, including the four representative CEMs (★, VL-CEM; ▽, L-CEM; △, M-CEM; ○, H-CEM; ▲, other CD20-CEMs) (B, **D**). CD20-MFI data were analyzed in three independent experiments with similar results. CD20-MFI data in (A), (B), and (D) were collected in different experiments. (**C**) Cytotoxicity of CD20CAR–T cells against the four representative CD20-CEMs. Bars represent the cytotoxicity of CD20CAR–T cells against the four CD20-CEMs or untransduced CEMs (parental CEMs) at the indicated E:T ratios in the [^{51}Cr] release assay. The means ± SD of triplicate wells are shown (**$p < 0.01$, ***$p < 0.0001$, two-way ANOVA analysis). (D) The correlation between the CD20-MFI of CD20-CEMs and the cytotoxicity of CD20CAR–T cells. The cytotoxicity of CD20CAR-T cells against each CD20-CEM cell line was determined as in (C). The cytotoxicity of each CD20-CEM cell line at an E:T ratio of 10:1 was plotted against the CD20-MFI of CD20-CEMs. Data were pooled from four independent experiments with CD20CAR–T cells from four donors (mean and SEM). The solid line represents the fitted curve obtained with the nonlinear regression model using Prism5 software. (**E**) CD20CAR–T cells eradicated CD20-CEMs in coculture assays according to CD20 expression levels. CAR-T cells and CFSE-labeled CEMs were cultured in a 1:1 ratio without IL-2 supplementation for 72 h. The percentage of surviving CAR–T cells and residual CEMs within the live cell gates are shown. Data are representative of three independent experiments using three independent CD20CAR–T cell lines.

Table I. Surface CD20 expression of CD20-CEMs and other tumor cell lines

	MFI	sABC
CEM		
Parental	121	0
#2	9,683	120,208
#3	11,403	142,921
#4	6,905	83,978
#7	7,491	91,567
#19	14,228	180,597
#23	1,293	13,675
#27	11,388	142,722
#29	8,045	98,770
#31	15,550	198,366
#37	845	8,414
#47	1,209	12,680
#71	563	5172
#72	6,494	78,675
#73	8,049	98,822
#76	126	240
#82	641	6,062
#85	9,922	123,353
#94	576	5,320
w6	15,672	200,009
w7	13,180	166,571
w12	1,063	10,960
w40	5,414	64,824
w54	17,930	230,546
w114	1,125	11,689
w127	749	7,303
w132	1,497	16,104
w141	669	6,383
w147	2,396	26,990
w149	11,363	142,390
Tumor cell line		
RRBL1	1,436	15,376
WILL2	510	4,571
DHL-4	33,076	390,664
DHL-6	31,713	371,994
DHL-10	6,983	564,656
Ly-3	6,798	73,049
Ly-10	9,206	100,965
Raji	9,949	108,985

and 4869 molecules per cell, respectively (Fig. 2B, ◇ and ×, respectively). Relative to other cell lines, CD20-CEMs represented a very wide range of CD20 expression, from 240 to 230,546 molecules per cell, which was considered very low to high (Fig. 2B, Table I).

To evaluate the potential influence of costimulation, inhibitory signals, and adhesion molecule, the expression of CD80, CD86, CD54 (ICAM-1), CD58 (leukocyte function–associated molecule-3), and PD-L1 on target tumor cells was investigated. CEM cells demonstrated a tolerogenic phenotype, expressing low levels of CD80 and CD86 and relatively high levels of the inhibitory ligand PD-L1. CD54 was positive in all examined cell lines, whereas CD58 was negative in WILL2 cells (Supplemental Fig. 2) (35).

Determination of the minimum threshold of CD20 expression that CAR-T cells require for recognition and lysis

The level of CD20 Ag expression for rituximab-induced complement-dependent cytotoxicity (CDC) was determined using the same set of CD20-CEMs (28). We performed the rituximab-induced CDC assay and obtained almost the same results using human complement (Supplemental Fig. 3A). As demonstrated previously, Ab-dependent cellular cytotoxicity (ADCC) with rituximab against CD20-CEMs did not show a clear threshold of CD20 expression (data not shown) (28). CD20-CEMs with an MFI <1000 (equivalent to sABC of 10^4) did not induce significant CDC, whereas CD20-CEMs with an MFI of 1000–3000 (equivalent to sABC of 10^4–10^5) did. CD20-CEMs with an MFI >3000 effectively induced cytotoxicity, and maximal CDC was obtained at an MFI >5000 (sABC of 10^5) (Supplemental Fig. 3A). CDC induced by the humanized anti-CD20 mAb OUBM was also examined. OUBM mAb, with which CD20CAR was constructed, induced marked CDC with half-maximum cytotoxicity at a CD20 expression level similar (MFI of 3000) to that of rituximab (MFI of 3000) (Supplemental Fig. 3).

In contrast to the weak CDC caused by rituximab and OUBM mAb, CD20-CEMs were more efficiently lysed by CD20CAR–T cells, with the exception of VL-CEMs, which underwent a significantly lower degree of lysis (Fig. 2C).

To determine the threshold expression level of the CD20 Ag required to induce CAR-T cytotoxicity, we performed a [^{51}Cr] release assay with CD20CAR–T cells against the clones of CD20-CEMs expressing various levels of CD20 (CD20-MFI: 126–6924/CD20-sABC: 240–230,546 molecules). CD20CAR–T cells lysed VL-CEMs, which had the lowest level of CD20 (MFI: 126/sABC: 240 molecules, 22.8 ± 2% lysis). In addition, CD20CAR–T cells induced similar lysis (40–60% lysis) of various CD20-CEMs with higher expression of CD20 (CD20-MFI: 157/CD20-sABC: $\geq$5172 molecules, E:T ratio of 10:1) (Fig. 2D). CD20CAR–T cells exhibited efficient cytotoxicity against CD20-CEMs with an MFI <1000; at this level, rituximab and OUBM mAb did not induce significant CDC (Supplemental Fig. 3A, 3B, Fig. 2D). Half-maximum cytotoxicity by CD20CAR–T cells was observed at an MFI of ~200–300 (equivalent to sABC of 10^3). Therefore, the minimum threshold number of surface target molecules that CAR-T recognized and lysed was markedly low, at approximately a few hundred molecules.

A coculture assay was performed as a more physiological model. In this assay, CD20CAR–T cells partially, but not completely, eradicated VL-CEMs. Conversely, CAR-T cells completely eradicated L-, M-, and H-CEMs after a 72-h coculture (Fig. 2E).

Intracellular signaling, cytokine production, and cell division after stimulation with the four representative CD20-CEMs

An advantage of CAR-T cell therapy over mAb therapy is that CAR-T cells can become activated and proliferate upon specific stimulation of the target Ag, enabling CAR-T cells to exhibit long-lasting efficacy in vivo (1, 3–5, 9). Although we titrated the threshold Ag density for CAR-T–induced lysis, the threshold for cytotoxicity and full activation, including cytokine production and proliferation, are uncoupled in Ag-specific T cells (36). Thus, we examined the threshold Ag density for CAR-T activation. To define the minimum threshold of CD20 expression that was needed for effective activation and expansion of CAR-T cells, we examined phosphorylation of the signaling molecules ERK and ZAP70 after stimulation with the four representative CD20-CEMs. The CD20-CEMs, except for VL-CEMs, induced similar phosphorylation of ERK (pERK) and ZAP70 in CAR-T cells (Fig. 3A and data not shown). pERK was equally upregulated when CAR-T cells were stimulated with L-, M-, and H-CEMs, but not with VL-CEMs, after 10 min (Fig. 3A). Time-course analysis showed that the pERK MFI responses were almost equal after L-, M-, and H-CEM stimulation, and the peak time was 5–10 min after stimulation. Nevertheless, VL-CEM induced only minimal phosphorylation of ERK in CAR-T cells, similar to that of parental CEMs (Fig. 3A, 3B).

Cytokine production and proliferation were evaluated following different stimuli. Stimulation with VL-CEM did not induce the production of cytokines from CAR-T cells. Conversely, L-, M-, and H-CEMs induced equivalent production of IFN-γ (Fig. 3C–E), IL-2 (Fig. 3F, 3G), and TNF-α (Fig. 3H). IL-2 production after H-CEM

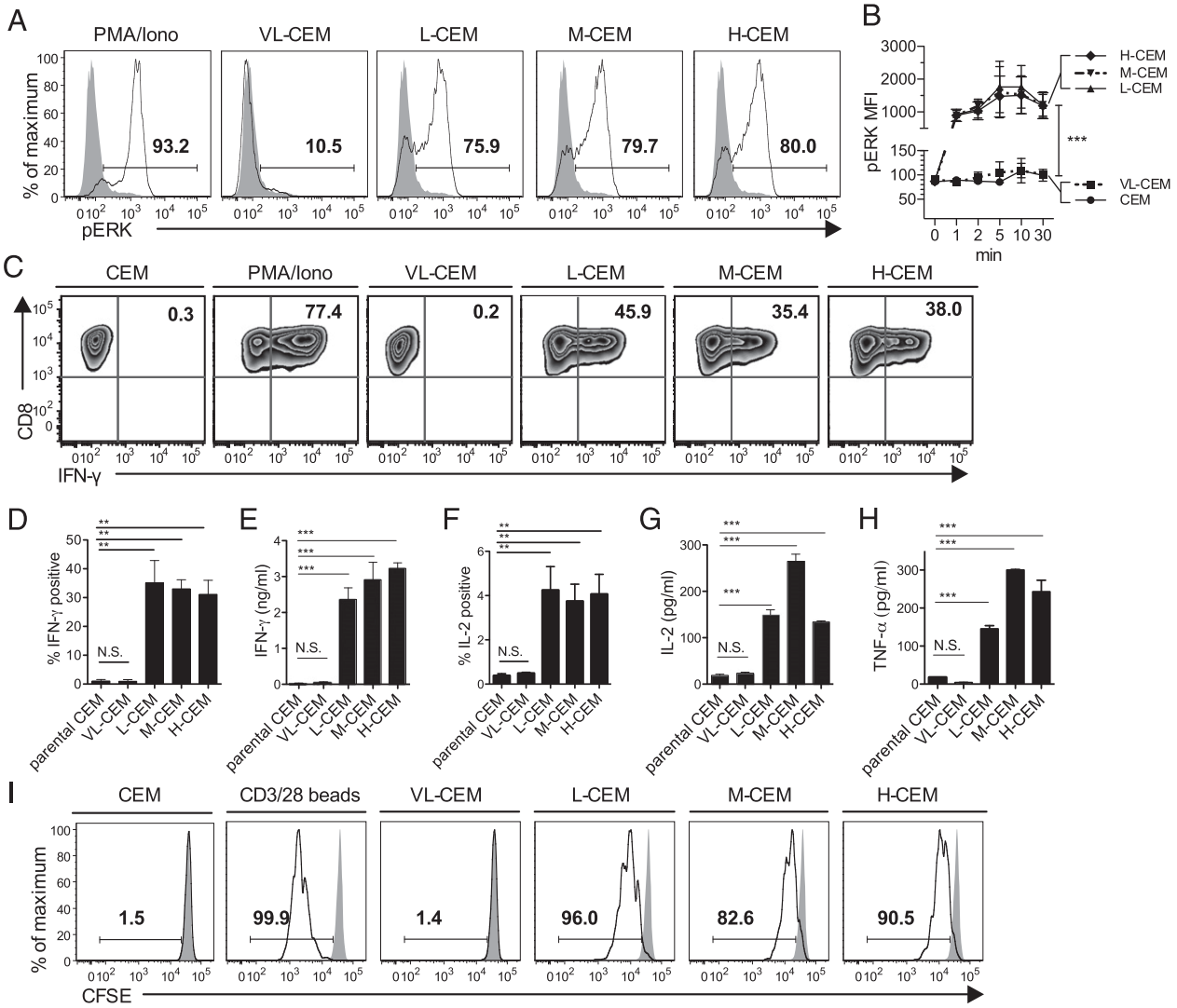

FIGURE 3. Titration of the threshold of CD20 expression for CD20CAR–T cell activation upon stimulation. (**A**) Phosphorylation of a distal signaling molecule, ERK (pERK). CD20CAR–T cells were stimulated with the four representative CD20-CEMs, untransduced CEMs at a responder to stimulator ratio of 1:5, or PMA/ionomycin (Iono) for 10 min, and were then fixed, permeabilized, and stained with pERK-specific Ab. Gray histograms show data obtained from T cells stimulated with parental CEMs. (**B**) Time-course analysis of pERK. The phosphorylation of ERK in CD20CAR–T cells was analyzed 1, 2, 5, 10, and 30 min after stimulation with the four representative CD20-CEMs or parental CEMs at a 1:5 ratio. MFI of pERK after stimulation is shown. Data were pooled from three independent experiments with CD20CAR–T cells from three donors. Means and SEM are shown (***$p < 0.0001$, two-way ANOVA analysis). (**C**) IFN-γ production after stimulation. CD20CAR–T cells were stimulated with the four representative CD20-CEMs, parental CEMs at a 1:1 ratio, or PMA/Iono for 4 h, and were then permeabilized and stained for IFN-γ. (**D** and **F**) The percentages of T cells that stained positive for IFN-γ and IL-2, respectively, are shown. Data were pooled from three independent experiments with CD20CAR–T cells from three donors (mean and SEM, **$p < 0.01$). The secretion of (**E**) IFN-γ, (**G**) IL-2, and (**H**) TNF-α upon CD20-CEM stimulation. CD20CAR–T cells were stimulated with the indicated CEMs at a 1:1 ratio, and culture supernatants were harvested at 16 h and analyzed with ELISA (mean and SEM, ***$p < 0.001$, one-way ANOVA). (**I**) Division of CD20CAR–T cells upon CD20 ligation. CD20CAR–T cells were labeled with CFSE and stimulated with CD20-CEMs, untransduced CEMs, or anti-CD3/28 beads at a 1:1 ratio, and the CFSE staining intensity was then analyzed with FCM 96 h after stimulation. Gray histograms show data of nonstimulated CD20CAR–T cells. Data are representative of at least three independent experiments with CD20CAR–T cells from three donors (A, C, and I).

stimulation was approximately half that after M-CEM stimulation in repeated experiments ($n = 3$). Because we observed no significant difference in intracellular IL-2 production (Fig. 3F), the low IL-2 concentration after H-CEM stimulation may have reflected an increase in cytokine consumption. Regarding proliferation, VL-CEM did not induce cell division of CAR-T cells, whereas other CEMs induced efficient cell division 72 and 96 h after stimulation (Fig. 3I and data not shown). The kinetics of CD20CAR–T cell division increased with higher CD20 expression on CD20-CEMs, but the percentages of proliferating cells were equivalent among L-, M-, and H-CEM stimulation (Fig. 3I). The kinetics of division appeared to be partly dependent on target Ag density (Fig. 3I).

Taken together, the minimum threshold required to induce activation and proliferation of CAR-T cells was between the levels expressed by VL-CEMs and L-CEMs. This threshold was very low: less than the CD20 expression level of L-CEMs (CD20-MFI: 576/CD20-sABC: 5320). CD20 expression above the threshold significantly activated CAR-T cells.

Effects on CD20^{lo} cell lines and CD20^{lo} primary tumor cells isolated from patients with rituximab-refractory B cell lymphoma

Because we demonstrated that CD20CAR–T cells recognized markedly low expression of CD20, we examined the effectiveness of

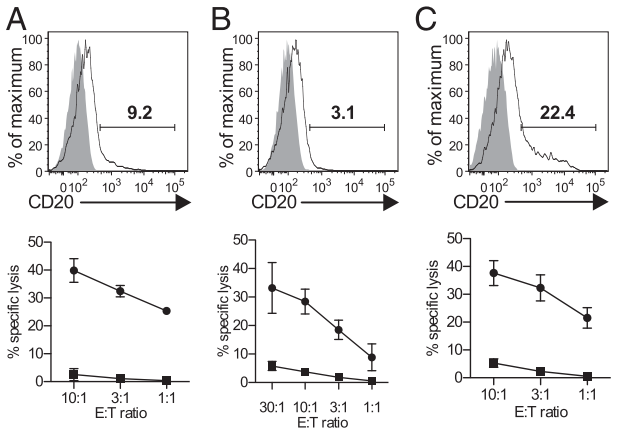

FIGURE 4. Cytotoxicity of CD20CAR–T cells against CD20-downregulated tumor cell lines and primary lymphoma cells. (**A** and **B**) CD20 expression and cytotoxicity by CD20CAR–T cells against CD20-downregulated tumor cell lines RRBL1 and WILL2, respectively. (**C**) CD20 expression and cytotoxicity by CD20CAR–T cells against primary tumor cells isolated from the pleural effusion of a patient with rituximab-refractory B cell lymphoma. Throughout the figure, *upper panels* show CD20 staining (solid line), isotype control staining (gray shaded), and percentages of CD20-positive fractions. *Lower panels* show the cytotoxicity by CD20CAR–T cells against the cell lines at the indicated E:T ratios in the [^{51}Cr] release assay. The means ± SEM of three independent experiments with CD20CAR–T cells from three donors are shown. • and ■ denote cytotoxicity by CD20CAR-T and untransduced T cells, respectively.

CD20CAR–T cell therapy against CD20^{lo} tumor cells. First, the cytotoxicity of CD20CAR–T cells against CD20^{lo} tumor cell lines was investigated. CD20CAR–T cells lysed both CD20^{lo} cell lines, RRBL1 and WILL2, very efficiently (Fig. 2B, 4A, 4B, *lower panel*).

We also evaluated cytotoxicity against CD20^{lo} primary cells from a patient with DLBCL (double-hit lymphoma). The patient exhibited disease recurrence after a full course of R-hyper CVAD (37), and lymphoma cells were obtained from pleural effusion. At the time of relapse, CD20 expression was reduced in most cells, and only ∼20% of cells showed low CD20 expression (Fig. 4C, *upper panel*). CD20CAR–T cells efficiently lysed CD20^{lo} primary DLBCL cells. This lytic activity was higher than the percentage of the CD20^{+} cell fraction, suggesting that CD20CAR–T cells partially lysed the cell fraction expressing low levels of CD20 (Fig. 4C, *lower panel*).

CD20CAR–T cells recognized and lysed residual CLL cells after ofa therapy

CLL is a chronic lymphoproliferative disease in which the anti-CD20 mAb is a choice for standard care (38). The expression of CD20 by CLL cells is generally lower than that of other CD20^{+} lymphoid malignancies such as ALL and lymphoma (39). To compare the potency of CD20 recognition by anti-CD20 mAb, we examined cytotoxicity and cytokine production following stimulation of CD20-downregulated CLL cells. Before starting mAb therapy, the expression of CD20 by CLL cells was intact, and the lytic activity of CD20CAR–T cells was remarkable (Fig. 5A). The patient then became chemorefractory following repeated administration of rituximab (the clinical course of this patient is summarized in Supplemental Fig. 4). In this patient, CLL cells could not be controlled with rituximab-combined chemotherapy. The expression of CD20 by CLL cells decreased, and the MFI showed two peaks: the nearly negative fraction and the CD20 low fraction (Fig. 5B, *upper panel*). However, cytotoxicity by CD20CAR–T cells was maintained (Fig. 5B, *lower panel*). The patient was then treated with the novel anti-CD20 mAb ofa (40). A marked decrease in the number of CLL cells and regression of lymphadenopathy were observed after a single course of ofa, whereas the CD20 very low fraction, which was confirmed to consist of CD5^{+} CLL cells (data not shown), remained in the peripheral

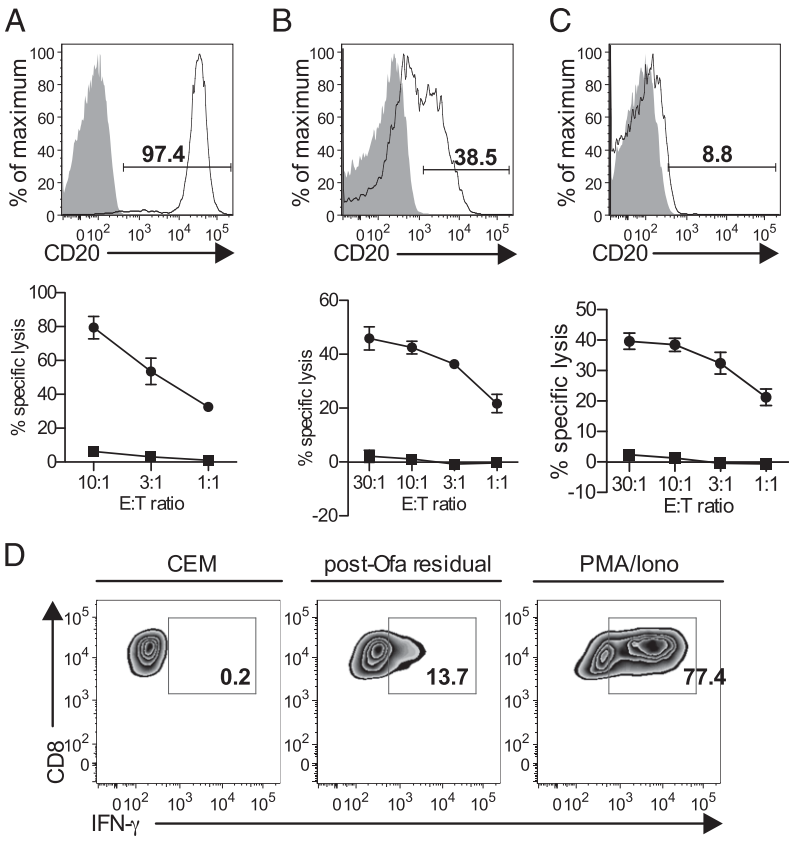

FIGURE 5. Cytotoxicity of CD20CAR–T cells against CD20-downregulated primary CLL cells. (**A**–**C**) CD20 expression and cytotoxicity against CLL cells isolated from an untreated patient (A), before administration of ofa (preofa) (B), and 14 d after the 10th course of ofa (postofa) (C). CLL cells were isolated from the peripheral blood of a patient with rituximab-refractory CLL. Residual CLL cells after rituximab treatment were isolated from the peripheral blood of a patient at two different time points, pre- and postofa. *Upper panels* show CD20 staining (solid line) and isotype control staining (gray shaded). *Lower panels* show cytotoxicity by CD20CAR–T cells against CLL cells at the indicated E:T ratios in the [^{51}Cr] release assay. Filled circles and squares denote cytotoxicity by CD20CAR-T and untransduced T cells, respectively. The means ± SEM of three independent experiments with CD20CAR–T cells from three donors are shown (A–C). (**D**) Cytokine production by CD20CAR–T cells upon stimulation with postofa CLL cells. CD20CAR–T cells were stimulated with postofa CLL cells, parental CEMs at a 1:1 ratio, or PMA/Iono for 4 h, and were then permeabilized and stained for IFN-γ.

blood. We obtained residual CLL cells from the peripheral blood of the patient after the 10th course of ofa. After ofa treatment, the CD20 relatively low fraction disappeared, and CD20 expression by CLL cells was almost uniformly nearly negative (Fig. 5C, *upper panel*). The residual cells were exposed once to the mAb therapy and survived. Therefore, the CD20 expression level of the residual cells was considered to be below the effective range of rituximab or ofa. In the [^{51}Cr] release assay using these primary CLL cells, CD20CAR–T cells efficiently recognized and lysed not only CLL cells before ofa but also CLL cells after ofa (Fig. 5B, 5C, *lower panel*). With an intracellular IFN-γ assay, after ofa, stimulation of CD20CAR–T cells with CLL cells, which were nearly CD20-negative, induced production of IFN-γ by CD20CAR–T cells (Fig. 5D).

Discussion

In the current study, we generated a novel CD20CAR based on a humanized anti-CD20 mAb (25). CD20CAR–T cells specifically and effectively lysed CD20-positive target cells. The expression of CD20CAR was precisely evaluated using the anti-Fc Ab and biotinylated Erbitux. Although we did not directly evaluate the copy number of the CD20CAR transgene, the variation observed in lytic activity against K562-CD20 cells was very low following tEGFR selection, suggesting that the expression of CD20CAR was similar among the CD20CAR–T cell lines. With cytotoxicity analysis of CD20CAR–T cells against CD20-CEMs expressing various levels of CD20, we first titrated the minimum threshold of CD20 expression that CAR-T cells could recognize and lyse. We demonstrated that CD20CAR–T cells lysed CD20-CEMs with CD20-ABC = 240 molecules, which was the lowest CD20 level in this set. This level was 1000-fold lower than that required to induce CDC with rituximab and OUBM mAb. The difference in cytolytic activity between CDC and CAR should mostly depend on the presence or absence of effector cells. Although CDC and CAR activity is similar against CD20-high CEM cells, CD20CAR–T cells demonstrated far better lytic activity than CDC against CD20-low CEM cells (Fig. 2D, Supplemental Fig. 3). This finding suggested that CAR-T therapy might show better effect in the case of only a limited number of target Ags on the tumor cells. The correlation between CD20-ABC and specific lysis was also represented with a saturation curve, which had a sharp inclination against CD20^{lo} targets. This phenomenon was attributed to CAR technology providing full activation with CD3ζ and the simultaneous costimulation of CD28 (3–6).

We next determined the threshold of CD20 expression that could activate and expand CD20CAR–T cells upon stimulation with the representative CD20-CEMs. Although cytotoxicity analysis revealed that CD20CAR–T cells lysed VL-CEMs, these cells did not induce downstream signaling, production of IFN-γ, or proliferation of CAR–T cells. Stimulation with L-, M-, and H-CEMs (CD20-ABC: ≥5320 molecules) effectively and equally activated CD20CAR–T cells. Taken together, these results indicated that the threshold of CD20 expression for recognition and lysis by CD20CAR–T cells, which we termed the "lytic threshold," was a few hundred molecules, and the threshold required for activation and expansion of CAR-T cells, termed the "activating threshold," was slightly higher, at a few thousand molecules. These results are consistent with previous findings in which the lytic threshold and activating threshold were different in TCR activation (36). Because endogenous T cells such as melanoma-specific T cells and virus-specific T cells require 10–100 epitope molecules per target cell to trigger specific lysis (13), both the lytic threshold and the activating threshold were slightly lower in endogenous T cells compared with CAR-T cells. Obviously, the thresholds are affected by the affinity of the mAb or TCR for the ligand or peptide/HLA complex. In our study, the affinity of the humanized anti-CD20 mAb (OUBM mAb), which was used to construct CD20CAR, was within the same range as that of rituximab (K_D value: OUBM mAb, 10.09 nM; rituximab, 5.35 nM) (25). Using a mAb with this range of affinity, both thresholds of CAR-T cells were close to those of endogenous T cells. Furthermore, CD20CAR–T cells recognized and lysed CD20-downregulated target cells that survived after mAb therapy, indicating that manufacturing a CAR with a mAb may reinforce target recognition more than the mAb itself.

The epitope location of the mAb is another important issue. Ofa exposure before sample collection may account for the apparent CD20 downregulation. However, we confirmed CD20 downregulation using another CD20 mAb, a B9E9 clone in which the epitope location is distinct from that of ofa (23). This confirmation indicated that CD20 downregulation after ofa treatment was not caused by competition between the analytical Ab and ofa. The epitope location targeted by OUBM mAb and ofa partially overlaps, but that of OUBM mAb and rituximab does not (25). Therefore, ofa can theoretically block the ligation of CD20CAR-T but rituximab cannot. We observed that CD20CAR–T cells indeed lysed CD20-downregulated target cells both after rituximab and ofa, suggesting that the potential effect of epitope blocking was minor in the current study.

The results of the current study led us to propose a novel concept for future searches for target Ag in CAR-T therapy. Suitable target Ags for CAR-T cell therapy are considerably different from those for mAb therapy in terms of their expression profiles and levels. Higher expression levels on the surface of tumor cells have been considered in target Ag searches for mAb therapy because off-tumor expression is usually negligible (41). However, for the target of CAR-T cell therapy, off-tumor expression of the target molecules must be strictly negative or at a very low level that is below the lytic threshold, at a few hundred molecules. Otherwise, severe adverse effects could occur as a result of off-tumor effects (10). The target Ag safety in the context of mAb therapy does not necessarily translate into the safety of Ag in the context of markedly more sensitive CAR-T cell therapy (10). Conversely, even if the threshold was below the mAb therapy range, low Ag expression above the activating threshold, such as at a few thousand molecules, could be considered a candidate for the target Ag of CAR-T cell therapy.

Acquired resistance to rituximab has become a problem in the treatment of patients with CD20-positive B cell tumors (20, 23). One suggested mechanism is downregulation of CD20 (20, 22, 26). A total of 15–20% of relapsed patients exhibit CD20 Ag loss, as observed with immunohistochemistry analysis in samples taken at relapse (20, 23). Our CD20CAR–T cells recognized and lysed primary cells isolated from patients with mAb therapy–refractory lymphoma and CLL, although the expression level of CD20 was very low. We also analyzed CD20CAR-T recognition against CD20-downregulated, mAb-refractory CLL in detail (21). The residual cells after CD20 mAb therapy expressed significantly low levels of CD20, and this expression level must have been below the effective range of the mAb in principle. CD20CAR–T cells lysed both postrituximab and postofa residual CLL cells, indicating that CD20CAR–T cells have a greater potential to recognize the target than mAbs. Even residual postofa CLL cells stimulated CD20CAR–T cells, and thus we conclude that the very low expression of CD20 on CLL cells could still efficiently provide stimulation for the further repopulation of CD20CAR–T cells.

In other CAR therapies targeting CD19, several patients were reported to have relapsed despite the completely negative con-

version of the Ag molecule after CAR-T cell therapy (2). Although CAR-T cells recognize very low levels of the target Ag, they cannot recognize completely Ag-negative cells. The strategy of administering CAR-T therapy as a first-line treatment, or in earlier phases with the aim of earlier eradication of target cells, may prevent immunological escape by negative conversion of the Ag.

One limitation of the current study is that we assessed the threshold using only CD20 and CD20CAR systems. Because the threshold may be influenced by many other factors, such as affinity (42), structure (43), epitope localization of individual CAR-Ag pairs (44, 45), and the expression of a coreceptor on target cells (46), the threshold may vary among mAbs and target Ags. We also could not investigate the relationship between the expression of CD20 and the ADCC activity of mAbs because NK cell activity is predominant in the CD20-CEM system, and a clear threshold has not been observed (28). Although the potential relationship between target Ag density and ADCC activity has been investigated in other experimental systems, $>10^4$ Ag molecules per cell are needed to demonstrate significant ADCC (47). In the current study, the minimum threshold of CAR recognition was 3-log units lower than that of mAbs to trigger CDC. CAR can also directly mobilize T cells to target cells, whereas mAb therapy mainly depends on indirect cytotoxicity such as CDC or ADCC (3–5, 19, 28). Thus, the lytic and activating thresholds of CAR are considered significantly lower than those of mAbs.

We concluded that CAR-T cells can recognize and lyse cells expressing considerably low levels of the target Ag and were activated and expanded upon such stimulation. CD20CAR–T cell therapy may also be applicable for the treatment of CD20-positive lymphoid malignancies.

Acknowledgments

We thank Yoko Matsuyama, Asako Watanabe, and Chika Wakamatsu for technical assistance.

Disclosures

H.K. has received research funding from Bristol-Myers Squibb, Chugai Pharmaceutical, Kyowa Hakko Kirin, Dainippon Sumitomo Pharma, Zenyaku Kogyo, and FUJIFILM. The other authors have no financial conflicts of interest.

References

1. Porter, D. L., B. L. Levine, M. Kalos, A. Bagg, and C. H. June. 2011. Chimeric antigen receptor-modified T cells in chronic lymphoid leukemia. *N. Engl. J. Med.* 365: 725–733.
2. Grupp, S. A., M. Kalos, D. Barrett, R. Aplenc, D. L. Porter, S. R. Rheingold, D. T. Teachey, A. Chew, B. Hauck, J. F. Wright, et al. 2013. Chimeric antigen receptor-modified T cells for acute lymphoid leukemia. *N. Engl. J. Med.* 368: 1509–1518.
3. Sadelain, M., R. Brentjens, and I. Riviere. 2013. The basic principles of chimeric antigen receptor design. *Cancer Discov.* 3: 388–398.
4. Jensen, M. C., and S. R. Riddell. 2014. Design and implementation of adoptive therapy with chimeric antigen receptor-modified T cells. *Immunol. Rev.* 257: 127–144.
5. Turtle, C. J., M. Hudecek, M. C. Jensen, and S. R. Riddell. 2012. Engineered T cells for anti-cancer therapy. *Curr. Opin. Immunol.* 24: 633–639.
6. Kowolik, C. M., M. S. Topp, S. Gonzalez, T. Pfeiffer, S. Olivares, N. Gonzalez, D. D. Smith, S. J. Forman, M. C. Jensen, and L. J. Cooper. 2006. CD28 costimulation provided through a CD19-specific chimeric antigen receptor enhances in vivo persistence and antitumor efficacy of adoptively transferred T cells. *Cancer Res.* 66: 10995–11004.
7. Imai, C., K. Mihara, M. Andreansky, I. C. Nicholson, C. H. Pui, T. L. Geiger, and D. Campana. 2004. Chimeric receptors with 4-1BB signaling capacity provoke potent cytotoxicity against acute lymphoblastic leukemia. *Leukemia* 18: 676–684.
8. Zhong, X. S., M. Matsushita, J. Plotkin, I. Riviere, and M. Sadelain. 2010. Chimeric antigen receptors combining 4-1BB and CD28 signaling domains augment PI3kinase/AKT/Bcl-XL activation and $CD8^+$ T cell-mediated tumor eradication. *Mol. Ther.* 18: 413–420.
9. Kochenderfer, J. N., M. E. Dudley, S. A. Feldman, W. H. Wilson, D. E. Spaner, I. Maric, M. Stetler-Stevenson, G. Q. Phan, M. S. Hughes, R. M. Sherry, et al. 2012. B-cell depletion and remissions of malignancy along with cytokine-associated toxicity in a clinical trial of anti-CD19 chimeric-antigen-receptor-transduced T cells. *Blood* 119: 2709–2720.
10. Morgan, R. A., J. C. Yang, M. Kitano, M. E. Dudley, C. M. Laurencot, and S. A. Rosenberg. 2010. Case report of a serious adverse event following the administration of T cells transduced with a chimeric antigen receptor recognizing ERBB2. *Mol. Ther.* 18: 843–851.
11. Hudis, C. A. 2007. Trastuzumab—mechanism of action and use in clinical practice. *N. Engl. J. Med.* 357: 39–51.
12. Ménard, S., P. Casalini, M. Campiglio, S. M. Pupa, and E. Tagliabue. 2004. Role of HER2/neu in tumor progression and therapy. *Cell. Mol. Life Sci.* 61: 2965–2978.
13. Purbhoo, M. A., D. H. Sutton, J. E. Brewer, R. E. Mullings, M. E. Hill, T. M. Mahon, J. Karbach, E. Jäger, B. J. Cameron, N. Lissin, et al. 2006. Quantifying and imaging NY-ESO-1/LAGE-1-derived epitopes on tumor cells using high affinity T cell receptors. *J. Immunol.* 176: 7308–7316.
14. Liddy, N., G. Bossi, K. J. Adams, A. Lissina, T. M. Mahon, N. J. Hassan, J. Gavarret, F. C. Bianchi, N. J. Pumphrey, K. Ladell, et al. 2012. Monoclonal TCR-redirected tumor cell killing. *Nat. Med.* 18: 980–987.
15. Sadelain, M., R. Brentjens, and I. Rivière. 2009. The promise and potential pitfalls of chimeric antigen receptors. *Curr. Opin. Immunol.* 21: 215–223.
16. Thomas, D. A., S. O'Brien, S. Faderl, G. Garcia-Manero, A. Ferrajoli, W. Wierda, F. Ravandi, S. Verstovsek, J. L. Jorgensen, C. Bueso-Ramos, et al. 2010. Chemoimmunotherapy with a modified hyper-CVAD and rituximab regimen improves outcome in de novo Philadelphia chromosome-negative precursor B-lineage acute lymphoblastic leukemia. *J. Clin. Oncol.* 28: 3880–3889.
17. Jaglowski, S. M., L. Alinari, R. Lapalombella, N. Muthusamy, and J. C. Byrd. 2010. The clinical application of monoclonal antibodies in chronic lymphocytic leukemia. *Blood* 116: 3705–3714.
18. Abramson, J. S., and M. A. Shipp. 2005. Advances in the biology and therapy of diffuse large B-cell lymphoma: moving toward a molecularly targeted approach. *Blood* 106: 1164–1174.
19. Jazirehi, A. R., and B. Bonavida. 2005. Cellular and molecular signal transduction pathways modulated by rituximab (rituxan, anti-CD20 mAb) in non-Hodgkin's lymphoma: implications in chemosensitization and therapeutic intervention. *Oncogene* 24: 2121–2143.
20. Hiraga, J., A. Tomita, T. Sugimoto, K. Shimada, M. Ito, S. Nakamura, H. Kiyoi, T. Kinoshita, and T. Naoe. 2009. Down-regulation of CD20 expression in B-cell lymphoma cells after treatment with rituximab-containing combination chemotherapies: its prevalence and clinical significance. *Blood* 113: 4885–4893.
21. Jilani, I., S. O'Brien, T. Manshuri, D. A. Thomas, V. A. Thomazy, M. Imam, S. Naeem, S. Verstovsek, H. Kantarjian, F. Giles, et al. 2003. Transient down-modulation of CD20 by rituximab in patients with chronic lymphocytic leukemia. *Blood* 102: 3514–3520.
22. Tsai, P. C., F. J. Hernandez-Ilizaliturri, N. Bangia, S. H. Olejniczak, and M. S. Czuczman. 2012. Regulation of CD20 in rituximab-resistant cell lines and B-cell non-Hodgkin lymphoma. *Clin. Cancer Res.* 18: 1039–1050.
23. Johnson, N. A., S. Leach, B. Woolcock, R. J. deLeeuw, A. Bashashati, L. H. Sehn, J. M. Connors, M. Chhanabhai, A. Brooks-Wilson, and R. D. Gascoyne. 2009. CD20 mutations involving the rituximab epitope are rare in diffuse large B-cell lymphomas and are not a significant cause of R-CHOP failure. *Haematologica* 94: 423–427.
24. Shimada, K., A. Tomita, S. Saito, and H. Kiyoi. 2014. Efficacy of ofatumumab against rituximab-resistant B-CLL/SLL cells with low CD20 protein expression. *Br. J. Haematol.* 166: 455–457.
25. Uchiyama, S., Y. Suzuki, K. Otake, M. Yokoyama, M. Ohta, S. Aikawa, M. Komatsu, T. Sawada, Y. Kagami, Y. Morishima, and K. Fukui. 2010. Development of novel humanized anti-CD20 antibodies based on affinity constant and epitope. *Cancer Sci.* 101: 201–209.
26. Tomita, A., J. Hiraga, H. Kiyoi, M. Ninomiya, T. Sugimoto, M. Ito, T. Kinoshita, and T. Naoe. 2007. Epigenetic regulation of CD20 protein expression in a novel B-cell lymphoma cell line, RRBL1, established from a patient treated repeatedly with rituximab-containing chemotherapy. *Int. J. Hematol.* 86: 49–57.
27. Sonoki, T., Y. Li, S. Miyanishi, H. Nakamine, N. Hanaoka, H. Matsuoka, I. Mori, and H. Nakakuma. 2009. Establishment of a novel CD20 negative mature B-cell line, WILL2, from a CD20 positive diffuse large B-cell lymphoma patient treated with rituximab. *Int. J. Hematol.* 89: 400–402.
28. van Meerten, T., R. S. van Rijn, S. Hol, A. Hagenbeek, and S. B. Ebeling. 2006. Complement-induced cell death by rituximab depends on CD20 expression level and acts complementary to antibody-dependent cellular cytotoxicity. *Clin. Cancer Res.* 12: 4027–4035.
29. Terakura, S., T. N. Yamamoto, R. A. Gardner, C. J. Turtle, M. C. Jensen, and S. R. Riddell. 2012. Generation of CD19-chimeric antigen receptor modified $CD8^+$ T cells derived from virus-specific central memory T cells. *Blood* 119: 72–82.
30. Lenkei, R., J. W. Gratama, G. Rothe, G. Schmitz, J. L. D'hautcourt, A. Arekrans, F. Mandy, and G. Marti. 1998. Performance of calibration standards for antigen quantitation with flow cytometry. *Cytometry* 33: 188–196.
31. Kumar, A., E. T. Petri, B. Halmos, and T. J. Boggon. 2008. Structure and clinical relevance of the epidermal growth factor receptor in human cancer. *J. Clin. Oncol.* 26: 1742–1751.
32. Wang, X., W. C. Chang, C. W. Wong, D. Colcher, M. Sherman, J. R. Ostberg, S. J. Forman, S. R. Riddell, and M. C. Jensen. 2011. A transgene-encoded cell surface polypeptide for selection, in vivo tracking, and ablation of engineered cells. *Blood* 118: 1255–1263.
33. Szymczak-Workman, A. L., K. M. Vignali, and D. A. Vignali. 2012. Design and construction of 2A peptide-linked multicistronic vectors. Cold Spring Harb. Protoc. 2012(2): 199–204.

34. Andris-Widhopf, J., P. Steinberger, R. Fuller, C. Rader, and C. F. Barbas, 3rd. 2011. Generation of human scFv antibody libraries: PCR amplification and assembly of light- and heavy-chain coding sequences. *Cold Spring Harb. Protoc.* 2011(9).
35. Weijtens, M. E., R. A. Willemsen, B. A. van Krimpen, and R. L. Bolhuis. 1998. Chimeric scFv/gamma receptor-mediated T-cell lysis of tumor cells is coregulated by adhesion and accessory molecules. *Int. J. Cancer* 77: 181–187.
36. Faroudi, M., C. Utzny, M. Salio, V. Cerundolo, M. Guiraud, S. Müller, and S. Valitutti. 2003. Lytic versus stimulatory synapse in cytotoxic T lymphocyte/target cell interaction: manifestation of a dual activation threshold. *Proc. Natl. Acad. Sci. USA* 100: 14145–14150.
37. Oki, Y., J. R. Westin, F. Vega, H. Chuang, N. Fowler, S. Neelapu, F. B. Hagemeister, P. McLaughlin, L. W. Kwak, J. E. Romaguera, et al. 2013. Prospective phase II study of rituximab with alternating cycles of hyper-CVAD and high-dose methotrexate with cytarabine for young patients with high-risk diffuse large B-cell lymphoma. *Br. J. Haematol.* 163: 611–620.
38. Hallek, M., B. D. Cheson, D. Catovsky, F. Caligaris-Cappio, G. Dighiero, H. Döhner, P. Hillmen, M. J. Keating, E. Montserrat, K. R. Rai, and T. J. Kipps, International Workshop on Chronic Lymphocytic Leukemia. 2008. Guidelines for the diagnosis and treatment of chronic lymphocytic leukemia: a report from the International Workshop on Chronic Lymphocytic Leukemia updating the National Cancer Institute-Working Group 1996 guidelines. *Blood* 111: 5446–5456.
39. Prevodnik, V. K., J. Lavrenčak, M. Horvat, and B. J. Novakovič. 2011. The predictive significance of CD20 expression in B-cell lymphomas. *Diagn. Pathol.* 6: 33.
40. Wierda, W. G., S. Padmanabhan, G. W. Chan, I. V. Gupta, S. Lisby, and A. Osterborg, Hx-CD20-406 Study Investigators. 2011. Ofatumumab is active in patients with fludarabine-refractory CLL irrespective of prior rituximab: results from the phase 2 international study. *Blood* 118: 5126–5129.
41. Scott, A. M., J. D. Wolchok, and L. J. Old. 2012. Antibody therapy of cancer. *Nat. Rev. Cancer* 12: 278–287.
42. Turatti, F., M. Figini, E. Balladore, P. Alberti, P. Casalini, J. D. Marks, S. Canevari, and D. Mezzanzanica. 2007. Redirected activity of human antitumor chimeric immune receptors is governed by antigen and receptor expression levels and affinity of interaction. *J. Immunother.* 30: 684–693.
43. Hudecek, M., M. T. Lupo-Stanghellini, P. L. Kosasih, D. Sommermeyer, M. C. Jensen, C. Rader, and S. R. Riddell. 2013. Receptor affinity and extracellular domain modifications affect tumor recognition by ROR1-specific chimeric antigen receptor T cells. *Clin. Cancer Res.* 19: 3153–3164.
44. Haso, W., D. W. Lee, N. N. Shah, M. Stetler-Stevenson, C. M. Yuan, I. H. Pastan, D. S. Dimitrov, R. A. Morgan, D. J. FitzGerald, D. M. Barrett, et al. 2013. Anti-CD22-chimeric antigen receptors targeting B-cell precursor acute lymphoblastic leukemia. *Blood* 121: 1165–1174.
45. Long, A. H., W. M. Haso, and R. J. Orentas. 2013. Lessons learned from a highly-active CD22-specific chimeric antigen receptor. *OncoImmunology* 2: e23621.
46. Casucci, M., B. Nicolis di Robilant, L. Falcone, B. Camisa, M. Norelli, P. Genovese, B. Gentner, F. Gullotta, M. Ponzoni, M. Bernardi, et al. 2013. CD44v6-targeted T cells mediate potent antitumor effects against acute myeloid leukemia and multiple myeloma. *Blood* 122: 3461–3472.
47. Tang, Y., J. Lou, R. K. Alpaugh, M. K. Robinson, J. D. Marks, and L. M. Weiner. 2007. Regulation of antibody-dependent cellular cytotoxicity by IgG intrinsic and apparent affinity for target antigen. *J. Immunol.* 179: 2815–2823.

OncoImmunology 4:2, e988098; February 2015; © 2015 Taylor & Francis Group, LLC

Oncolytic virus expressing RANTES and IL-15 enhances function of CAR-modified T cells in solid tumors

Nobuhiro Nishio[1] and Gianpietro Dotti[1,2,3,*]

[1]Center for Cell and Gene Therapy; Baylor College of Medicine; Houston, TX USA; [2]Department of Immunology; Baylor College of Medicine; Houston, TX USA; [3]Department of Medicine; Baylor College of Medicine; Houston, TX USA

Keywords: chimeric antigen receptor, GD2 antigen, IL-15, oncolytic virus, RANTES

We improved the migration and survival of chimeric antigen receptor (CAR)-modified T cells in solid tumors by combining CAR-T cells with an armed oncolytic virus. Local delivery of the chemokine RANTES and the cytokine IL-15 by the oncolytic virus enhanced the trafficking and persistence of the CAR-T cells, resulting in improved antitumor effects.

Adoptive transfer of T cells modified to express chimeric antigen receptors (CARs) has had clinical success in B-lymphocyte derived malignancies.[1] However, the clinical efficacy of CAR-T cells remains limited in solid tumors. This unfavorable outcome could be due to the insufficient migration of the infused T cells to the tumor site as well as to the immunosuppressive characteristics of the tumor environment that inhibits the effector function and proliferation of those few T cells that do reach the tumor.

CAR molecules have been further engineered to express co-stimulatory endodomains such as those derived from CD28 and tumor necrosis factor receptor superfamily member 9 (TNFRSF9, better known as 4–1BB) to promote T-cell proliferation and persistence upon encountering tumor cells. CD28 has proven effective in inducing CAR-T cell expansion in B-cell malignancies.[2,3] The incorporation of 4–1BB seems, however, to sustain more robust engraftment of CD19-specific CAR-T cells.[1] The incorporation of these co-stimulatory molecules in CARs targeting antigens expressed by solid tumors is anticipated to play a similarly crucial role.

CAR-T cells targeting CD19 seem to traffic physiologically to the bone marrow and lymph nodes, the primary sites of hematologic malignancies.[1,3] In addition, they can encounter both normal B lymphocytes and leukemic cells directly in the circulation. By contrast, T-cell migration remains a relevant problem for solid tumors. For instance, while tumor-infiltrating T lymphocytes (TILs) isolated from tumor biopsies and expanded *ex vivo* show dramatic migration to melanoma lesions, polyclonal T lymphocytes isolated from the peripheral blood and engineered with a T-cell receptor seem less effective. This disparity suggests that TILs and peripheral blood T cells may have a different pattern of homing molecules.[4] If the current CAR-T cell studies in solid tumors such as neuroblastoma, prostate cancer, pancreatic cancer, and mesothelioma reveal suboptimal migration, countermeasures to increase T-cell migration should be applied. Radiation or chemotherapy before the infusion of CAR-T cells in patients with solid tumors may favorably alter the pattern of T-cell migration. However, several preclinical models have already demonstrated that engineering CAR-T cells to express chemokine receptors that pair with chemokines produced by tumor cells is a strategy that can overcome the trafficking issue.[5]

When CAR-T cells reach the tumor bed in a sufficient number, tumor-associated inhibitory mechanisms are there to shutdown effective immune responses. In the treatment of small tumors, infusion of CAR-T cells after chemo or radiotherapy may partially reduce the impact of these inhibitory mechanisms. In addition, the recent introduction of antibodies that block T-cell inhibitory mechanisms, such as those abrogating the immune checkpoint CTLA-4 and PD1-PDL-1 pathways, shows great potential. Combinations of CAR-T cell therapies with these antibodies are anticipated to make a substantial difference in the near future. Similarly to the genetic modification of CAR-T cells aimed to express specific chemokine receptors, a plethora of genetic modifications has been proposed to increase the fitness of CAR-T cells within the tumor environment.[5] Some of the proposed modifications are currently under clinical investigation. Although each single modification seems to have specific beneficial effects, multiple mechanisms of resistance can be developed by tumors. T cells must accomplish simultaneously optimal trafficking and persistence, while also retaining an acceptable safety profile. In our recent study,[6] we developed an engineering strategy where an armed oncolytic virus (OV), another single biological agent, creates a favorable tumor environment for CAR-T cells.

OVs selectively infect, lyse and replicate in malignant cells without affecting non-malignant cells.[7] In addition, OVs

*Correspondence to: Gianpietro Dotti; Email: gdotti@bcm.edu
Submitted: 11/08/2014; Accepted: 11/12/2014
http://dx.doi.org/10.4161/21505594.2014.988098

have sufficient cargo capacity to insert multiple ectopic genes that can be beneficial for CAR-T cells. To investigate the effect of combining armed OV and CAR-T cells, we choose the neuroblastoma model since this tumor model has been previously targeted with CAR-T cells specific for the GD2 antigen.[8] We also selected an oncolytic adenovirus (Ad5Δ24) that has been extensively used in the clinic. We exploited the tropism of the OV for the tumor cells and engineered the virus to express both a chemokine and a growth factor for the T cells in order to achieve optimal trafficking of the engineered T cells to the tumor site and to generate a cytokine milieu that sustains T-cell growth and survival. Therefore, we armed Ad5Δ24 with chemokine (C-C motif) ligand 5 (CCL5, better known as RANTES) and interleukin (IL)-15 (**Fig. 1**), 2 immunomodulatory molecules selected on the basis of both clinical and preclinical data. RANTES is also a very potent chemokine and its receptors are maintained in T cells expanded *ex vivo*. Using this strategy, we anticipated that tumor cells, regardless of their tissue origin, could be forced to ectopically express RANTES after infection with the armed OV. We hypothesized that this strategy would promote efficient migration of the infused CAR-T cells without the need to select a chemokine/chemokine receptor pathway specific for each single tumor type. The cytokine IL-15 was selected for its multiple beneficial effects on T cells, and its overall ability to increase T-cell antitumor functions. In our experimental design, we demonstrated that neuroblastoma cells infected with Ad5Δ24.RANTES.IL-15 produce functional levels of RANTES and IL-15 both *in vitro* and *in vivo*, while the cytopathic effect of the virus is conserved. In a xenogenic mouse model, combined therapy with Ad5Δ24.RANTES.IL-15 and GD2.CAR-T cells significantly enhanced the survival of mice as compared with either of the monotherapies. Furthermore, both RANTES and IL-15 released by the armed OV were predominantly detected at the tumor site, rather than in the serum, indicating a preferential local expression of both factors. This strategy thereby circumvented the toxicities associated with systemic administration of cytokines.[6]

In conclusion, our preclinical study demonstrates that optimal trafficking and survival of CAR-T cells can be obtained in solid tumors by engineering an OV without compromising its cytopathic effect. In principle, similar genetic modifications can be applied to OVs such as vaccinia viruses and measles virus that have been administered intravenously into patients to treat metastatic tumors already.[9,10] Arming these viruses using this proposed strategy will not only favor the rapid recruitment of tumor-specific T cells to the primary lesions so infected but will also enhance the spread of the virus to other tumor cells, thus amplifying the therapeutic effect of the viruses. In addition, considering the cargo capacity of these viruses, other relevant genes that may further overcome inhibitory mechanisms can be accommodated.

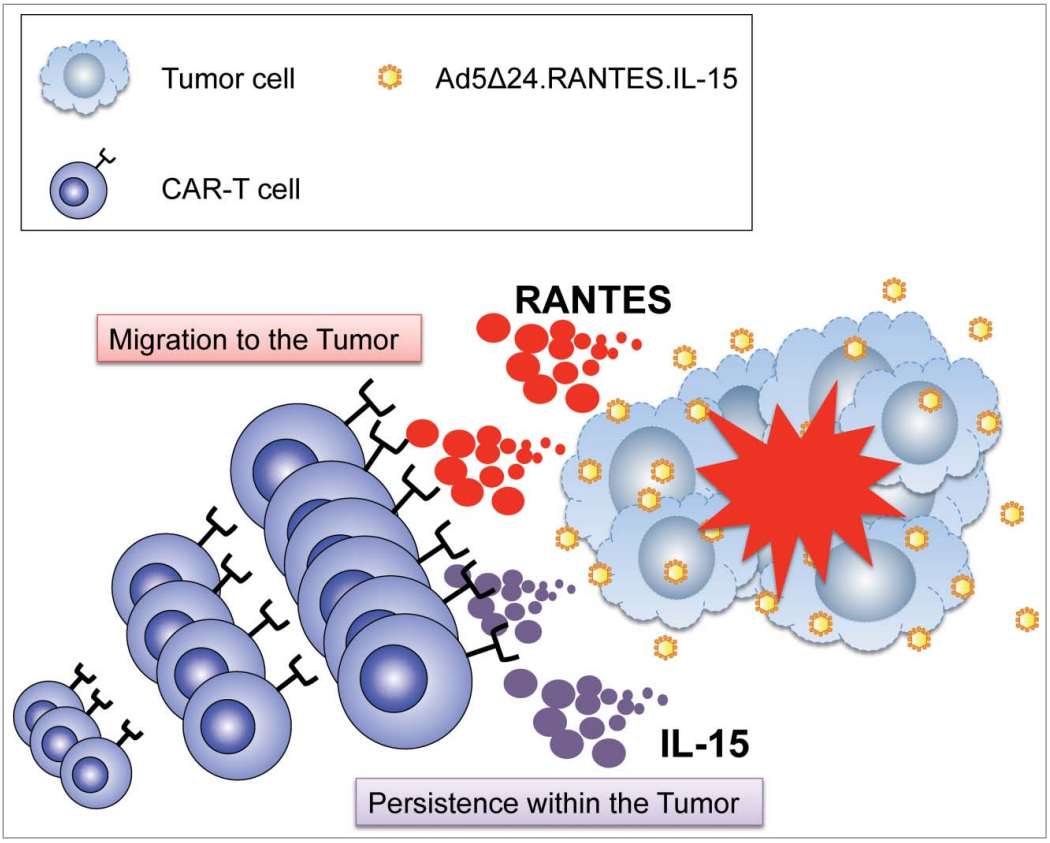

Figure 1. Combined therapy with CAR-T cells and Ad5Δ24 armed with RANTES and IL-15. Oncolytic viruses (OVs) selectively infect and lyse tumor cells, and then spread to neighboring tumor cells. Virus-infected tumor cells release both proteins and undergo apoptosis. The chemokine RANTES attracts circulating chimeric antigen receptor (CAR) modified T cells (CAR-T) to the virus infected tumor site and migrated CAR-T cells persist by virtue of interleukin 15 (IL-15) and specific antigen stimulation.

Disclosure of Potential Conflicts of Interest

No potential conflicts of interest were disclosed.

Acknowledgment

The authors would like to thank Catherine Gillespie for editing the invited auto commentary.

Funding

This work was supported in part by R01 CA142636 National Institute of Health-NCI and W81XWH-10–10425 Department of Defense and Technology/ Therapeutic Development Award.

References

1. Maude SL, Frey N, Shaw PA, Aplenc R, Barrett DM, Bunin NJ, Chew A, Gonzalez VE, Zheng Z, Lacey SF, et al. Chimeric antigen receptor T cells for sustained remissions in leukemia. N Engl J Med 2014; 371:1507-17; PMID:25317870; http://dx.doi.org/10.1056/NEJMoa1407222
2. Savoldo B, Ramos CA, Liu E, Mims MP, Keating MJ, Carrum G, Kamble RT, Bollard CM, Gee AP, Mei Z, et al. CD28 costimulation improves expansion and persistence of chimeric antigen receptor-modified T cells in lymphoma patients. J Clin Invest 2011; 121:1822-6; PMID:21540550; http://dx.doi.org/10.1172/JCI46110
3. Brentjens RJ, Davila ML, Riviere I, Park J, Wang X, Cowell LG, Bartido S, Stefanski J, Taylor C, Olszewska M, et al. CD19-targeted T cells rapidly induce molecular remissions in adults with chemotherapy-refractory acute lymphoblastic leukemia. Sci Transl Med 2013; 5:177ra38; PMID:23515080; http://dx.doi.org/10.1126/scitranslmed.3005930
4. Johnson LA, Morgan RA, Dudley ME, Cassard L, Yang JC, Hughes MS, Kammula US, Royal RE, Sherry RM, Wunderlich JR, et al. Gene therapy with human and mouse T-cell receptors mediates cancer regression and targets normal tissues expressing cognate antigen. Blood 2009; 114:535-46; PMID:19451549; http://dx.doi.org/10.1182/blood-2009-03-211714
5. Dotti G, Gottschalk S, Savoldo B, Brenner MK. Design and development of therapies using chimeric antigen receptor-expressing T cells. Immunol Rev 2014; 257:107-26; PMID:24329793; http://dx.doi.org/10.1111/imr.12131
6. Nishio N, Diaconu I, Liu H, Cerullo V, Caruana I, Hoyos V, Bouchier-Hayes L, Savoldo B, Dotti G. Armed oncolytic virus enhances immune functions of chimeric antigen receptor-modified T cells in solid tumors. Cancer Res 2014; 74:5195-205; PMID:25060519; http://dx.doi.org/10.1158/0008-5472.CAN-14-0697
7. Parato KA, Senger D, Forsyth PA, Bell JC. Recent progress in the battle between oncolytic viruses and tumours. Nat Rev Cancer 2005; 5:965-76; PMID:16294217; http://dx.doi.org/10.1038/nrc1750
8. Pule MA, Savoldo B, Myers GD, Rossig C, Russell HV, Dotti G, Huls MH, Liu E, Gee AP, Mei Z, et al. Virus-specific T cells engineered to coexpress tumor-specific receptors: persistence and antitumor activity in individuals with neuroblastoma. Nat Med 2008; 14:1264-70; PMID:18978797; http://dx.doi.org/10.1038/nm.1882
9. Heo J, Reid T, Ruo L, Breitbach CJ, Rose S, Bloomston M, Cho M, Lim HY, Chung HC, Kim CW, et al. Randomized dose-finding clinical trial of oncolytic immunotherapeutic vaccinia JX-594 in liver cancer. Nat Med 2013; 19:329-36; PMID:23396206; http://dx.doi.org/10.1038/nm.3089
10. Russell SJ, Federspiel MJ, Peng KW, Tong C, Dingli D, Morice WG, Lowe V, O'Connor MK, Kyle RA, Leung N, et al. Remission of disseminated cancer after systemic oncolytic virotherapy. Mayo Clin Proc 2014; 89:926-33; PMID:24835528; http://dx.doi.org/10.1016/j.mayocp.2014.04.003

Biol Blood Marrow Transplant 21 (2015) 517–525

Biology of Blood and Marrow Transplantation

journal homepage: www.bbmt.org

Comparison of Cord Blood Transplantation with Unrelated Bone Marrow Transplantation in Patients Older than Fifty Years

Masatsugu Tanaka [1,*], Koichi Miyamura [2], Seitaro Terakura [3], Kiyotoshi Imai [4], Naoyuki Uchida [5], Hiroatsu Ago [6], Toru Sakura [7], Tetsuya Eto [8], Kazuteru Ohashi [9], Takahiro Fukuda [10], Shuichi Taniguchi [5], Shinichiro Mori [11], Tokiko Nagamura-Inoue [12], Yoshiko Atsuta [13], Shin-ichiro Okamoto [14]

[1] *Department of Hematology, Kanagawa Cancer Center, Yokohama, Japan*
[2] *Department of Hematology, Japanese Red Cross Nagoya First Hospital, Nagoya, Japan*
[3] *Department of Hematology and Oncology, Nagoya University Graduate School of Medicine, Nagoya, Japan*
[4] *Department of Hematology, Sapporo Hokuyu Hospital, Sapporo, Japan*
[5] *Department of Hematology, Toranomon Hospital, Tokyo, Japan*
[6] *Department of Hematology and Oncology, Shimane Prefectural Central Hospital, Izumo, Japan*
[7] *Leukemia Research Center, Saiseikai Maebashi Hospital, Maebashi, Japan*
[8] *Department of Hematology, Hamanomachi Hospital, Fukuoka, Japan*
[9] *Division of Hematology, Tokyo Metropolitan Cancer and Infectious Disease Center Komagome Hospital, Tokyo, Japan*
[10] *Division of Hematopoietic Stem Cell Transplantation, National Cancer Center Hospital, Tokyo, Japan*
[11] *Division of Hematology and Oncology, St. Luke's International Hospital, Tokyo, Japan*
[12] *Department of Cell Processing and Transfusion, The Institute of Medical Science, The University of Tokyo, Tokyo, Japan*
[13] *Department of Hematopoietic Stem Cell Transplantation Data Management, Nagoya University School of Medicine, Nagoya, Japan*
[14] *Division of Hematology, Department of Medicine, Keio University School of Medicine, Tokyo, Japan*

Article history:
Received 30 June 2014
Accepted 30 November 2014

Key Words:
Unrelated bone marrow transplantation
Umbilical cord blood transplantation
Elderly patients

A B S T R A C T

We retrospectively compared the transplantation outcomes for patients 50 years or older who received umbilical cord blood transplantation (UCBT) with those who received unrelated bone marrow transplantation (UBMT) for hematologic malignancies. A total of 1377 patients who underwent transplantation between 2000 and 2009 were included: 516 received 8/8 HLA allele-matched UBMT, 295 received 7/8 HLA allele-matched UBMT, and 566 received 4/6 to 6/6 HLA-matched UCBT. Adjusted overall survival (OS) was significantly lower in those who underwent UCBT than those who underwent 8/8 HLA–matched UBMT but was similar to that of 7/8 HLA–matched UBMT (the 2-year OS after 8/8 HLA–matched UBMT, 7/8 HLA–matched UBMT, and UCBT were 49% [95% confidence interval (CI), 45% to 55%], 38% [95% CI, 32% to 45%], and 39% [95% CI, 34% to 43%], respectively). However, adjusted OS was similar between 8/8 HLA–matched UBMT and UCBT receiving $\geq .84 \times 10^5$ $CD34^+$ cells/kg among those with acute myeloid leukemia and those with acute lymphoblastic leukemia (the 2-year OS was 49% [95% CI, 43% to 55%], and 49% [95% CI, 41% to 58%], respectively). These data suggest that UCB is a reasonable alternative donor/stem cell source for elderly patients with similar outcomes compared with UBM from 8/8 HLA–matched unrelated donors when the graft containing $\geq .84 \times 10^5$ $CD34^+$ cells/kg is available.

INTRODUCTION

Allogeneic hematopoietic stem cell transplantation (HSCT) is a curative treatment for patients with high-risk hematologic malignancies. The frequency of adverse cytogenetic abnormalities is higher in elderly patients with acute myeloid leukemia (AML) or acute lymphoblastic leukemia (ALL) than in younger patients, and overall survival (OS) after intensive chemotherapy in elderly patients is shorter than that in younger patients [1,2]. Inductions of reduced-intensity and nonmyeloablative stem cell transplantations allow elderly patients to receive allogeneic HSCT [3,4], and these patients have increasingly received this type of transplantation [5]. Only approximately 30% of patients

Financial disclosure: See Acknowledgments on page 524.

* Correspondence and reprint requests: Dr. Masatsugu Tanaka, Department of Hematology, Kanagawa Cancer Center, 2-3-2 Nakao, Asahi-ku, Yokohama 241-8515, Japan.
E-mail address: tanakam@kcch.jp (M. Tanaka).

http://dx.doi.org/10.1016/j.bbmt.2014.11.685
1083-8791/

have an HLA-identical sibling, and some elderly patients have siblings who cannot serve as a donor because of their age or underlying comorbidities; in such cases, an alternative donor is needed.

HLA-matched unrelated bone marrow or peripheral blood stem cells have been used as an alternative to an HLA-identical sibling donor. Umbilical cord blood has been used more frequently over the past decade, and several studies and meta-analyses have compared the outcomes of umbilical cord blood transplantation (UCBT) with that of unrelated bone marrow transplantation (UBMT) or unrelated peripheral blood stem cell transplantation (UPBSCT) [6-15]. However, the findings of those reports varied, and most of those studies included a small number of elderly patients. To the best of our knowledge, there has been no report that compared the outcomes of elderly patients who received UCBT with those who received UBMT or UPBSCT. Therefore, the main objective of this study was to compare the outcomes of patients 50 years or older who received UCBT with those who received UBMT using the Japanese nationwide registry data.

METHODS

Data Collection

Data regarding transplantations were extracted from the Transplant Registry Unified Management Program system of the Japan Society for Hematopoietic Cell Transplantation [16]. A total of 171 transplantation centers performed unrelated HSCT for adults and reported transplantation data to Japan Society for Hematopoietic Cell Transplantation between 2000 and 2009. All patients gave written informed consent at each transplantation center. The trial was conducted in accordance with the Declaration of Helsinki.

Patients with acute leukemia or myelodysplastic syndrome (MDS) who were 50 years or older and who received unrelated HSCT between 2000 and 2009 were included. Because the bone marrow was exclusively harvested from volunteer unrelated donors in Japan, cases of peripheral blood stem cell transplantation were not included in this analysis. Only 7 patients received double UCBT; therefore, these patients were also excluded. For the bone marrow recipients, recipients whose HLA matched 8/8 or 7/8 with their donor at the allelic level for HLA-A, HLA-B, HLA-C, and HLA-DRB1 were included. For UCBT, recipients whose HLA matched 4/6 to 6/6 with their donor at the antigen level for HLA-A and HLA-B and at the allelic level for HLA-DRB1, and who received a single unit of umbilical cord blood containing 2.0×10^7 or more total nucleated cells per kilogram of recipient's body weight at cryopreservation were included. Patients who had previously received autologous or allogeneic transplantation were excluded.

A myeloablative conditioning (MAC) regimen was defined as a total busulfan dose of more than 8 mg/kg, total melphalan dose of more than 140 mg/kg, fractionated total body irradiation (TBI) of 8 Gy or more, or single TBI of 5 Gy or more [17,18]. Other conditioning regimen was defined as reduced-intensity conditioning (RIC). Acute leukemia in the first complete remission (CR), refractory anemia with or without ringed sideroblasts, and refractory cytopenia with multilineage dysplasia for MDS were defined as early phase; acute leukemia in the second or subsequent CR were defined as intermediate phase; and all other statuses were defined as advanced phase. The karyotype at diagnosis for AML, ALL, and MDS were classified as previously reported [2,19,20]. The year of transplantation was divided into 2 groups: 2000 to 2004 was defined as the early period and 2005 to 2009 was defined as the recent period. Neutrophil recovery was defined as the first 3 consecutive days in which absolute neutrophil counts rose to greater than or equal to 500/mm^3. Acute graft-versus-host disease (GVHD) was evaluated based on standard criteria [21]. Chronic GVHD was defined according to the classical classification [22]. Relapse was defined as disease recurrence detected by hematological examination or detected by cytogenetic or molecular examination and requiring any treatment. Patients who did not obtain CR after HSCT were defined as patients who had a relapse the next day after HSCT. Nonrelapse mortality (NRM) was defined as death without relapse. OS was defined as the survival time from the date of transplantation to death from any cause or the last follow-up.

Statistical Analysis

The demographic factors and disease characteristics were compared between patients who underwent transplantation with 8/8 HLA–matched unrelated bone marrow, 7/8 HLA–matched bone marrow, and umbilical cord blood using Fisher's exact test for the categorical data and the Mann-Whitney U test for the continuous variables. OS was calculated from the date of transplantation to death from any cause or last follow-up and was estimated by the Kaplan-Meier method. Cox proportional hazards regression model was used for the multivariate analyses. Adjusted comparison of the stem cell source on OS was performed using the Cox proportional hazards regression model. Gray's test was employed for the comparison of cumulative incidence curves for relapse, NRM, neutrophil and platelet recoveries, and GVHD [23]. NRM and relapse were the competing event for each other. For neutrophil and platelet recovery, death before neutrophil or platelet recovery was the competing event; for GVHD, death without GVHD was the competing event. Fine and Gray's proportional hazard regression model was employed for multivariate analyses with competing risks [24]. Multivariate analyses to compare the effect of stem cell source on transplantation outcomes were performed with the consideration of other significant clinical variables in the final models, which were built with the significant variables ($P < .10$) from the univariate analysis, which were then deleted in a stepwise fashion from the model when a variable was not statistically significant ($P > .05$). The stem cell source was added in the final model. The following variables were considered: patient age at transplantation, sex, primary disease (AML versus ALL versus MDS), karyotype at diagnosis (favorable versus intermediate versus adverse), disease status at transplantation (early phase versus intermediate phase versus advanced phase), year of transplantation (early period versus recent period), conditioning regimen (MAC versus RIC), use of TBI, and GVHD prophylaxis (cyclosporine alone versus cyclosporine and other agent versus tacrolimus alone versus tacrolimus and other agent versus other). All tests were 2-sided, and $P < .05$ was considered to indicate statistical significance. Analyses were performed with EZR version 1.20 (Saitama Medical Center, Jichi Medical University) [25], which is a graphical user interface for R version 3.0.2 (R Development Core Team, Vienna, Austria).

RESULTS

Patients and Transplantation Characteristics

Patients and transplantation characteristics are shown in Table 1. A total of 1377 patients were included in this analysis, and of those, 516 patients received 8/8 HLA allele-matched UBMT, 295 patients received 7/8 HLA allelic-matched UBMT, and 566 patients underwent transplantation from 4/6 to 6/6 HLA–matched UCBT. The UCBT recipients were significantly older than the 8/8 or 7/8 HLA–matched UBMT recipients ($P < .001$), and more UCBT recipients underwent RIC or nonmyeloablative transplantation ($P < .001$) and received a TBI-containing conditioning regimen than did the 8/8 or 7/8 HLA–matched UBMT recipients ($P < .001$). More UCBT recipients had advanced phase disease ($P < .001$). Female donor to male recipient transplantation was included in UCBT more than in UBMT ($P < .001$). Compared with those receiving UBMT, more UCBT recipients had AML ($P < .001$) and received GVHD prophylaxis with a single-agent regimen ($P < .001$). The distribution of karyotype at diagnosis was similar (Supplemental Tables 1–3). The distribution of recipients' sex and year of transplantation were similar among the 3 groups. The median duration of follow-up for the surviving patients who underwent transplantation with 8/8 HLA–matched UBMT, 7/8 HLA–matched UBMT, and 4/6 to 6/6 HLA-matched UCBT was 23.7 months (range, 1.8 to 125.2 months), 18.6 months (range, 1.6 to 94.0 months), and 22.3 months (range, .1 to 107.5 months), respectively.

Hematopoietic Recovery

The median time from transplantation to neutrophil recovery in patients who underwent 8/8 HLA–matched UBMT, 7/8 HLA–matched UBMT, and 4/6 to 6/6 HLA–matched UCBT was 17 days (range, 1 to 100 days), 17 days (range, 4 to 169 days), and 24 days (range, 0 to 95 days), respectively. Neutrophil recovery was faster in recipients with early phase disease or intermediate phase disease than in those with advanced phase disease ($P < .001$). MAC was an independent negative predictor for neutrophil engraftment ($P = .007$). The

Table 1
Patients, Disease, and Transplantation Characteristics

Characteristic	Total	8/8 HLA–Matched Bone Marrow	7/8 HLA–Matched Bone Marrow	Umbilical Cord Blood	*P* Value
Number	1377	516	295	566	
Sex (male)	816 (59%)	310 (60%)	188 (64%)	318 (56%)	.091
Age, median (range), yr	57 (50-82)	56 (50-70)	57 (50-71)	58 (50-82)	<.001
50-59	892 (65%)	376 (73%)	198 (67%)	318 (56%)	
60-69	468 (34%)	138 (27%)	96 (33%)	234 (41%)	
70 or older	17 (1%)	2 (<1%)	1 (<1%)	14 (3%)	
Sex matching					<.001
Female donor to male recipient	1030 (75%)	73 (14%)	67 (23%)	153 (27%)	
Others	293 (21%)	443 (86%)	227 (77%)	360 (64%)	
Unknown	54 (4%)	0 (0%)	1 (<1%)	53 (9%)	
Body weight, median (range), kg	56 (32.0-102.4)	58.5 (32.0-102.4)	58.9 (35.1-92.0)	54.0 (32.0-86.0)	<.001
Disease					<.001
AML	902 (65%)	314 (61%)	180 (61%)	408 (72%)	
ALL	244 (18%)	96 (19%)	47 (16%)	101 (18%)	
MDS	231 (17%)	106 (20%)	68 (23%)	57 (10%)	
Disease status at transplantation					<.001
Early phase	471 (34%)	223 (43%)	94 (32%)	154 (27%)	
Intermediate phase	221 (16%)	82 (16%)	58 (20%)	81 (14%)	
Advanced phase	685 (50%)	211 (41%)	143 (48%)	331 (59%)	
Year of transplantation					
2000-2004	343 (25%)	128 (25%)	74 (25%)	141 (25%)	1
2005-2009	1034 (75%)	388 (75%)	221 (75%)	425 (75%)	
Conditioning regimen					
Myeloablative	653 (47%)	291 (56%)	147 (50%)	215 (38%)	<.001
CY + TBI (≥8 Gy)	174 (12%)	79 (15%)	43 (15%)	52 (9%)	
CY + TBI (≥8 Gy) + other	135 (10%)	46 (9%)	19 (6%)	70 (13%)	
BU + CY	110 (8%)	64 (12%)	33 (12%)	13 (2%)	
FLU + BU (>8 mg/kg)	44 (3%)	34 (7%)	5 (2%)	5 (1%)	
FLU + BU (>8 mg/kg) + TBI (<8 Gy)	40 (3%)	14 (3%)	7 (2%)	19 (3%)	
FLU + MEL (>140 mg/m^2)	57 (4%)	28 (5%)	20 (7%)	9 (2%)	
Other TBI-based regimen	66 (5%)	19 (4%)	13 (4%)	34 (6%)	
Other BU-based regimen	27 (2%)	7 (1%)	7 (2%)	13 (2%)	
RIC/NMA	712 (52%)	217 (42%)	145 (49%)	350 (62%)	
FLU + BU (≤8 mg/kg)	25 (2%)	5 (1%)	5 (2%)	15 (3%)	
FLU + BU (≤8 mg/kg) + TBI (<8 Gy)	206 (15%)	91 (17%)	58 (20%)	57 (10%)	
FLU + BU (≤8 mg/kg) + MEL (≤140 mg/m^2)	26 (2%)	13 (3%)	5 (2%)	8 (1%)	
FLU + BU (≤8 mg/kg) + other	33 (2%)	12 (2%)	16 (5%)	5 (1%)	
FLU + MEL (≤140 mg/m^2)	64 (5%)	33 (6%)	16 (5%)	15 (3%)	
FLU + MEL (≤140 mg/m^2) + TBI (<8 Gy)	219 (16%)	33 (6%)	26 (9%)	160 (28%)	
FLU + MEL (≤140 mg/m^2) + TBI (<8 Gy) + other	20 (2%)	3 (1%)	1 (<1%)	16 (3%)	
FLU + CY + TBI (<8 Gy)	56 (4%)	3 (1%)	2 (1%)	51 (9%)	
Other regimen including TBI (<8 Gy)	33 (2%)	13 (3%)	10 (3%)	10 (2%)	
Other regimen not including TBI (<8 Gy)	30 (2%)	11 (2%)	6 (2%)	13 (2%)	
Unknown	12 (1%)	8 (2%)	3 (1%)	1 (<1%)	
TBI-containing conditioning regimen	962 (70%)	306 (59%)	184 (62%)	472 (83%)	<.001
Addition of ATG to conditioning regimen	46 (3%)	17 (3%)	19 (6%)	10 (2%)	.001
GVHD prophylaxis					
CyA + other	370 (27%)	129 (25%)	52 (18%)	189 (33%)	<.001
CyA alone	68 (5%)	5 (1%)	3 (1%)	60 (11%)	
TAC + other	775 (56%)	359 (70%)	226 (76%)	190 (33%)	
TAC alone	138 (10%)	15 (3%)	11 (4%)	112 (20%)	
Others	13 (1%)	7 (1%)	3 (1%)	3 (1%)	
None	13 (1%)	1 (<1%)	0 (0%)	12 (2%)	
Total cell dose (range, ×10^7/kg)				2.56 (2.00-5.62)	
CD34$^+$ cell dose (range, ×10^5/kg)				.83 (.01-14.02)	
HLA-A, B, DR antigen level					
Matched (6/6)		516 (100%)	295 (100%)	46 (8%)	
One-antigen mismatched (5/6)		0	0	159 (28%)	
Two-antigen mismatched (4/6)		0	0	361 (64%)	

HLA indicates human leukocyte antigen; TBI, total body irradiation; GVHD, graft-versus-host disease; CY, cyclophosphamide; BU, busulfan; FLU, fludarabine; MEL, melphalan; NMA, nonmyeloablative; ATG, antithymocyte globulin; CyA, cyclosporine A; TAC, tacrolimus.

probability of neutrophil recovery by day 50 was significantly lower in recipients of 4/6 to 6/6 HLA–matched UCBT (72% [95% confidence interval (CI), 68% to 75%]) than in those of 8/8 HLA–matched UBMT (95% [95% CI, 92% to 96%]) or 7/8 HLA–matched UBMT (90% [95% CI, 85% to 93%]). On multivariate analysis, the 4/6 to 6/6 HLA–matched UCBT was an independent negative predictor for neutrophil engraftment when compared with the 8/8 HLA–matched UBMT (hazard ratio [HR], .43 [95% CI, .38 to .50]; $P < .001$) and the 7/8 HLA–matched UBMT (HR, .47 [95% CI, .40 to .56]; $P < .001$) (Table 2).

The probability of platelet recovery by day 180 was also significantly lower in the 4/6 to 6/6 HLA–matched UCB recipients (54% [95% CI, 50% to 58%]) than in those who received the 8/8 HLA–matched UBMT (83% [95% CI, 79% to 86%]) or the 7/8 HLA–matched UBMT (75% [95% CI, 70% to 80%]). The median times from transplantation to platelet recovery in the recipients of 8/8 HLA–matched

Table 2
Multivariate Analysis of Transplantation Outcomes

Outcome	HR (95% CI)	*P* Value
Overall survival*	Overall	<.001
4/6-6/6–Matched UCB versus 8/8 HLA–matched UBM	1.47 (1.24-1.74)	<.001
4/6-6/6–Matched UCB versus 7/8 HLA–matched UBM	1.03 (.86-1.24)	.75
Relapse†	Overall	.02
4/6-6/6–Matched UCB versus 8/8 HLA–matched UBM	1.35 (1.05-1.74)	.02
4/6-6/6–Matched UCB versus 7/8 HLA–matched UBM	1.18 (.89-1.56)	.26
NRM‡	Overall	.013
4/6-6/6–Matched UCB versus 8/8 HLA–matched UBM	1.32 (1.06-1.64)	.013
4/6-6/6–Matched UCB versus 7/8 HLA–matched UBM	.98 (.77-1.25)	.88
Neutrophil recovery§	Overall	<.001
4/6-6/6–Matched UCB versus 8/8 HLA–matched UBM	.42 (.37-.48)	<.001
4/6-6/6–Matched UCB versus 7/8 HLA–matched UBM	.47 (.40-.55)	<.001
Platelet recovery‖	Overall	<.001
4/6-6/6–Matched UCB versus 8/8 HLA–matched UBM	.36 (.30-.42)	<.001
4/6-6/6–Matched UCB versus 7/8 HLA–matched UBM	.44 (.37-.53)	<.001
Grade II-IV acute GVHD¶	Overall	.36
4/6-6/6–Matched UCB versus 8/8 HLA–matched UBM	1.10 (.89-1.36)	.38
4/6-6/6–Matched UCB versus 7/8 HLA–matched UBM	.69 (.56-.87)	.001
Extensive chronic GVHD#	Overall	.022
4/6-6/6–Matched UCB versus 8/8 HLA–matched UBM	.65 (.46-.92)	.015
4/6-6/6–Matched UCB versus 7/8 HLA–matched UBM	.56 (.38-.82)	.003

UCB indicates umbilical cord blood; UBM, unrelated bone marrow.

* For overall survival, hazard ratio is adjusted with recipient age, sex, primary disease, disease status at transplantation, and year of transplantation.

† For relapse, hazard ratio is adjusted with primary disease, the use of TBI, the use of antithymocyte globulin, and disease status at transplantation.

‡ For NRM, hazard ratio is adjusted with recipient sex, the use of TBI, and year of transplantation.

§ For neutrophil recovery, hazard ratio is adjusted with disease status at transplantation, conditioning regimen, the use of TBI, and GVHD prophylaxis.

‖ For platelet recovery, hazard ratio is adjusted with recipient sex, disease status at transplantation, the use of TBI, year of transplantation, and GVHD prophylaxis.

¶ For grade II to IV acute GVHD, hazard ratio is adjusted with age, disease status at transplantation, and the use of TBI.

For extensive chronic GVHD, hazard ratio is adjusted with recipient sex.

UBMT, 7/8 HLA–matched UBMT, and 4/6 to 6/6 HLA–matched UCBT were 29 days (range, 1 to 228 days), 32 days (range, 1 to 323 days), and 66 days (range, 8 to 230 days), respectively. Platelet recovery was also faster in recipients with early phase disease or intermediate phase disease than in those with advanced phase disease in ($P < .001$). A 4/6 to 6/6 HLA–matched UCBT was a strong independent negative predictor for platelet engraftment within the multivariate analysis (versus 8/8 HLA–matched UBMT, HR, .36 [95% CI, .30 to .42]; $P < .001$, versus 7/8 HLA–matched UBMT, HR, .44 [95% CI, .37 to .53]; $P < .001$, respectively) (Table 2). MAC was not a negative predictor for platelet engraftment.

GVHD

The cumulative incidence of grade II to IV acute GVHD by 100 days after transplantation was lower in recipients of an 8/8 HLA–matched UBMT (34% [95% CI, 30% to 39%]) than in recipients of a 7/8 HLA–matched UBMT (50% [95% CI, 44% to 56%]) or a 4/6 to 6/6 HLA–matched UCBT (41% [95% CI, 36% to 45%]). More recipients who received a TBI-containing regimen experienced grade II to IV acute GVHD by day 100 than did those who received a non-TBI regimen (43% [95% CI, 40% to 46%] versus 34% [95% CI, 29% to 39%], $P = .001$). The 4/6 to 6/6 HLA–matched UCBT recipients had a similar risk of grade II to IV acute GVHD to the 8/8 HLA–matched UBMT recipients within the multivariate analysis (HR, 1.10 [95% CI, .89 to 1.36]; $P = .38$) (Table 2). However, the 4/6 to 6/6 HLA–matched UCBT recipients had a significantly lower risk of grade II to IV acute GVHD than did the 7/8 HLA–matched UBMT recipients (HR, .69 [95% CI, .56 to .87]; $P = .001$) (Table 2).

The cumulative incidence of the extensive type of chronic GVHD by 2 years after transplantation was lower in recipients of the 4/6 to 6/6 HLA–matched UCB (15% [95% CI, 11% to 19%]) than in those who received the 8/8 HLA–matched UBMT or 7/8 HLA–matched UBMT (23% [95% CI, 19% to 27%] and 25% [95% CI, 20% to 32%], respectively). The same relationship was observed when performing the multivariate analysis (versus 8/8 HLA–matched UBMT, HR, .65 [95% CI, .46 to .92]; $P = .015$, versus 7/8 HLA–matched UBMT, HR, .56 [95% CI, .38 to .82]; $P = .003$, respectively) (Table 2).

Relapse

The cumulative incidence of relapse by 2 years was significantly higher in patients receiving the 4/6 to 6/6 HLA–matched UCBT (26% [95% CI, 22% to 30%]) than in those who received the 8/8 HLA–matched UBMT (18% [95% CI, 15% to 22%]) or those who received the 7/8 HLA–matched UBMT (21% [95% CI, 16% to 26%]). However, according to disease status at transplantation, the relapse rate by 2 years after the 8/8 HLA–matched UBMT, 7/8 HLA–matched UBMT, and 4/6 to 6/6 HLA–matched UCBT were not statistically different regardless of disease status at transplantation (8/8 HLA–matched UBMT, 7/8 HLA–matched UBMT, and 4/6 to 6/6 HLA–matched UCBT; early phase disease, 11% [95% CI, 7% to 16%], 15% [95% CI, 8% to 23%], and 19% [95% CI, 12% to 26%]; intermediate phase disease, 22% [95% CI, 13% to 32%], 26% [95% CI, 15% to 39%], and 17% [95% CI, 10% to 27%]; advanced phase disease, 35% [95% CI, 28% to 42%], 36% [95% CI, 28% to 44%], and 43% [95% CI, 38% to 49%], respectively) (Figure 1A–C). On multivariate analysis, the 4/6 to 6/6 HLA–matched UCBT recipients had a significantly higher risk of relapse than did the recipients of the 8/8 HLA–matched UCBT (HR, 1.35 [95% CI, 1.05 to 1.74]; $P = .02$) and had a similar risk to that of the 7/8 HLA–matched UBMT recipients (HR, 1.18 [95% CI, .89 to 1.56]; $P = .26$) (Table 2).

According to primary disease, the cumulative incidence of relapse after the 4/6 to 6/6 HLA–matched UCBT was higher than that after the 8/8 HLA–matched UBMT only in MDS patients and was similar both in AML patients and in ALL patients (Supplemental Table 4).

According to conditioning regimen, the cumulative incidence of relapse after the 4/6 to 6/6 HLA–matched UCBT was higher than that after the 8/8 HLA–matched UBMT only in recipients of MAC (Supplemental Table 5). Among the patients who received RIC, the cumulative incidence of relapse after the 4/6 to 6/6 HLA–matched UCBT was significantly higher than that after the UBMT in recipients without extensive chronic GVHD. However, the cumulative incidence of relapse after the 4/6 to 6/6

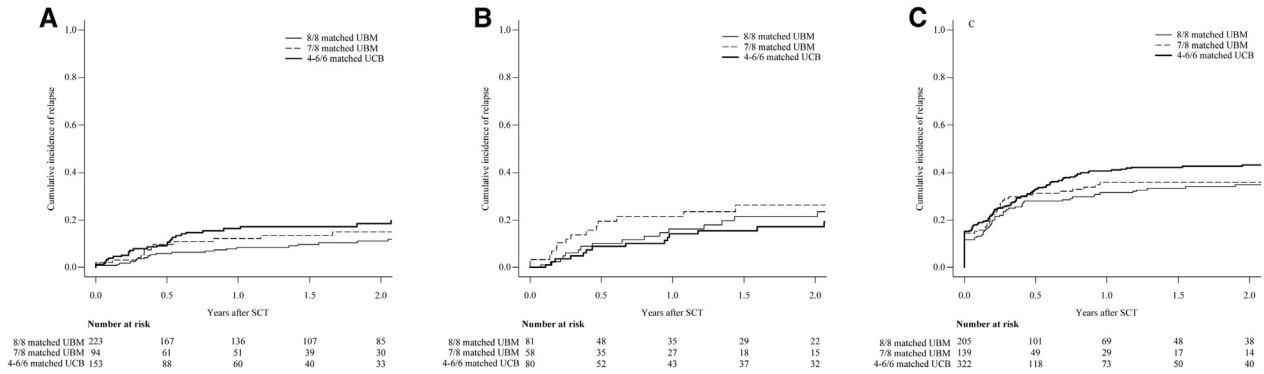

Figure 1. Cumulative incidence of relapse in patients with early phase disease, in those with intermediate phase disease, and in those with high-risk disease according to hematopoietic stem cell source and donor-recipient HLA match. (A) The cumulative incidences of relapse in patients with early phase disease by 2 years after an 8/8 HLA–matched unrelated bone marrow transplantation (UBMT), a 7/8 HLA–matched UBMT, and a 4/6 to 6/6 HLA–matched umbilical cord blood transplantation (UCBT) were 11% (95% CI, 7% to 16%), 15% (95% CI, 8% to 23%), and 19% (95% CI, 12% to 26%), respectively. (B) The cumulative incidences of relapse in patients with intermediate phase disease by 2 years after an 8/8 HLA–matched UBMT, a 7/8 HLA–matched UBMT, and a 4/6 to 6/6 HLA–matched UCBT were 22% (95% CI, 13% to 32%), 26% (95% CI, 15% to 39%), and 17% (95% CI, 10% to 27%), respectively. (C) The cumulative incidences of relapse in patients with intermediate phase disease by 2 years after an 8/8 HLA–matched UBMT, a 7/8 HLA–matched UBMT, and a 4/6 to 6/6 HLA–matched UCBT were 35% (95% CI, 28% to 42%), 36% (95% CI, 28% to 44%), and 43% (95% CI, 38% to 49%), respectively.

HLA–matched UCBT was not statistically different from that after UBMT among the recipients of MAC (Supplemental Figure 1).

NRM

The 2-year cumulative incidences of NRM after the 8/8 HLA–matched UBMT, 7/8 HLA–matched UBMT, and 4/6 to 6/6 HLA–matched UCBT were 32% (95% CI, 27% to 36%), 40% (95% CI, 33% to 46%), and 38% (95% CI, 34% to 43%), respectively. Among patients with early phase disease, the cumulative incidence of NRM at 2 years after the 8/8 HLA–matched UBMT was significantly lower than that after the 7/8 HLA–matched UBMT or 4/6 to 6/6 HLA–matched UCBT (25% [95% CI, 19% to 32%], 35% [95% CI, 25% to 45%], and 37% [95% CI, 29% to 46%]) (Figure 2A). Among patients with intermediate phase disease or advanced phase disease, NRM by 2 years was not statistically different among 3 groups (8/8 HLA–matched UBMT, 7/8 HLA–matched UBMT, and 4/6 to 6/6 HLA–matched UCBT; intermediate phase disease; 32% [95% CI, 31% to 43%], 27% [95% CI, 16% to 40%], and 28% [95% CI, 18% to 38%]; advanced phase disease, 34% [295% CI, 7% to 41%], 41% [95% CI, 32% to 50%], and 36% [95% CI, 30% to 41%], respectively) (Figure 2B,C). On multivariate analysis, the 4/6 to 6/6 HLA–matched UCBT recipients had a higher risk of NRM than the 8/8 HLA–matched UBMT recipients (HR, 1.32 [95% CI, 1.06 to 1.64]; $P = .013$); however, they had a similar risk to the 7/8 HLA–matched UBMT recipients (HR, .98 [95% CI, .77 to 1.25]; $P = .88$) (Table 2). According to primary disease, NRM by 2 years after the 4/6 to 6/6 HLA–matched UCBT was likely higher than that after the 8/8 HLA–matched UBMT only among patients with MDS; however, the difference was not significant regardless of primary diseases (Supplemental Table 4). On multivariate analysis of subgroup analysis according to conditioning regimen, NRM after the 8/8 HLA–matched UBMT was significantly lower than that after the 7/8 HLA–matched UBMT and 4/6 to 6/6 HLA–matched UCBT only among recipients of RIC (Supplemental Table 5).

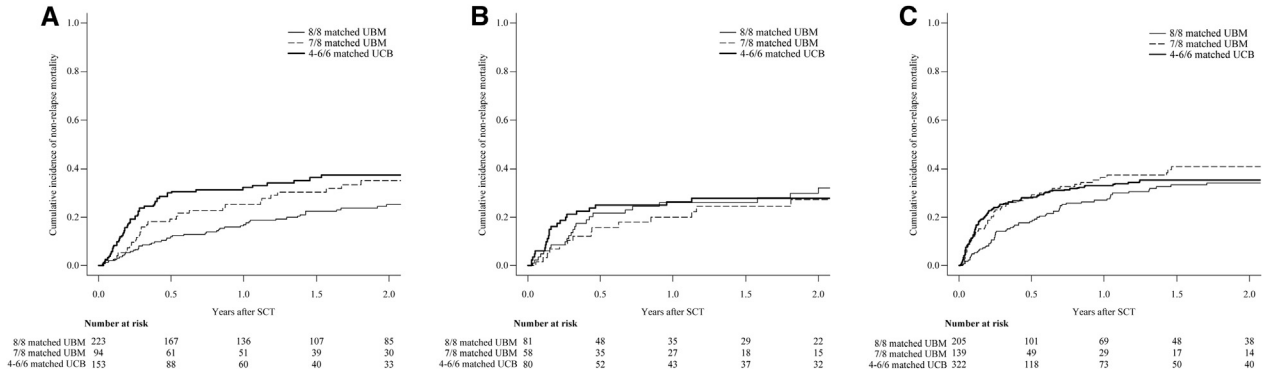

Figure 2. Cumulative incidence of NRM in patients with early phase disease, in those with intermediate phase disease, and in those with advanced phase disease according to hematopoietic stem cell source and donor-recipient HLA match. (A) The cumulative incidences of NRM in patients with early phase disease by 2 years after an 8/8 HLA–matched unrelated bone marrow transplantation (UBMT), a 7/8 HLA–matched UBMT, and a 4/6 to 6/6 HLA–matched umbilical cord blood transplantation (UCBT) were 25% (95% CI, 95% CI, 19% to 32%), 35% (95% CI, 95% CI, 25% to 45%), and 37% (95% CI, 29% to 46%), respectively. (B) The cumulative incidences of NRM in patients with intermediate phase disease by 2 years after an 8/8 HLA–matched UBMT, a 7/8 HLA–matched UBMT, and a 4/6 to 6/6 HLA–matched UCBT were 32% (95% CI, 31% to 43%), 27% (95% CI, 16% to 40%), and 28% (95% CI, 18% to 38%), respectively. (C) The cumulative incidences of NRM in patients with advanced phase disease by 2 years after an 8/8 HLA–matched UBMT, a 7/8 HLA–matched UBMT, and a 4/6 to 6/6 HLA–matched UCBT were 34% (95% CI, 27% to 41%), 41% (95% CI, 32% to 50%), and 36% (95% CI, 30% to 41%), respectively.

Survival

The 2-year unadjusted probabilities of OS after the 8/8 HLA–matched UBMT (51% [95% CI, 46% to 56%]) were significantly higher than those of the 7/8 HLA–matched UBMT (39% [95% CI, 32% to 45%]) and 4/6 to 6/6 HLA–matched UCBT (35% [95% CI, 31% to 39%]) recipients, respectively. The adjusted probabilities of OS at 2 years were also significantly better in recipients of the 8/8 HLA–matched UBMT than in the recipients of the 7/8 HLA–matched UBMT or 4/6 to 6/6 HLA–matched UCBT (49% [95% CI, 44% to 54%], 38% [95% CI, 32% to 45%], 39% [95% CI, 35% to 44%], respectively). This finding was also observed in the subgroup analysis for disease status (at early phase: the adjusted probabilities of OS at 2 years after the 8/8 HLA–matched UBMT, 7/8 HLA–matched UBMT, and 4/6 to 6/6 HLA–matched UCBT were 69% [95% CI, 62% to 76%], 54% [95% CI, 44% to 66%], and 46% [95% CI, 38% to 56%]; at intermediate phase: 53% [95% CI, 42% to 67%], 55% [95% CI, 42% to 72%], and 62% [95% CI, 52% to 74%], respectively; at advanced phase: 31% [95% CI, 24% to 39%], 24% [95% CI, 17% to 33%], and 25% [95% CI, 21% to 31%], respectively) (Figure 3).

According to the multivariate analysis, the 4/6 to 6/6 HLA–matched UCBT recipients had a significantly higher risk of overall mortality than did the 8/8 HLA–matched UBMT recipients (HR, 1.47 [95% CI, 1.24 to 1.74]; $P < .001$) (Table 2). However, the 4/6 to 6/6 HLA–matched UCBT recipients had a similar risk of overall mortality when compared with the 7/8 HLA–matched UBMT recipients (HR, 1.03 [95% CI, .86 to 1.24]; $P = .75$) (Table 2). The adjusted probabilities of OS at 2 years after 8/8 HLA–matched UBMT were superior to those after 4/6 to 6/6 HLA–matched UCBT, regardless of primary disease and conditioning regimen, especially in the patients with MDS (Supplemental Figure 2, Supplemental Tables 4 and 5).

To identify the population of UCBT recipients who had a similar OS to those of 8/8 HLA–matched UBMT, we evaluated the impact of cell dose, HLA matching, and GVHD prophylaxis on the OS of UCBT recipients. The 2-year unadjusted OS of UCBT recipients who received $\geq .84 \times 10^5$ $CD34^+$ cells/kg, which was median cell dose, was significantly higher than those who received $< .84 \times 10^5$ $CD34^+$ cells/kg (Supplemental Figure 3A). HLA matching did not have an effect on OS (Supplemental Figure 3B). GVHD prophylaxis with calcineurin inhibitor (CNI) and other agents improved OS compared with that with CNI alone (Supplemental Figure 3C). Therefore, we compared the OS of 4/6 to 6/6 HLA–matched UCBT recipients who received umbilical cord blood units containing $\geq .84 \times 10^5$ $CD34^+$ cells/kg with 8/8 HLA–matched UBMT recipients, among those with AML and those with ALL who received GVHD prophylaxis with CNI and other agent. The unadjusted 2-year OS after 8/8 HLA–matched UBMT was higher than 4/6 to 6/6 HLA–matched UCBT in patients with early phase disease. Among those with intermediate phase disease, the unadjusted 2-year OS after 4/6 to 6/6 HLA–matched UCBT was likely higher than 8/8 HLA–matched UBMT. Among those with advanced phase disease, the 2-year OS were similar between 2 groups (8/8 HLA–matched UBMT versus 4/6 to 6/6 HLA–matched UCBT; the unadjusted OS of early phase disease, 67% [95% CI, 59% to 74%] versus 55% [95% CI, 40% to 67%], $P = .044$; the unadjusted OS of intermediate disease, 52% [95% CI, 39% to 64%] versus 77% [95% CI, 56% to 89%], $P = .08$; the unadjusted OS of advanced phase disease, 25% [95% CI, 17% to 33%] versus 26% [95% CI, 16% to 36%], $P = .82$) (Figure 4A,C). The adjusted probability of OS were similar between 2 groups (8/8 HLA–matched UBMT versus 4/6 to 6/6 HLA–matched UCBT; the adjusted OS, 49% [95% CI, 43% to 55%] versus 49% [95% CI, 41% to 58%], $P = .74$, respectively) (Figure 4D).

DISCUSSION

The primary objectives of this study were to compare OS after 4/6 to 6/6 HLA–matched UCBT with those after 8/8 and 7/8 HLA–matched UBMT in patients with hematologic malignancies ages 50 years or older and to provide useful data for the selection of an appropriate unrelated stem cell source for those patients who do not have an available HLA-identical sibling. Our findings suggested that an 8/8 HLA allele–matched unrelated donor is the best alternative to a HLA-identical sibling donor. Four of 6 to 6/6 HLA–matched UCBT had a similar OS to 8/8 HLA–matched UBMT for patients with AML and for those with ALL when the umbilical cord blood unit containing $\geq .84 \times 10^5$ $CD34^+$ cells/kg is available.

Neutrophil and platelet recovery were significantly slower after the 4/6 to 6/6 HLA–matched UCBT than after the

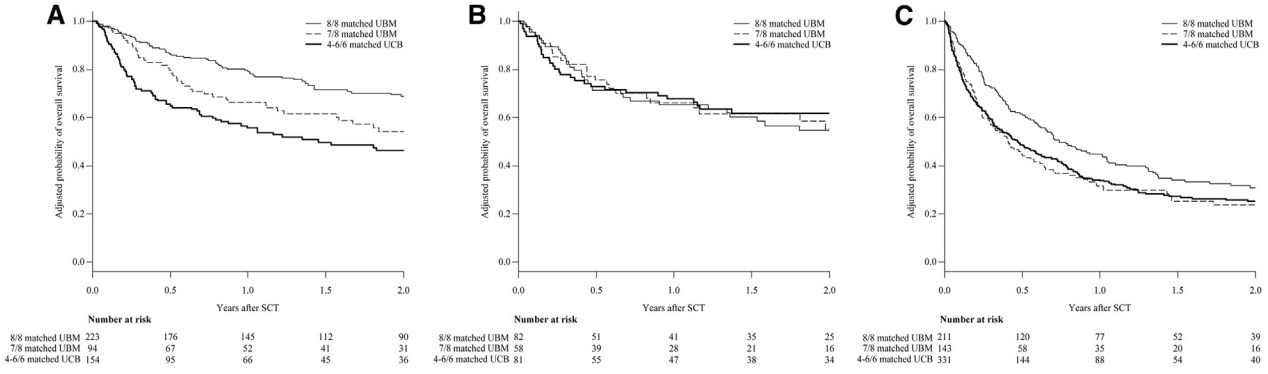

Figure 3. Adjusted probabilities of OS in patients with early phase disease, in those with intermediate phase disease, and in those with advanced phase disease according to hematopoietic stem cell source and donor-recipient HLA match. (A) The adjusted probabilities of the 2-year OS after transplantation in patients with early phase disease who received an 8/8 HLA–matched unrelated bone marrow transplantation (UBMT), a 7/8 HLA–matched UBMT, and a 4/6 to 6/6 HLA–matched umbilical cord blood transplantation (UCBT) were 69% (95% CI, 62% to 76%), 54% (95% CI, 44% to 66%), and 46% (95% CI, 38% to 56%), respectively. (B) The adjusted probabilities of the 2-year OS after transplantation in patients with intermediate phase disease who received an 8/8 HLA–matched UBMT, a 7/8 HLA–matched UBMT, and a 4/6 to 6/6 HLA–matched UCBT were 53% (95% CI, 42% to 67%), 55% (95% CI, 42% to 72%), and 62% (95% CI, 52% to 74%), respectively. (C) The adjusted probabilities of the 2-year OS after transplantation in patients with intermediate phase disease who received an 8/8 HLA–matched UBMT, a 7/8 HLA–matched UBMT, and a 4/6 to 6/6 HLA–matched UCBT were 31% (95% CI, 24% to 39%), 24% (95% CI, 17% to 33%), and 25% (95% CI, 21% to 31%), respectively.

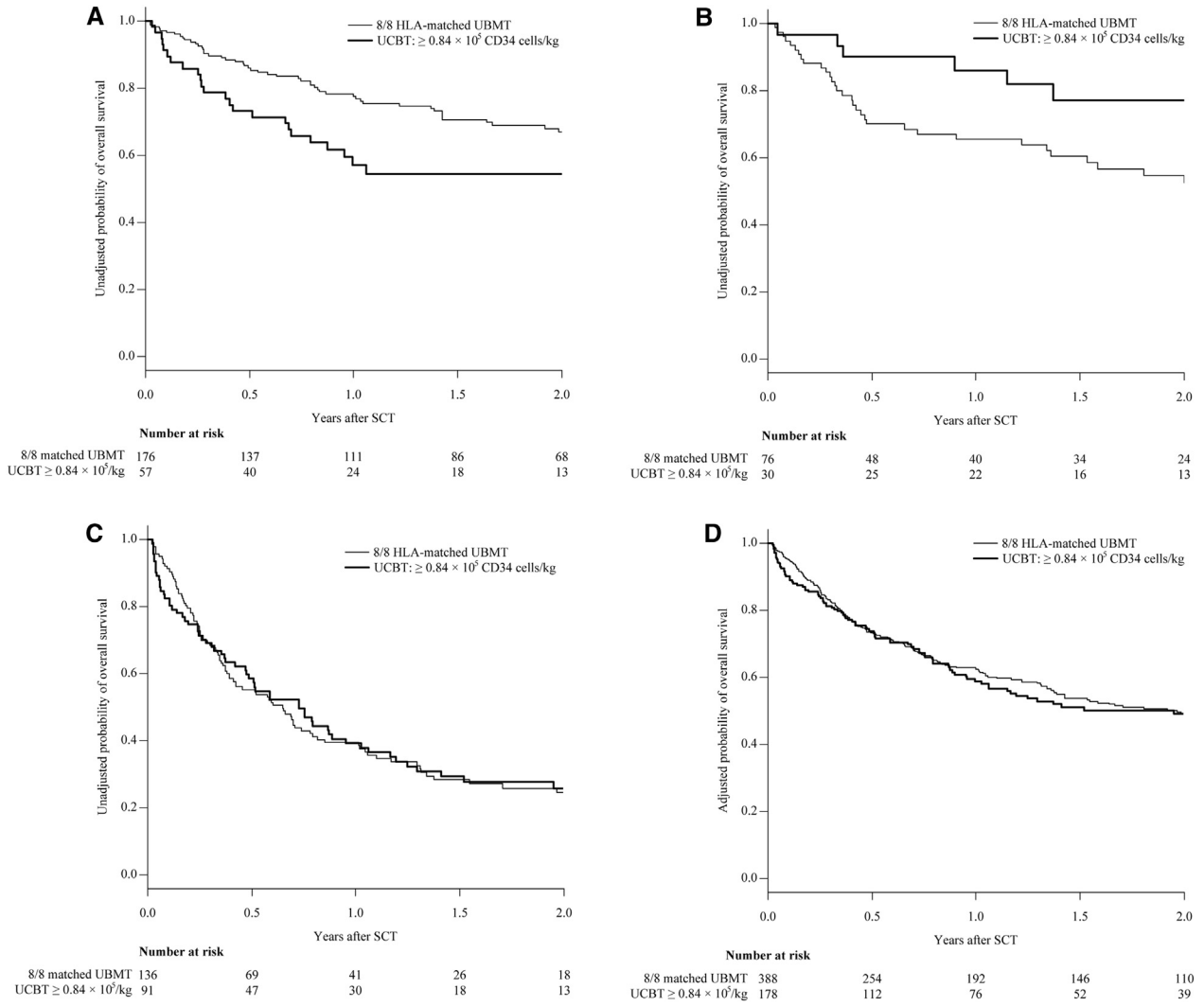

Figure 4. OS in UCBT recipient who received ≥ .84 × 10^5/kg CD34 cells compared with 8/8 HLA–matched UBMT recipients, among those with AML and ALL who prevented graft-versus-host disease with CNI and other agents. (A) The unadjusted probabilities of the 2-year OS after transplantation in patients with acute myeloid leukemia (AML) and acute lymphoblastic leukemia (ALL) at early phase disease and prevented GVHD with CNI and other agent who received an 8/8 HLA–matched unrelated bone marrow transplantation (UBMT) and a 4/6 to 6/6 HLA–matched umbilical cord blood transplantation (UCBT) receiving ≥.84 × 10^5/kg CD34 cells were 67% (95% CI, 59% to 74%) and 55% (95% CI, 40% to 67%), respectively, $P = .044$. (B) The unadjusted probabilities of the 2-year OS after transplantation in patients with AML and ALL at intermediate phase disease and prevented GVHD with CNI and other agent who received an 8/8 HLA–matched UBMT and a 4/6 to 6/6 HLA–matched UCBT receiving ≥.84 × 10^5/kg CD34 cells were 52% (95% CI, 39% to 64%) and 77% (95% CI, 56% to 89%), respectively, $P = .08$. (C) The unadjusted probabilities of the 2-year OS after transplantation in patients with AML and ALL at advanced phase disease and prevented GVHD with CNI and other agent who received an 8/8 HLA–matched UBMT and a 4/6 to 6/6 HLA–matched UCBT receiving ≥.84 × 105/kg CD34 cells were 25% (95% CI, 17% to 33%) and 26% (95% CI, 16% to 36%), respectively, $P = .82$. (D) The adjusted probabilities of the 2-year OS after transplantation in patients with AML and ALL prevented GVHD with CNI and other agent who received an 8/8 HLA–matched UBMT and a 4/6 to 6/6 HLA–matched UCBT receiving ≥.84 × 10^5/kg CD34 cells were 49% (95% CI, 43% to 55%) and 49% (95% CI, 41% to 58%), respectively, $P = .74$.

8/8 and 7/8 HLA–matched UBMT, which was consistent with findings from previous studies [6-9,11,15]. Neutrophil recovery in patients with early phase disease and intermediate phase disease at transplantation was significantly faster than in those with advanced phase disease, which was consistent with the findings in allogeneic peripheral blood stem cell transplantation that had been previously reported [26]. This may be associated with the fact that patients with advanced phase disease were likely pretreated more heavily than those with early phase disease and intermediate phase disease and that they had damage in the microenvironment of the bone marrow.

UCBT recipients had a lower risk of extensive chronic GVHD and a higher risk of relapse compared with 8/8 HLA–matched UBMT recipients. These findings suggested that the graft-versus-leukemia effect in the UCBT recipients was lower than that in the recipients of 8/8 HLA–matched UBMT.

Several studies comparing transplantation outcomes after UBMT versus after UCBT have been reported [6-9]. In some studies, serological HLA class I typing was used for UBMT [6-8]. In another study, UCBT recipients were significantly younger than UBMT recipients, and all patients received a MAC regimen. As a result, only a small number of patients aged 50 years or older were included [9], so direct comparisons of our findings with previous studies are difficult. We had previously demonstrated that HR of overall mortality after a 4/6 to 6/6 HLA–matched UCBT was significantly

higher than that after an 8/8 HLA–matched UBMT among AML patients but not among ALL patients [15]. By contrast, this study showed that the overall survival after an 8/8 HLA–matched UBMT was superior to that after a 4/6 to 6/6 HLA–matched UCBT for patients with AML and for patients with ALL. The present study included patients 50 years or older who received HSCT between 2000 and 2009 regardless of intensity of the conditioning regimen, whereas our previous study had included the recipients of MAC between 2000 and 2005 ages 16 years or older. Therefore, 20% of the 8/8 HLA–matched UBMT recipients and 10% of the 4/6 to 6/6 HLA–matched UCBT recipients in the present study were also included in our previous study. The discrepancy of the results for ALL may be partly due to differences in conditioning regimens (only recipients of MAC regimens were described in our previous report, whereas more than one half of the patients in this study received RIC regimen). Older patients with ALL had a higher risk of relapse and tended to receive RIC when compared with younger patients [27]; therefore, these patients would need a strong graft-versus-leukemia effect. In addition, short-term methotrexate improved OS in the UCBT recipients [28]. In our cohort, approximately 30% of UCBT recipients received GVHD prophylaxis with cyclosporine or tacrolimus alone, and this reduced OS in UCBT recipients. As previously described [29], UCBT recipients receiving higher $CD34^+$ cells had a higher OS than those receiving lower $CD34^+$ cells. For patients with AML and for patients with ALL, UCBT recipients receiving $\geq .84 \times 10^5$ $CD34^+$ cells/kg had a similar adjusted and unadjusted OS to 8/8 HLA–matched UBMT recipients. These findings suggest that the outcomes of UCBT may improve with graft selection based on $CD34^+$ cell dose. The HR of overall mortality after a 4/6 to 6/6 HLA–matched UCBT was similar to that after a 7/8 HLA–matched UBMT, regardless of disease status at transplantation. To the best of our knowledge, this is the first report to compare transplantation outcomes in patients 50 years or older who received a 4/6 to 6/6 HLA–matched UCBT with those who received a 7-8/8 HLA–matched UBMT in a large cohort.

This study had several limitations. Although we adjusted for known risk factors using multivariate analysis, we could not exclude selection bias because this was a retrospective study based on registry data. Further, donor selection was influenced by several factors that were not statistically adjustable. Some patients with urgent disease who could not wait for the preparation of UBMT received UCBT; in other cases, a suitable UCB unit with enough cell doses was not available, and these patients therefore received UBMT. Patients who planned to receive UBMT and could not receive transplantation because of disease progression during the donor coordination were not included in this analysis. In addition, only 5% of recipients of UBMT received GVHD prophylaxis using only a CNI; on the other hand, approximately 30% of UCBT recipients employed the same protocol, which may have influenced the occurrence of GVHD and overall survival. A randomized controlled trial comparing UCBT with UBMT is needed to validate the findings from the present study; however, a study of that design is very difficult to conduct. Clinical decision analysis may help to address any selection bias caused by the donor search process. From 2000 onwards, UPBSCT was more common than UBMT [5]; however, we could not compare the transplantation outcomes of the 4/6 to 6/6 HLA–matched UCBT with the UPBSCT because more than 99% of the unrelated donors from Japan Marrow Donor Program were harvested bone marrow. A randomized controlled trial comparing UPBSCT with UBMT had shown similar outcomes for OS, NRM, and relapse rate [30]. Taken together, UCBT may also be an alternative stem cell source when a HLA-matched peripheral blood stem cell donor is not available.

In conclusion, UCB is a reasonable alternative donor/stem cell source for elderly patients with AML and for those with ALL with similar outcomes compared with UBM from a 8/8 HLA–matched unrelated donor when UCB unit containing $\geq .84 \times 10^5$ $CD34^+$ cells/kg is available. If urgently needed or if there is no 8/8 HLA–matched unrelated donor, a 4/6 to 6/6 HLA–matched UCBT is an acceptable treatment.

ACKNOWLEDGMENTS

The authors thank all the staff members of the collaborating institutes of the Japan Cord Blood Bank Network and Japan Marrow Donor Program for their assistance and cooperation.

Financial disclosure: The authors have nothing to disclose.

Conflict of interest statement: There are no conflicts of interest to report.

Authorship statement: M.T. and K.M. designed the study. M.T. prepared and analyzed data and had primary responsibility for drafting the manuscript. K.M., S.T., K.I., and Y.A. participated in data interpretation and critically reviewed the manuscript. N.U., H.A., T.S., T.E., K.O., T.F., S.T., S.M., T.N.I., and S.O. interpreted data and critically reviewed the manuscript. All authors contributed equally to the interpretation of data, manuscript preparation, and approval of the final report.

Supplementary information is available at Leukemia's website.

SUPPLEMENTARY DATA

Supplementary data related to this article can be found at http://dx.doi.org/10.1016/j.bbmt.2014.11.685

REFERENCES

1. Appelbaum FR, Gundacker H, Head DR, et al. Age and acute myeloid leukemia. *Blood*. 2006;107:3481-3485.
2. Pullarkat V, Slovak ML, Kopecky KJ, et al. Impact of cytogenetics on the outcome of adult acute lymphoblastic leukemia: results of Southwest Oncology Group 9400 study. *Blood*. 2008;111:2563-2572.
3. Slavin S, Nagler A, Naparstek E, et al. Nonmyeloablative stem cell transplantation and cell therapy as an alternative to conventional bone marrow transplantation with lethal cytoreduction for the treatment of malignant and nonmalignant hematologic diseases. *Blood*. 1998;91:756-763.
4. McSweeney PA, Niederwieser D, Shizuru JA, et al. Hematopoietic cell transplantation in older patients with hematologic malignancies: replacing high-dose cytotoxic therapy with graft-versus-tumor effects. *Blood*. 2001;97:3390-3400.
5. Pasquini MC Wang Z. Current use and outcome of hematopoietic stem cell transplantation: CIBMTR Summary Slides. 2011. http://www.cibmtr.org/ReferenceCenter/SlidesReports/SummarySlides/pages/index.aspx.
6. Laughlin MJ, Eapen M, Rubinstein P, et al. Outcomes after transplantation of cord blood or bone marrow from unrelated donors in adults with leukemia. *N Engl J Med*. 2004;351:2265-2275.
7. Rocha V, Labopin M, Sanz G, et al. Transplants of umbilical-cord blood or bone marrow from unrelated donors in adults with acute leukemia. *N Engl J Med*. 2004;351:2276-2285.
8. Takahashi S, Iseki T, Ooi J, et al. Single-institute comparative analysis of unrelated bone marrow transplantation and cord blood transplantation for adult patients with hematologic malignancies. *Blood*. 2004;104:3813-3820.
9. Eapen M, Rocha V, Sanz G, et al. Effect of graft source on unrelated donor haemopoietic stem-cell transplantation in adults with acute leukaemia: a retrospective analysis. *Lancet Oncol*. 2010;11:653-660.
10. Tomblyn MB, Arora M, Baker KS, et al. Myeloablative hematopoietic cell transplantation for acute lymphoblastic leukemia: analysis of graft sources and long-term outcome. *J Clin Oncol*. 2009;27:3634-3641.

11. Brunstein CG, Eapen M, Ahn KW, et al. Reduced-intensity conditioning transplantation in acute leukemia: the effect of source of unrelated donor stem cells on outcomes. *Blood*. 2012;119:5591-5598.
12. Hwang WY, Samuel M, Tan D, et al. A meta-analysis of unrelated donor umbilical cord blood transplantation versus unrelated donor bone marrow transplantation in adult and pediatric patients. *Biol Blood Marrow Transplant*. 2007;13:444-453.
13. Zhang H, Chen J, Que W. A meta-analysis of unrelated donor umbilical cord blood transplantation versus unrelated donor bone marrow transplantation in acute leukemia patients. *Biol Blood Marrow Transplant*. 2012;18:1164-1173.
14. Wang J, Zhan P, Ouyang J, et al. Unrelated donor umbilical cord blood transplantation versus unrelated donor bone marrow transplantation in adult and pediatric patients: A meta-analysis. *Leuk Res*. 2010;34:1018-1022.
15. Atsuta Y, Suzuki R, Nagamura-Inoue T, et al. Disease-specific analyses of unrelated cord blood transplantation compared with unrelated bone marrow transplantation in adult patients with acute leukemia. *Blood*. 2009;113:1631-1638.
16. Atsuta Y, Suzuki R, Yoshimi A, et al. Unification of hematopoietic stem cell transplantation registries in Japan and establishment of the TRUMP System. *Int J Hematol*. 2007;86:269-274.
17. Bacigalupo A, Ballen K, Rizzo D, et al. Defining the intensity of conditioning regimens: working definitions. *Biol Blood Marrow Transplant*. 2009;15:1628-1633.
18. Giralt S, Ballen K, Rizzo D, et al. Reduced-intensity conditioning regimen workshop: defining the dose spectrum. Report of a workshop convened by the center for international blood and marrow transplant research. *Biol Blood Marrow Transplant*. 2009;15:367-369.
19. Grimwade D, Hills RK, Moorman AV, et al. Refinement of cytogenetic classification in acute myeloid leukemia: determination of prognostic significance of rare recurring chromosomal abnormalities among 5876 younger adult patients treated in the United Kingdom Medical Research Council trials. *Blood*. 2010;116:354-365.
20. Greenberg PL, Tuechler H, Schanz J, et al. Revised international prognostic scoring system for myelodysplastic syndromes. *Blood*. 2012;120:2454-2465.
21. Przepiorka D, Weisdorf D, Martin P, et al. 1994 Consensus Conference on Acute GVHD Grading. *Bone Marrow Transplant*. 1995;15:825-828.
22. Shulman HM, Sullivan KM, Weiden PL, et al. Chronic graft-versus-host syndrome in man. A long-term clinicopathologic study of 20 Seattle patients. *Am J Med*. 1980;69:204-217.
23. Gray RJ. A class of K-sample tests for comparing the cumulative incidence of a competing risk. *Ann Stat*. 1988;16:1141-1154.
24. Fine JP, Gray RJ. A proportional hazards model for the subdistribution of a competing risk. *J Am Stat Assoc*. 1999;94:496-509.
25. Kanda Y. Investigation of the freely available easy-to-use software 'EZR' for medical statistics. *Bone Marrow Transplant*. 2013;48:452-458.
26. Lee HS, Park LC, Lee EM, et al. Predictive factors for rapid neutrophil and platelet engraftment after allogenic peripheral blood stem cell transplantation in patients with acute leukemia. *Ann Hematol*. 2013;92:1685-1693.
27. Rowe JM, Buck G, Burnett AK, et al. Induction therapy for adults with acute lymphoblastic leukemia: results of more than 1500 patients from the international ALL trial: MRC UKALL XII/ECOG E2993. *Blood*. 2005;106:3760-3767.
28. Narimatsu H, Terakura S, Matsuo K, et al. Short-term methotrexate could reduce early immune reactions and improve outcomes in umbilical cord blood transplantation for adults. *Bone Marrow Transplant*. 2007;39:31-39.
29. Wagner JE, Barker JN, DeFor TE, et al. Transplantation of unrelated donor umbilical cord blood in 102 patients with malignant and nonmalignant diseases: influence of CD34 cell dose and HLA disparity on treatment-related mortality and survival. *Blood*. 2002;100:1611-1618.
30. Anasetti C, Logan BR, Lee SJ, et al. Peripheral-blood stem cells versus bone marrow from unrelated donors. *N Engl J Med*. 2012;367:1487-1496.

OPEN ACCESS Freely available online

PLOS ONE

Dexamethasone Palmitate Ameliorates Macrophages-Rich Graft-versus-Host Disease by Inhibiting Macrophage Functions

Satoshi Nishiwaki[1,2,3], Takayuki Nakayama[4]*, Makoto Murata[1], Tetsuya Nishida[1], Seitaro Terakura[1], Shigeki Saito[1], Tomonori Kato[1], Hiroki Mizuno[1], Nobuhiko Imahashi[1,3], Aika Seto[3], Yukiyasu Ozawa[3], Koichi Miyamura[3], Masafumi Ito[5], Kyosuke Takeshita[6], Hidefumi Kato[4], Shinya Toyokuni[7], Keisuke Nagao[8], Ryuzo Ueda[9], Tomoki Naoe[1]

1 Department of Hematology and Oncology, Nagoya University Graduate School of Medicine, Nagoya, Aichi, Japan, **2** Japan Society for the Promotion of Science, Japanese Red Cross Nagoya First Hospital, Nagoya, Aichi, Japan, **3** Department of Hematology, Japanese Red Cross Nagoya First Hospital, Nagoya, Aichi, Japan, **4** Department of Transfusion Medicine, Aichi Medical University, Nagakute, Aichi, Japan, **5** Department of Pathology, Japanese Red Cross Nagoya First Hospital, Nagoya, Aichi, Japan, **6** Department of Cardiology, Nagoya University Graduate School of Medicine, Nagoya, Aichi, Japan, **7** Department of Pathology and Biological Responses, Nagoya University Graduate School of Medicine, Nagoya, Aichi, Japan, **8** Department of Dermatology, Keio University School of Medicine, Shinjyuku-ku, Tokyo, Japan, **9** Department of Tumor Immunology, Aichi Medical University, Nagakute, Aichi, Japan

Abstract

Macrophage infiltration of skin GVHD lesions correlates directly with disease severity, but the mechanisms underlying this relationship remain unclear and GVHD with many macrophages is a therapeutic challenge. Here, we characterize the macrophages involved in GVHD and report that dexamethasone palmitate (DP), a liposteroid, can ameliorate such GVHD by inhibiting macrophage functions. We found that host-derived macrophages could exacerbate GVHD in a mouse model through expression of higher levels of pro-inflammatory TNF-α and IFN-γ, and lower levels of anti-inflammatory IL-10 than resident macrophages in mice without GVHD. DP significantly decreased the viability and migration capacity of primary mouse macrophages compared to conventional dexamethasone *in vitro*. DP treatment on day 7 and day 14 decreased macrophage number, and attenuated GVHD score and subsequent mortality in a murine model. This is the first study to provide evidence that therapy for GVHD should be changed on the basis of infiltrating cell type.

Citation: Nishiwaki S, Nakayama T, Murata M, Nishida T, Terakura S, et al. (2014) Dexamethasone Palmitate Ameliorates Macrophages-Rich Graft-versus-Host Disease by Inhibiting Macrophage Functions. PLoS ONE 9(5): e96252. doi:10.1371/journal.pone.0096252

Editor: Derya Unutmaz, New York University, United States of America

Received August 21, 2013; **Accepted** March 5, 2014; **Published** May 7, 2014

Funding: This study was supported in part by a grant from the Japan Society for the Promotion of Science to S.N., and in part by a Japanese Grant-in-Aid for Scientific Research [(C) 20591118] to T. Nakayama. The funders had no role in study design, data collection and analysis, decision to publish, or preparation of the manuscript.

Competing Interests: The authors have declared that no competing interests exist.

* E-mail: tnaka@aichi-med-u.ac.jp

Introduction

Macrophages are recruited by chemokines including CCL2 to the inflammatory site and, primarily, play an indispensable role in both innate and acquired immunity [1]. Macrophage phenotypes and functions can vary with different external stimuli, and macrophages are divided into two major classifications: classically activated, i.e. inflammatory, and alternatively activated, i.e. anti-inflammatory macrophages [1]. Persistence of activated macrophages can occasionally be harmful to the host [2,3].

Graft-versus-host (GVHD) is often a prominent complication after allogeneic stem cell transplantation (allo-SCT) and can be fatal despite aggressive interventions including corticosteroids [4]. It has been reported that GVHD can be divided into 3 subtypes based on the number of macrophages and T lymphocytes infiltrated in the skin, and that GVHD with many $CD163^+$ macrophages was refractory with poor prognosis and a therapeutic challenge [5]. However, those macrophages were CD163 positive, a member of the scavenger receptor cysteine-rich superfamily, which was one of anti-inflammatory macrophage markers [6]. Thus, the pathogenesis between macrophage infiltration and refractory GVHD is currently unclear. These facts prompted us to characterize the phenotypes of macrophages related to refractory GVHD.

Corticosteroids inhibit functions of inflammatory cells via glucocorticoid receptors in the cytoplasm [7]. Therefore, efficient delivery of corticosteroids into the cytoplasm could enhance their therapeutic effect. It is known that a dexamethasone palmitate emulsion (DP) is readily taken up by macrophages via phagocytosis and is strongly retained in the cytoplasm [8]. Here, we report that the macrophages increased in fatal GVHD are inflammatory and that DP treatment efficiently attenuated such GVHD by inhibiting macrophage functions.

Materials and Methods

1. Mice

Male 6- to 8-week-old male C57BL/6J mice and female BALB/c mice were purchased from Chubu Kagaku Shizai (Nagoya, Japan). The animal GVHD experiments using spontaneous death

as an endpoint were approved by the Institutional Ethics Committee for Laboratory Animal Research, Nagoya University School of Medicine (protocol 24298), and were performed according to the guidelines of the institute. Animals were maintained at constant ambient temperature (22±1°C) under a 12-h light/dark cycle (lights on between 9:00 and 21:00), with food and water available ad libitum.

2. Cells and reagents

A murine macrophage cell line, RAW264.7, was purchased from American Type Culture Collection (Manassas, VA, USA). Primary peritoneal macrophages and skin macrophages were obtained from the peritoneal lavages of C57BL/6J mice and from the ears of mice after BMT, respectively, as described elsewhere with slight modification [9,10]. Briefly, peritoneal lavages were collected 3 days after intraperitoneal injection of 1 mL of 2% thioglycolate (Kanto Chemical Co., Inc., Tokyo, Japan) and macrophages were positively selected from the lavages by AutoMACS system with anti CD11b immunomagnetic microbeads (Miltenyi Biotec, Bergisch Gladbach, Germany). To prepare single cell suspensions from dermis, the ears were split into dorsal and ventral halves with removal of subcutaneous tissues such as cartilage and the dermal sheets were incubated in RPMI containing 2% Liberase (Liberase TL Research Grade, Roche Applied Science) for 2 hours at 37°C. After digestion, residual tissue was minced in RPMI and disaggregated by using a tissue homogenizer (Medimachine; Becton Dickinson, San Jose, CA). Dermal macrophages were positively selected from the suspension cells by AutoMACS as described above. FACS analysis using a monoclonal antibody (mAb) (F4/80: BM8, BioLegend, San Diego, CA, USA) showed that the purity of isolated macrophages were > 90%. Primary T cells were positively isolated from splenocytes of BALB/c mice by using anti CD90.2 immunomagnetic microbeads (Miltenyi Biotec). T cell-depleted (TCD) donor bone marrow (BM) cells was obtained from BALB/c mice by negative selection by using CD90.2 microbeads.

Dexamethasone sodium phosphate (DSP) and Dexamethasone palmitate emulsion (DP) were from MSD K.K. (Tokyo, Japan) and Mitsubishi Tanabe Pharma (Tokyo, Japan), respectively.

3. Induction and assessment of GVHD

A fatal murine GVHD model was established by allogeneic BM transplantation. Lethally irradiated C57/BL6 recipient mice (5 Gy×2; days -2 and -1) were co-transplanted with TCD-BM (5×10^6) and T lymphocytes (1×10^7) from BALB/c donor mice via tail vein without anesthesia. DP or DSP (10 mg/kg as dexamethasone) were administrated intravenously into the mice on day 7 and 14 after transplantation (control: n = 9, DSP: n = 9, DP: n = 10). The conditions and survival of animals after BMT were monitored daily with all efforts to alleviate pain and suffering, and the degree of GVHD was evaluated clinically (3 times/week) for 28 days (until day 42) after the last administration of DP or DSP (day 14) because our preliminary experiments showed that GVHD-related complications were neither worsen nor cause of death after 28 days of DSP treatment. The reasons why we set spontaneous death as an endpoint are as follows. GVHD also possesses an antitumor effect; so-called graft-versus-leukemia (GVL), and 'mild' GVHD confers a survival benefit [11][12]. Thus, physicians try to modulate the GVL-GVHD balance by immune-suppressants such as steroid and cyclosporine A. However, GVHD, once became refractory to conventional therapies, could cause high mortalities [13]. To determine whether DP can improve overall survival outcomes or not in a GVHD mouse model brings a lot of useful information to physicians. The animals survived by DP treatment were humanely euthanized by overexposure to carbon dioxide after day 42. Mice treated with no steroid or with DSP had all died of GVHD before day 42. The detailed clinical GVHD scoring system by using 5 parameters is as follows: weight loss, posture, activity, fur texture, and skin integrity (maximum index = 10) [14]. Acute GVHD was also assessed in a blind fashion by detailed histopathologic analysis in hematoxylin and eosin-stained tissue sections (the skin from the interscapular region, ears and descending colon). Skin sections were scored on the basis of the following criteria: epidermis (0, normal; 1, foci of interface damage in <20% of section with occasional necrotic keratinocytes; 2, widespread interface damage in >20% of section); dermis (0, normal; 1, slightly altered with mild increased collagen density; 2, marked increased collagen density); inflammation (0, none; 1, focal infiltrates; 2, widespread infiltrates); subctaneous fat (0, normal; 1, reduced number of normal adipocytes; 2, serous fat atrophy); and follicles (0, normal number of hair follicles, ~5 per linear millimeter;1, between 1 and 5 follicles per linear millimeter; 2, <1 follicle per linear millimeter) [15]. Seven parameters were scored for gut (crypt regeneration, crypt epithelial cell apoptosis, crypt loss, surface colonocyte vacuolization, surface colonocyte attenuation, lamina propria inflammatory cell infiltrate, and mucosal ulceration). The scoring system for each parameter denoted 0 as normal; 0.5 as focal and rare; 1 as focal and mild; 2 as diffuse and mild; 3 as diffuse and moderate; and 4 as diffuse and severe, as previously described [16].

To assess the direct effect of inflammatory macrophages on GVHD, 1×10^6 thioglycolate-stimulated peritoneal macrophages from C57BL/6J mice were subcutaneously injected in interscapular region on day 5. All mice were humanely euthanized by overexposure to carbon dioxide on day 7 and GVHD score was pathologically evaluated as described above.

4. Analysis of donor-cell chimerism

Donor-cell chimerism of macrophages in the skin after BMT was analyzed by FACS using anti-MHC haplotype antibodies. An anti-H-2Kb mAb (AF6-88.5) and an anti- H-2Kd (SF1-1.1) recognized cells from C57/BL6 recipient mice and cells from BALB/c donor mice, respectively. Both mAbs were obtained from PharMingen (San Diego, CA).

5. RNA preparation and real-time PCR analysis

Total RNA was extracted from the skin and gut of mice using TRIzol (Invitrogen Carlsbad, CA, USA). The mRNA levels of CCL2 in the skin and gut, and those of TNF-α, IFN-γ and IL-10 in skin macrophages were evaluated using quantitative RT-PCR. Primer pairs (TNF-α: Mm00443258_m1, IFN-γ: Mm01168134_m1, CCL-2: Mm00441242_m1, IL-10: Mm00439614_m1, Arginase-1: Mm00475988_m1, Eukaryotic 18s rRNA: 4333760T) were from Applied Biosystems (Foster City, CA, USA). Obtained data were normalized to internal 18 s rRNA expression and were analyzed using the $2^{-\Delta\Delta}C_T$ Method [17].

6. *In vitro* assay for the effects of DP on macrophages and lymphocytes

The viability of RAW264.7 after DSP or DP treatment was assessed using a colorimetric assay as described elsewhere [18]. Briefly, 10 μl of TetraColor-One (Seikagaku Co., Tokyo, Japan) was added to each well of a 96-well plate, where RAW264.7 cells (10,000 cells/well) were pretreated with various concentrations of DSP or DP (48 hours, 37°C), and the mixture was incubated for

an additional 4 hours. Absorbance at 450 nm was monitored. The viability of splenic T lymphocytes after exposure to DSP or DP was assessed by trypan blue exclusion. Briefly, cells were washed twice with PBS, suspended in culture medium (RPMI containing 10% FBS), plated (1.0×10^5 cells/well in 0.2 mL culture medium) in three independent determinations with DSP or DP (25 nM) onto 96-well plates, and incubated for 48 hours. Viable cells were determined as Trypan blue- negative cells. The percent viability was calculated as follows: (viability in DSP or DP group/viability in control group) $\times100$ (%).

CCR2 expression on the surface of macrophages after DSP or DP treatment was analyzed by FACS as described previously [19]. Briefly, thioglycolate-recruited peritoneal macrophages were pretreated with 25 μM (as dexamethasone) of DSP or DP for 3 hours, and then, were exposed to LPS (O55:B5, 100 ng/mL, List Biological Laboratories, Inc. Campbell, CA) for 18 hours. After washings with PBS, the cells were incubated for 30 minutes on ice with a rabbit anti-mouse CCR2 polyclonal antibody (pAb) (1: 25 dilution, E68, Novus Biologicals, Littleton, CO) in the presence of an anti-mouse CD16/32 mAb (BioLegend, San Diego, CA) to reduce non-specific binding of a primary antibody to Fc receptor. The cells were washed twice with PBS and were incubated with a fluorescein isothiocyanate -conjugated donkey anti-rabbit IgG pAb (1: 25 dilution, BioLegend, San Diego, CA) as a secondary antibody for 30 minutes. CCR2 expression was assessed from 1.0×10^4 viable cells using a FACSAria flow cytometer (BD Biosciences, San Jose, CA), and the data were analyzed using FlowJo software (TreeStar, San Carlos, CA). Background fluorescence was assessed through staining with the isotype-matched antibody.

To assess the inhibitory effect of DP and DSP on the CCL2-CCR2 axis, transwell migration assays were performed as described elsewhere [18]. Briefly, RAW264.7 cells were pretreated with DSP or DP (25 μM) for 3 hours and then, were serum-starved in DMEM with 1% FBS and 100 ng/ml LPS overnight. After washing, the cells were seeded (2×10^5 cells in DMEM with 1% FBS per well) onto the upper chamber of a cell culture insert with a pore size of 8 μm (BD Biosciences, San Jose, CA). Recombinant murine CCL2 (final concentration, 20 ng/ml; PeproTech, Rocky Hill, NJ) was added to the lower chamber, to which cells were allowed to migrate for 4 hours. The membranes were fixed with 4% paraformaldehyde and were stained with Giemsa. For quantitative analysis, four fields were randomly selected, and migrated cells were counted under a light microscope.

7. Immunohistochemistry

Immunostaining of murine skin and gut specimens was carried out on sections from paraffin-embedded tissues fixed in 10% neutral-buffered formalin solution (Sigma-Aldrich, St. Louis, MO) using streptavidin-biotinylated HRP detection (Beckeman Coulter, Brea, CA) as previously described with slight modification [20]. For antigen retrieval, sections (3.5 μm thickness) on silane-coated slides were heated in a microwave oven for 45 minutes at 98°C in immunosaver (1:200 dilution, Nisshin EM Corp. Tokyo, Japan). After blocking nonspecific binding with normal rabbit serum (1:75 dilution; Dako Inc. Via Real (Carpinteria, CA), sections were incubated with an anti F4/80 mAb (CI:A3-1, Novus, Littleton, CO) (1:100) or an isotype-matched mAb for 15 minutes using intermittent microwave irradiation [21,22]. Sections were then incubated with biotin-labeled rabbit anti-mouse IgG pAb (1:300 dilution; Dako Inc.) and 3,3′-diaminobenzidine (DAB; Vector Laboratories Inc. Burlingame, CA) was used as chromogen. Finally they were counterstained with hematoxylin.

8. Statistical Analysis

Statistical significance of group differences was evaluated using Student's *t*-test between two groups and ANOVA followed by bonferroni test for multiple comparisons using STATA software (StataCorp, Lakeway, TX). Kaplan-Meier product-limit estimates were performed to determine survival, while the different subgroups were compared for significance using the log-rank test.

Results

1. Murine GVHD model mimics human severe GVHD

In a BMT model, mice received TCD-BM (5×10^6) and T lymphocytes (1×10^7) or TCD-BM (5×10^6) alone. Cotransplantation of TCD-BM and T lymphocytes resulted weight loss, poor activity, damaged fur texture and all of the mice died on day 12 even though all of the mice received TCD-BM alone were active and survived. Pathological analysis of the skin showed necrotic keratinocytes, increased collagen density, infiltration of inflammatory cells and serous fat atrophy in mice with TCD-BM and T lymphocytes, but minimal damage in mice with TCD-BM alone (Figure 1A, left panel). The gut was similarly severely damaged in mice with TCD-BM and T lymphocytes (data not shown). A higher number of macrophages infiltrated the skin of mice had received TCD-BM and T lymphocytes compared to the skin of mice had received TCD-BM alone (Figure 1A, middle panel). These results clearly suggest that this fatal mouse GVHD model mimics human severe GVHD with many macrophages [5].

To analyze the mechanism of macrophage infiltration in the skin, we focused on the role of CCL2-CCR2 axis since CCL2 is a potent inducer of macrophage recruitment and activation [23]. Quantitative RT-PCR analysis showed that CCL2 expression in the skin of mice with TCD-BM and T lymphocytes was 10-times higher than that in the skin of mice with TCD-BM alone (Figure 1A, right panel).

2. Characterization of macrophages increased in GVHD

The phenotypes of dermal macrophages isolated on day 7 after BMT (the purity of macrophages >90%, not shown) were evaluated by quantitative RT-PCR analyses. Macrophages from GVHD mice showed that skin macrophages from GVHD mice expressed much higher levels of TNF-α and IFN-γ, and a significantly lower level of IL-10 than those of sham mice (no GVHD) (Figure 1B), suggesting that the macrophages involved in GVHD possess inflammatory properties [1]. To assess the direct effect of inflammatory macrophages on GVHD, 1×10^6 thioglycolate-stimulated peritoneal macrophages from C57BL/6J mice were subcutaneously injected in the interscapular region on day 5 and evaluated on day 7. Skin pathological score of the injected site was significantly higher among mice injected macrophages than PBS-injected control mice (Figure 1C). Donor-cell chimerism analyzed by FACS showed that >90% of dermal macrophages possessed the recipient phenotype (data not shown). These data indicated that recipient monocytes recruited to the skin GVHD site acquired inflammatory phenotypes and deteriorated GVHD subsequently.

3. Effects of DP on macrophage functions in vitro

Based on these results, we hypothesized that GVHD with many macrophages would be ameliorated by inhibiting macrophage functions. We therefore compared DP with conventional DSP on macrophage functions. Both DSP and DP inhibited proliferation of RAW 264.7 cells in a dose dependent manner. However, DP possessed a significantly higher ability than DSP (Figure 2A left panel). DP decreased the viability of RAW 264.7 cells by 75% at a

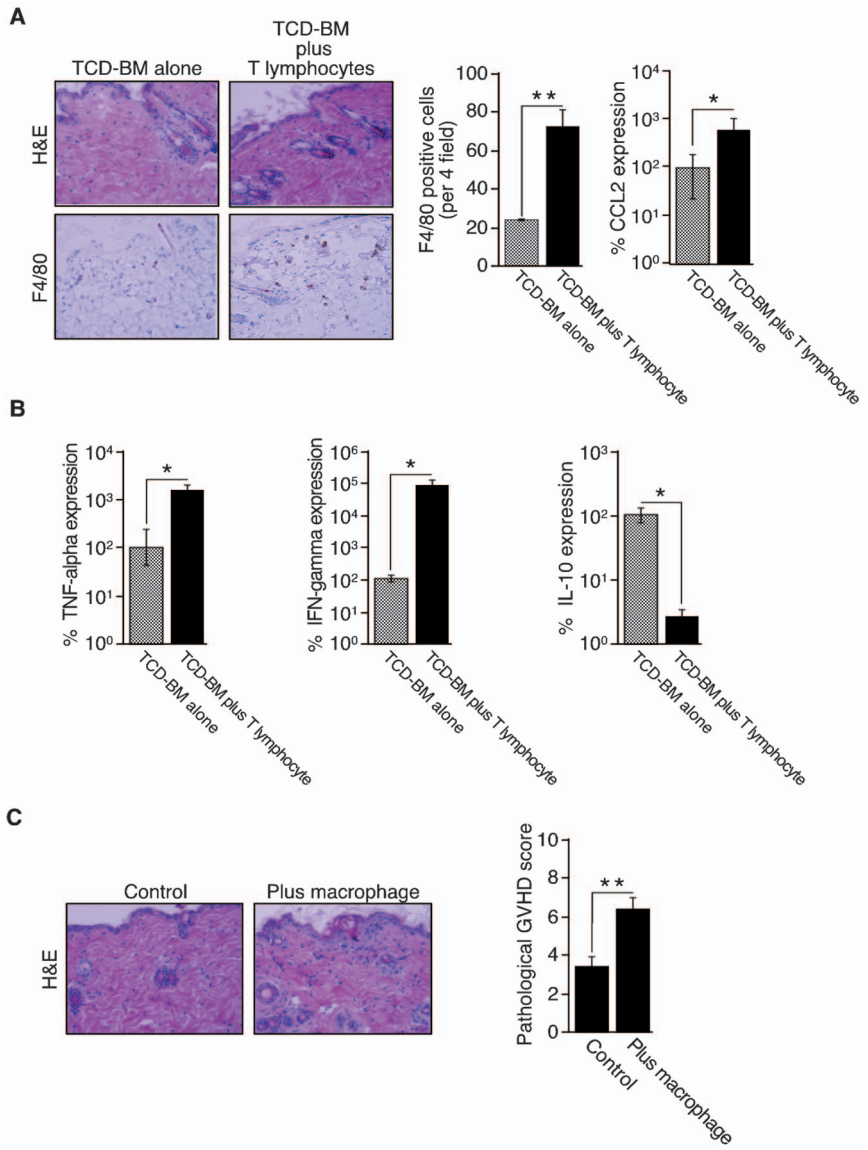

Figure 1. Characterization of macrophage-involvement in GVHD. A: Skin specimens from mice in which T-cell depleted bone marrow (TCD-BM) cells and spleen-derived T lymphocytes were co-transplanted were histopathologically compared with those of mice transplanted with TCD-BM alone. Skin specimens (7 days after transplantation) were stained with H&E (upper left panels) and macrophages were detected with the anti-mouse F4/80 monoclonal antibody (lower left panels). Original magnification, ×400. Representative images of two independent experiments are shown. For quantitative analysis of macrophage numbers, 4 microscopic fields were randomly selected from each of three mice and the total number of $F4/80^+$ cells was counted. The mean number of $F4/80^+$ cells per 4 fields ± SD is shown for each group (middle panel). Original magnification, ×200. The results are representative of two independent experiments. Statistical significance: $^{**}P<0.01$. CCL2 mRNA expression was evaluated using quantitative real-time RT-PCR. Total RNA was extracted from the skin (3 specimens per group) and was subjected to RT-PCR using specific primer pairs. Each reaction was performed in duplicate sets. The obtained data were normalized to internal eukaryotic 18 s rRNA expression, were analyzed using the $2^{-\Delta\Delta}C_T$ Method and are expressed as percent expression, where expression of the control is designated as 100%. The results reflect the mean ± SD of three independent determinations. The results are representative of two independent experiments. Statistical significance: $^{*}P<0.05$. **B:** Macrophages in the skin were characterized by measurement of TNF-α, IFN-γ and IL-10 mRNA expression. Skin dermis was incubated in RPMI containing 2% Liberase for 2 h at 37°C. After digestion, residual tissue was minced and mechanically disaggregated. After separation of dermal macrophages by using the magnetic isolation system, total RNA was extracted and mRNA levels of TNF-α, IFN-γ and IL-10 were quantified by RT-PCR using specific primer pairs (3 specimens per group). Each reaction was performed in duplicate sets. The obtained data were normalized to internal eukaryotic 18 s rRNA expression, were analyzed using the $2^{-\Delta\Delta}C_T$ Method and are expressed as percent expression, where expression of the control is designated as 100%. The results reflect the mean ± SD of three independent determinations. Statistical significance: $^{*}P<0.05$. The results are representative of two independent experiments. **C:** Direct effects of inflammatory macrophages on GVHD were assessed by injecting thioglycolate-stimulated macrophages (1×10^6 cells per mouse) or PBS (three mice per group) subcutaneously into the interscapular region of GVHD mice 5 days after BMT. The animals were killed 7 days after BMT. Skin specimens of the injected sites stained with H&E were photographed (left panel) and skin GVHD was pathologically scored based on five parameters (epidermal damage, alteration of dermis, degree of inflammation, alteration of subcutaneous fat and number of follicles). The results reflect the mean ± SD of three independent determinations. Statistical significance: $^{**}P<0.01$. The results are representative of two independent experiments.

doi:10.1371/journal.pone.0096252.g001

concentration of 10 μM, which is 25-fold lower than the concentration at which DSP similarly worked (by 71% at 250 μM) (Figure 2A left panel). Interestingly, the toxic effect of DP on splenic T lymphocytes is rather weak toxic than DSP, when tested at 25 μM as dexamethasone (Figure 2A right panel). DP also significantly decreased CCR2 expression on the surface of primary peritoneal macrophages (Figure 2B) and RAW 264.7 cells (data not shown), and subsequently decreased migration of primary macrophages towards CCL2 (Figure 2C) compared to DSP. This decreased number of macrophage migration could not be attributed to decreased number of the input cells, as 3 hour-treatment with DSP or DP at 25 μM minimally affected on macrophage viabilities (data not shown). These results clearly suggest that DP attenuates macrophage functions more efficiently than DSP.

4. The effect of DP on murine fatal GVHD

We next investigated whether DP could affect the fatal murine GVHD with many macrophages. DP or DSP was administered 10 mg/kg as dexamethasone on day 7 and day14 (control: n = 9, DSP: n = 9, DP: n = 10). DP significantly lowered the clinical GVHD score compared to DSP. The difference became apparent 5 days after second administration (Figure 3A, left panel). Subsequently DP could rescue about 20% of these mice, whereas mice treated with no steroid or with DSP had all died by days 12 and 30, respectively (Figure 3A, right panel). The effect of DP was also confirmed by pathological analyses, where tissue damage and pathological GVHD scores in the skin (Figure 3B, left panel) and gut (Figure 3B, right panel) were significantly improved in mice treated with DP. The number of $F4/80^+$ macrophages was also lower in mice treated with DP. Since DP had a weaker effect on lymphocytes than DSP (Figure 2A, right panel), the combined facts suggest that DP can attenuate GVHD with many macrophages by inhibiting inflammatory macrophages.

Discussion

Macrophage infiltration in the skin of patients with GVHD is a maker of poor prognosis [5]. Here, we identify macrophages in the GVHD sites are inflammatory and an exacerbator of GVHD, and provide evidence that such GVHD can be effectively treated by DP, not conventional DSP in a mouse model.

Inflammatory cells such as macrophages and mast cells have been proved to be durable to even high dose chemotherapy and irradiation [24,25]. Accordingly, donor-cell chimerism analysis showed that >90% of dermal macrophages possessed the recipient phenotype (not shown).

Macrophages are divided into two major classifications: classically activated, i.e. inflammatory, and alternatively activated, i.e. anti-inflammatory macrophages [26]. Since persistence of macrophage activation can be harmful to the host, phenotypic switch from inflammatory macrophages to anti-inflammatory macrophages can be occurred via various stimuli [27]. We revealed by RT-PCR that macrophages in the skin of a murine GVHD model possessed inflammatory properties (Figure 1B) although the macrophages in patients with GVHD expressed CD163 [5], a marker of the alternatively activated macrophages [26]. Recently, compelling studies revealed that $CD163^+$ macrophages could be unrestrained proinflammatory macrophage population with an incomplete switch to anti-inflammatory macrophages under certain circumstances such as iron-overloading condition [28]. An elevated level of ferritin, a marker of tissue iron overload, closely correlates with increased risk of acute GVHD, higher mortality and lower overall survival [29]. These

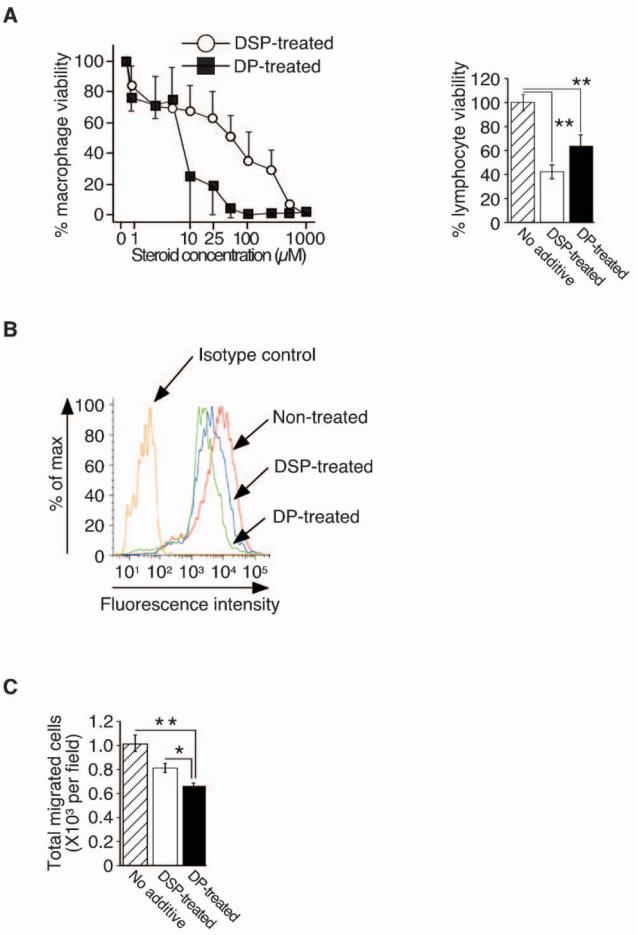

Figure 2. Effect of dexamethasone palmitate on macrophages *in vitro*. **A:** The viability of mouse macrophage-like RAW264.7 cells after dexamethasone sodium phosphate (DSP) or dexamethasone palmitate (DP) treatment (48 hours) was evaluated by using a colorimetric assay (left panel). The percentage viability was calculated as follows: (O.D value in the presence of each concentration of steroid/O.D value without steroid) ×100. The results reflect the mean ± SD of three independent determinations (representative experiment of three performed). The viability of splenic T lymphocytes after exposure to DSP or DP (25 nM each, 48 hours) was assessed by trypan blue exclusion (right panel). Viable cells were determined as Trypan blue-negative cells. The percent viability was calculated as follows: (viability in DSP or DP group/viability in control group) ×100 (%). The results reflect the mean ± SD of three independent determinations (representative experiment of three performed). **B:** CCR2 expression on the surface of mouse primary peritoneal macrophages after DSP or DP treatment was evaluated by FACS. The results are representative of three independent experiments (left panel). **C:** The migration of peritoneal macrophages towards CCL2 after DSP or DP treatment was analyzed using transwell assays. For quantitative analysis, four fields were randomly selected, and migrated cells were counted under a light microscope (×200). The results reflect the mean ± SD of four independent determinations. Representative results of three independent experiments are shown (right panel). Statistical significance: $*P<0.05$ and $**P<0.01$.
doi:10.1371/journal.pone.0096252.g002

evidences and results suggest that $CD163^+$ macrophages in patients with GVHD can be inflammatory and exacerbate GVHD similarly with the mouse GVHD model.

CCL2-CCR2 signaling is known to play a major role in recruitment of monocytes/macrophages [23]. Inflammatory mediators released from activated macrophages not only induce tissue

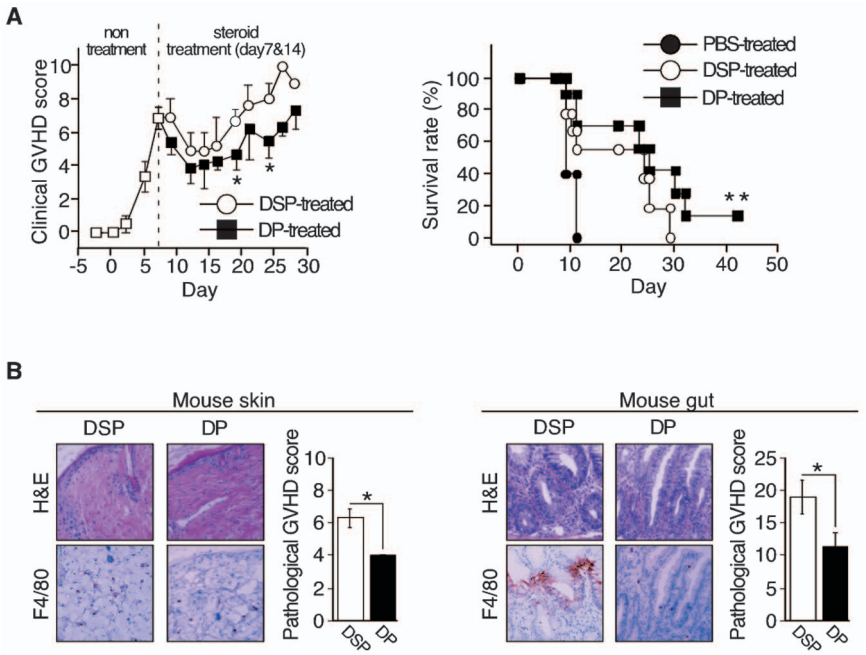

Figure 3. Effect of dexamethasone palmitate on macrophages in mice with fatal GVHD. A: Clinical assessment of GVHD after DP or DSP treatment. Mice were treated with DP or DSP (10 mg/kg/each day) on day 7 and day14 after co-transplantation of TCD-BM and spleen-derived T lymphocytes (control: n = 9, DSP: n = 9, DP: n = 10). Clinical GVHD was assessed 3 times a week, using a scoring system consisting of 5 clinical parameters: weight loss, posture, activity, fur texture, and skin integrity (maximum index = 10, left panel). Statistical significance: $*P<0.05$ (days 19 and 24). Mortalities were counted daily for up to 42 days after transplantation (right panel). Statistical significance: $**P<0.01$ (PBS-treated versus DP-treated). **B:** Pathological assessment of GVHD after DP or DSP treatment. Skin (left panels) and gut (right panels) specimens were stained with H&E (top panels) and skin macrophages were detected with the anti-mouse F4/80 monoclonal antibody (bottom panels). Original magnification, ×400. Representative images of the skin of three mice are shown. Skin and gut GVHD were scored based on five parameters (epidermal damage, alteration of dermis, degree of inflammation, alteration of subcutaneous fat and number of follicles) and seven parameters (crypt regeneration, crypt epithelial cell apoptosis, crypt loss, surface colonocyte vacuolization, surface colonocyte attenuation, lamina propria inflammatory cell infiltrate and mucosal ulceration), respectively, and are presented as histograms. Statistical significance: $*P<0.05$.
doi:10.1371/journal.pone.0096252.g003

damage but also recruit and activate macrophages [1]. DP treatment in a mouse GVHD model decreased the number of macrophages in the skin and gut, and attenuated GVHD without severe complications compared to DSP treatment (Figure 3), suggesting that DP inhibited the positive feedback loop between macrophages and inflammation more efficiently than by DSP.

Not a few attempts to prevent severe acute GVHD in animal models by inhibiting macrophage function as an antigen-presenting cell or modulating macrophage phenotype have been reported and some were successful [30–35]. However, severe adverse effects such as infections occurred occasionally [31] since inflammatory macrophages play important roles in both innate and acquired immune response. Minimal risk of infection can give DP treatment an advantage over those pretreatment.

Our small preclinical study showed that DP treatment in patients with macrophage-rich GVHD (3 day, 5 mg/day) ameliorated GVHD with efficient reduction of skin macrophages. Severe adverse effects such as infections were not observed during and after DP treatment (not published).

Again, these observations provide further evidence that macrophages directly exacerbate GVHD and that DP treatment against such macrophages improves the outcome of refractory GVHD.

Acknowledgments

We thank Ms. Chika Wakamatsu, Ms. Yukiji Ando and Ms. Rie Goto for their contributions to various aspects of this work.

Author Contributions

Conceived and designed the experiments: SN T. Nakayama MM T. Naoe. Performed the experiments: SN T. Nakayama MM S. Terakura SS TK HM. Analyzed the data: SN T. Nakayama MM S. Terakura SS HM T. Naoe. Contributed reagents/materials/analysis tools: AS YO MI S. Toyokuni KN. Wrote the paper: SN T. Nakayama MM T. Nishida S. Terakura SS KT HM NI KM HK MI RU T. Naoe.

References

1. Mantovani A, Sica A, Sozzani S, Allavena P, Vecchi A, et al. (2004) The chemokine system in diverse forms of macrophage activation and polarization. Trends Immunol 25: 677–686.
2. Stoy N (2001) Macrophage biology and pathobiology in the evolution of immune responses: a functional analysis. Pathobiology 69: 179–211.
3. Sindrilaru A, Peters T, Wieschalka S, Baican C, Baican A, et al. (2011) An unrestrained proinflammatory M1 macrophage population induced by iron impairs wound healing in humans and mice. J Clin Invest 121: 985–997.
4. Van Lint MT, Milone G, Leotta S, Uderzo C, Scime R, et al. (2006) Treatment of acute graft-versus-host disease with prednisolone: significant survival advantage for day +5 responders and no advantage for nonresponders receiving anti-thymocyte globulin. Blood 107: 4177–4181.
5. Nishiwaki S, Terakura S, Ito M, Goto T, Seto A, et al. (2009) Impact of macrophage infiltration of skin lesions on survival after allogeneic stem cell transplantation: a clue to refractory graft-versus-host disease. Blood 114: 3113–3116.

6. Schaer DJ, Alayash AI, Buehler PW (2007) Gating the radical hemoglobin to macrophages: the anti-inflammatory role of CD163, a scavenger receptor. Antioxid Redox Signal 9: 991–999.
7. Muller M, Renkawitz R (1991) The glucocorticoid receptor. Biochim Biophys Acta 1088: 171–182.
8. Pak CC, Fidler IJ (1991) Liposomal delivery of biological response modifiers to macrophages. Biotherapy 3: 55–64.
9. Xia W, Hilgenbrink AR, Matteson EL, Lockwood MB, Cheng JX, et al. (2009) A functional folate receptor is induced during macrophage activation and can be used to target drugs to activated macrophages. Blood 113: 438–446.
10. Nagao K, Ginhoux F, Leitner WW, Motegi S, Bennett CL, et al. (2009) Murine epidermal Langerhans cells and langerin-expressing dermal dendritic cells are unrelated and exhibit distinct functions. Proc Natl Acad Sci U S A 106: 3312–3317.
11. Ringden O, Hermans J, Labopin M, Apperley J, Gorin NC, et al. (1996) The highest leukaemia-free survival after allogeneic bone marrow transplantation is seen in patients with grade I acute graft-versus-host disease. Acute and Chronic Leukaemia Working Parties of the European Group for Blood and Marrow Transplantation (EBMT). Leuk Lymphoma 24: 71–79.
12. Gratwohl A, Hermans J, Apperley J, Arcese W, Bacigalupo A, et al. (1995) Acute graft-versus-host disease: grade and outcome in patients with chronic myelogenous leukemia. Working Party Chronic Leukemia of the European Group for Blood and Marrow Transplantation. Blood 86: 813–818.
13. Baron F, Labopin M, Niederwieser D, Vigouroux S, Cornelissen JJ, et al. (2012) Impact of graft-versus-host disease after reduced-intensity conditioning allogeneic stem cell transplantation for acute myeloid leukemia: a report from the Acute Leukemia Working Party of the European group for blood and marrow transplantation. Leukemia 26: 2462–2468.
14. Cooke KR, Kobzik L, Martin TR, Brewer J, Delmonte J, Jr., et al. (1996) An experimental model of idiopathic pneumonia syndrome after bone marrow transplantation: I. The roles of minor H antigens and endotoxin. Blood 88: 3230–3239.
15. Kaplan DH, Anderson BE, McNiff JM, Jain D, Shlomchik MJ, et al. (2004) Target antigens determine graft-versus-host disease phenotype. J Immunol 173: 5467–5475.
16. Hill GR, Cooke KR, Teshima T, Crawford JM, Keith JC, Jr., et al. (1998) Interleukin-11 promotes T cell polarization and prevents acute graft-versus-host disease after allogeneic bone marrow transplantation. J Clin Invest 102: 115–123.
17. Livak KJ, Schmittgen TD (2001) Analysis of relative gene expression data using real-time quantitative PCR and the 2(-Delta Delta C(T)) Method. Methods 25: 402–408.
18. Saito S, Nakayama T, Hashimoto N, Miyata Y, Egashira K, et al. (2011) Mesenchymal stem cells stably transduced with a dominant-negative inhibitor of CCL2 greatly attenuate bleomycin-induced lung damage. Am J Pathol 179: 1088–1094.
19. Nakayama T, Mutsuga N, Yao L, Tosato G (2006) Prostaglandin E2 promotes degranulation-independent release of MCP-1 from mast cells. J Leukoc Biol 79: 95–104.
20. Kondo S, Toyokuni S, Tsuruyama T, Ozeki M, Tachibana T, et al. (2002) Peroxynitrite-mediated stress is associated with proliferation of human metastatic colorectal carcinoma in the liver. Cancer Lett 179: 87–93.
21. Toyokuni S, Kawaguchi W, Akatsuka S, Hiroyasu M, Hiai H (2003) Intermittent microwave irradiation facilitates antigen-antibody reaction in Western blot analysis. Pathol Int 53: 259–261.
22. Leong AS, Milios J (1986) Rapid immunoperoxidase staining of lymphocyte antigens using microwave irradiation. J Pathol 148: 183–187.
23. Qian BZ, Li J, Zhang H, Kitamura T, Zhang J, et al. (2011) CCL2 recruits inflammatory monocytes to facilitate breast-tumour metastasis. Nature 475: 222–225.
24. Thiele J, Kvasnicka HM, Beelen DW, Wenzel P, Koepke ML, et al. (2000) Macrophages and their subpopulations following allogenic bone marrow transplantation for chronic myeloid leukaemia. Virchows Arch 437: 160–166.
25. Blirando K, Milliat F, Martelly I, Sabourin JC, Benderitter M, et al. (2011) Mast cells are an essential component of human radiation proctitis and contribute to experimental colorectal damage in mice. Am J Pathol 178: 640–651.
26. Mantovani A, Sozzani S, Locati M, Allavena P, Sica A (2002) Macrophage polarization: tumor-associated macrophages as a paradigm for polarized M2 mononuclear phagocytes. Trends Immunol 23: 549–555.
27. Shin S, Moon S, Park Y, Kwon J, Lee S, et al. (2009) Role of Cordycepin and Adenosine on the Phenotypic Switch of Macrophages via Induced Anti-inflammatory Cytokines. Immune Netw 9: 255–264.
28. Fuentes-Duculan J, Suarez-Farinas M, Zaba LC, Nograles KE, Pierson KC, et al. (2010) A subpopulation of CD163-positive macrophages is classically activated in psoriasis. J Invest Dermatol 130: 2412–2422.
29. Pullarkat V, Blanchard S, Tegtmeier B, Dagis A, Patane K, et al. (2008) Iron overload adversely affects outcome of allogeneic hematopoietic cell transplantation. Bone Marrow Transplant 42: 799–805.
30. Hashimoto D, Chow A, Greter M, Saenger Y, Kwan WH, et al. (2011) Pretransplant CSF-1 therapy expands recipient macrophages and ameliorates GVHD after allogeneic hematopoietic cell transplantation. J Exp Med 208: 1069–1082.
31. Everse LA, Anderson LD, Jr., van Rooijen N, Mullen CA (2001) Bone marrow transplant conditioning intensified with liposomal clodronate to eliminate residual host antigen presenting cells fails to ameliorate GVHD and increases PERI-BMT mortality. Transplantation 71: 611–618.
32. Shlomchik WD, Couzens MS, Tang CB, McNiff J, Robert ME, et al. (1999) Prevention of graft versus host disease by inactivation of host antigen-presenting cells. Science 285: 412–415.
33. Merad M, Hoffmann P, Ranheim E, Slaymaker S, Manz MG, et al. (2004) Depletion of host Langerhans cells before transplantation of donor alloreactive T cells prevents skin graft-versus-host disease. Nat Med 10: 510–517.
34. Wilson J, Cullup H, Lourie R, Sheng Y, Palkova A, et al. (2009) Antibody to the dendritic cell surface activation antigen CD83 prevents acute graft-versus-host disease. J Exp Med 206: 387–398.
35. Li N, Chen Y, He W, Yi T, Zhao D, et al. (2009) Anti-CD3 preconditioning separates GVL from GVHD via modulating host dendritic cell and donor T-cell migration in recipients conditioned with TBI. Blood 113: 953–962.

Immunology Letters 160 (2014) 99–101

Contents lists available at ScienceDirect

Immunology Letters

journal homepage: www.elsevier.com/locate/immlet

Letter to the Editor

Successful unrelated cord blood transplantation for adult acquired aplastic anemia using reduced intensity conditioning without ATG

Acquired aplastic anemia (aAA) patients who are transfusion-dependent and who have failed or relapsed after immunosuppressive therapy need further treatment. In cases in which a human leukocyte antigen (HLA)-identical sibling donor is not available, the use of alternative donor including HLA-matched unrelated donor and unrelated cord blood (CB) are commonly considered, but this strategy is associated with worse outcomes [1]. Because of the abundant availability of acceptable CB units, the use of cord blood transplantation (CBT) has been increasing. Although the use of CBT in patients with aAA has recently been evaluated [2], relatively little information is available on how to achieve proper engraftment with a reduced intensity conditioning (RIC) regimen in aAA patients undergoing CBT. We describe here three adult patients with aAA who underwent transplantation with unrelated CB after a RIC regimen without ATG. The patient characteristics are shown in Table 1. All three patients received single-unit CB containing more than 2.2×10^7/kg of total nucleated cell (TNC) with no more than two of six HLA-mismatches. The conditioning regimen consisted of six doses of fludarabine (Flu) 30 mg/m^2, two doses of cyclophosphamide (CY) 60 mg/kg and total body irradiation (TBI) 2 Gy × 2 with no use of anti-thymocyte globulin (ATG). The graft-versus-host disease (GVHD) prophylaxis regimen was a combination of short-term methotrexate (15, 10, and 10 mg/m^2 on days 1, 3, 6, respectively) and tacrolimus. Because patient #3 had a high titer of anti-HLA antibody, a CB unit that was not cross-reactive with this antibody was chosen.

All three patients rapidly exhibited sustained CB engraftment (Table 2). Chimerism analyses of the CD3$^+$ fraction using various numbers of tandem repeats showed initial full-donor conversion from the first point of analysis in all patients. No secondary graft-failure was observed. Acute GVHD was observed in patient #2 (skin only stage 2, Grade I) and resolved spontaneously. Chronic GVHD was observed in patient #3 (skin, oral involvement) and symptoms resolved quickly after the administration of 0.5 mg/kg oral prednisolone. The regimen was generally well tolerated, and no significant organ damage or severe toxicity occurred. The patients remain alive without transfusion dependence at 68, 44 and 9 months, with Karnofsky scores of 70% (due to postherpetic neuralgia), 100% and 100%, respectively.

Here we report three CBT recipients who received successful single-unit CBT after a RIC regimen. All three patients exhibited sustained full donor-type hematopoiesis without further intervention to increase donor-type chimerism. The conditioning regimen included 180 mg/m^2 Flu and 120 mg/kg CY with 2 Gy × 2 TBI, which may be regarded as a relatively strong regimen in terms of immunosuppressive and cytotoxic ability. Thus, one might think this regimen too potent for the induction of sustained engraftment of CB. However, Liu et al. reported that RIC regimen, consisting of Flu 120 mg/m^2, CY 1200 mg/m^2 (equivalent to 40 mg/kg if the patient's body weight was 50 kg) and rabbit ATG 30 mg/kg, was not sufficiently potent enough to induce engraftment after CBT in patients with aAA. They reported two early deaths and 16 graft-failures among the 18 CBT recipients conditioned with the above regimen [3]. Thus, it is reasonable to use a CY dose >40 mg/kg, and further study to determine the optimal CY dose between 40 and 120 mg/kg is warranted.

To ensure rapid and proper CB engraftment, graft cell contents, such as TNC, CD34$^+$ cell count and CD8$^+$ cell count, are important factors [4]. In Western countries, ATG is commonly used as the conditioning regimen for CBT. Nevertheless, the use of ATG will decrease lymphocytes, including graft-facilitating CD8$^+$ lymphocytes, which may lead to attenuation of total potency for the facilitation of engraftment in exchange for the beneficial effect of reducing the incidence of severe acute GVHD. Indeed, only one of seven CB recipients for aAA who received ATG-containing regimen achieved engraftment in a previous retrospective study in Japan [5]. Thus, we replaced ATG with 4 Gy TBI in our regimen, which may be another reason for successful engraftment.

One of the biggest differences in CBT between Western countries and Japan may be the attitude toward the use of ATG. In the recent protocol of European group, two doses of ATG 2.5 mg/kg and a single agent GVHD prophylaxis are recommended [6]. To reduce the incidence of severe acute GVHD, physicians in Europe and US would be likely to use ATG more frequently, which might result in failure to observe better engraftment. In fact, it is reported that a conditioning regimen without ATG provided a low incidence of graft-failure [7]. Taken together, we believe that ATG should not be included in the conditioning regimen for CBT, not only for a single-unit CBT but also for a double-unit CBT. We also have shown the superiority of two-drug GVHD prophylaxis (including methotrexate) over single-drug prophylaxis in CBT [8]. To compensate prophylactic effect of ATG to control severe GVHD, it would be preferable to develop the GVHD prophylaxis after transplantation without ATG. Further study to determine whether or not ATG should be used in order to achieve prompt engraftment and subsequent higher quality of life and survival after RIC-CBT is warranted.

http://dx.doi.org/10.1016/j.imlet.2014.01.013

Table 1
Patient demographics and CB unit characteristics.

Pt no.	Age/sex	BW (kg)	Disease status at transplant	Interval from diagnosis to CBT (year)	Transfusion dependency	ABO mismatch	HLA serological mismatch	HLA allele mismatch	HLA-antibody	Donor-specific antibody	TNCC (10^7/kg)	$CD34^+$ (10^5/kg)
1	48/M	51	Severe	1.2	RBC	Match	2/6	3/8	–	–	3.67	0.50
2	53/M	65	Severe	22.1	RBC/PC	Major/minor	1/6	4/8	–	–	2.79	0.44
3	37/F	51	Non-severe	26.9	RBC/PC	Major/minor	2/6	3/8	+	–	2.24	0.55

Pt, patient; M, male; F, female; BW, body weight; RBC, red blood cell concentration; PC, platelet concentration; HLA, human leukocyte antigen; TNCC, total nucleated cell count.

Table 2
Engraftment, chimerism and other outcomes.

Pt no.	Days to ANC >500/μl	Days to reticulocyte >1%	Days to plt > 20,000/μl	Days to plt > 50,000/μl	Chimerism after CBT	Acute GVHD	Chronic GVHD	Other complications	Survival, mo	KS (%)
1	19	30	25	191	Day 20, 95% donor	No	No	Postherpetic neuralgia	Alive, 68	70
2	21	28	37	44	Day 19, 100% donor	Grade I (skin 2)	No	Polymyalgia rheumatica	Alive, 44	100
3	22	37	32	43	Day 25, 100% donor	No	Yes (skin, oral)	No	Alive, 9	100

Pt, patient; ANC, absolute neutrophil count;plt, platelet; KS, Karnofsky score.

Conflict of interest

All authors declare that there are no competing financial interests.

References

[1] Passweg JR, Pérez WS, Eapen M, Camitta BM, Gluckman E, Hinterberger W, et al. Bone marrow transplants from mismatched related and unrelated donors for severe aplastic anemia. Bone Marrow Transplant 2006;37:641–9.
[2] Yamamoto H, Kato D, Uchida N, Ishiwata K, Araoka H, Takagi S, et al. Successful sustained engraftment after reduced-intensity umbilical cord blood transplantation for adult patients with severe aplastic anemia. Blood 2011;117:3240–2.
[3] Liu HL, Sun ZM, Geng LQ, Wang XB, Ding KY, Tang BI, et al. Unrelated cord blood transplantation for newly diagnosed patients with severe acquired aplastic anemia using a reduced-intensity conditioning: high graft rejection, but good survival. Bone Marrow Transplant 2012;47:1186–90.
[4] Terakura S, Azuma E, Murata M, Kumamoto T, Hirayama M, Atsuta Y, et al. Hematopoietic engraftment in recipients of unrelated donor umbilical cord blood is affected by the CD34(+) and CD8(+) cell doses. Biol Blood Marrow Transplant 2007;13:822–30.
[5] Yoshimi A, Kojima S, Taniguchi S, Hara J, Matsui T, Takahashi Y, et al. Unrelated cord blood transplantation for severe aplastic anemia. Biol Blood Marrow Transplant 2008;14:1057–63.
[6] Peffault de Latour R, Rocha V, Socie G. Cord blood transplantation in aplastic anemia. Bone Marrow Transplant 2013;48:201–2.
[7] Ostronoff F, Milano F, Gooley T, Gutman JA, McSweeney P, Petersen FB, et al. Double umbilical cord blood transplantation in patients with hematologic malignancies using a reduced-intensity preparative regimen without antithymocyte globulin. Bone Marrow Transplant 2013;48:782–6.
[8] Narimatsu H, Terakura S, Matsuo K, Oba T, Uchida T, Iida H, et al. Short-term methotrexate could reduce early immune reactions and improve outcomes in umbilical cord blood transplantation for adults. Bone Marrow Transplant 2007;39:31–9.

Seitaro Terakura*
Tetsuya Nishida
Yoshihiro Inamoto
Department of Hematology and Oncology, Nagoya University Graduate School of Medicine, Nagoya, Japan

Haruhiko Ohashi
Clinical Research Center, National Hospital Organization Nagoya Medical Center, Nagoya, Japan

Tomoki Naoe
Makoto Murata
Department of Hematology and Oncology, Nagoya University Graduate School of Medicine, Nagoya, Japan

* Corresponding author at: Department of Hematology and Oncology, Nagoya University Graduate School of Medicine, 65 Tsurumai-cho, Showa-ku, Nagoya, Aichi 466-8550, Japan. Tel.: +81 52 744 2145; fax: +81 52 744 2161.
E-mail address: tseit@med.nagoya-u.ac.jp (S. Terakura)

3 December 2013

Available online 29 January 2014

Int J Hematol (2014) 99:169–174
DOI 10.1007/s12185-013-1495-5

ORIGINAL ARTICLE

RUNX1 mutation associated with clonal evolution in relapsed pediatric acute myeloid leukemia with t(16;21)(p11;q22)

Olfat Ismael · Akira Shimada · Shaimaa Elmahdi · Momen Elshazley · Hideki Muramatsu · Asahito Hama · Yoshiyuki Takahashi · Miho Yamada · Yuka Yamashita · Keizo Horide · Seiji Kojima

Received: 23 October 2012 / Revised: 9 December 2013 / Accepted: 10 December 2013 / Published online: 28 December 2013

Abstract *TLS/FUS-ERG* chimeric fusion transcript resulting from translocation changes involving chromosomes 16 and 21 is a rare genetic event associated with acute myeloid leukemia (AML). The distinct t(16;21) AML subtype exhibits unique clinical and morphological features and is associated with poor prognosis and a high relapse rate; however, the underlying mechanism remains to be clarified. Recently, whole-genome sequencing revealed a large set of genetic alterations that may be relevant for the dynamic clonal evolution and relapse pathogenesis of AML. Here, we report three pediatric AML patients with t(16;21) (p11; q22). The *TLS/FUS-ERG* fusion transcript was detected in all diagnostic and relapsed samples, with the exception of one relapsed sample. We searched for several genetic lesions, such as *RUNX1*, *FLT3*, *c-KIT*, *NRAS*, *KRAS*, *TP53*, *CBL*, *ASXL1*, *IDH1/2*, and *DNMT3A*, in primary and relapsed AML samples. Interestingly, we found *RUNX1* mutation in relapsed sample of one patient in whom cytogenetic analysis showed the emergence of a new additional clone. Otherwise, there were no genetic alterations in *FLT3*, *c-KIT*, *NRAS*, *KRAS*, *TP53*, *CBL*, *ASXL1*, *IDH1/2*, or *DNMT3A*. Our results suggest that precedent genetic alterations may be essential to drive the progression and relapse of t(16;21)-AML patients.

Keywords *RUNX1* · AML · Translocation · *TLS/FUS-ERG*

Introduction

Translocation t(16;21) (p11;q22) is a rare reciprocal chromosomal change observed in Ewing's sarcoma [1], blast crisis of chronic myelocytic leukemia (CML) [2] and acute myeloid leukemia (AML) [3–5]. This translocation leads to the formation of *TLS/FUS-ERG* fusion gene, resulting in *TLS/FUS-ERG* chimeric protein [6]. The incidence of t(16;21) AML is estimated to be 1 % of all de novo and

O. Imael, S. Elmahdi contributed equally to this work.

O. Ismael (✉) · A. Shimada · S. Elmahdi · H. Muramatsu · A. Hama · Y. Takahashi · S. Kojima (✉)
Department of Pediatrics, Nagoya University Graduate School of Medicine, 65 Tsuruma-cho, Showa-ku, Nagoya, Aichi 466-8550, Japan
e-mail: olfat_80@yahoo.com

S. Kojima
e-mail: kojimas@med.nagoya-u.ac.jp

O. Ismael
Department of Pediatrics, EL-Hilal Hospital, General Authority for Health Insurance, Sohag, Egypt

A. Shimada · M. Yamada · Y. Yamashita · K. Horide
Clinical Research Center, National Hospital Organization, Nagoya Medical Center, Nagoya, Aichi, Japan

A. Shimada
Department of Pediatrics, Okayama University Hospital, Okayama, Japan

M. Elshazley
Department of Respiratory Medicine, Nagoya University Graduate School of Medicine, Nagoya, Aichi, Japan

M. Elshazley
Industrial Medicine and Occupational Diseases Unit, Faculty of Medicine, Sohag University, Sohag, Egypt

secondary AML cases [7]. The chromosomal translocation t(16;21)(p11;q22) has been diagnosed in adult and childhood AML with a wide range of age (1–60 years) and with no sex predilection [6]. AML with t(16;21) is a unique cytogenetic subtype that showed distinct clinical and hematological characteristics. Unfavorable prognosis and poor survival are considered the most prominent features of t(16;21) AML [7], while hemophagocytosis, micromegakaryocytes, increases of eosinophils in bone marrow (BM), and vacuolation of leukemic cells are frequently detected in t(16;21) AML [6, 7]. Treatment of AML with t(16;21)(p11;q22) represents significant therapeutic challenges with high relapse rate. Furthermore, post-relapse treatment outcomes remain unsatisfactory for this group of patients [6, 7]. Recently, it has been shown that CD56, a neural cell adhesion molecule, is frequently expressed in adult t(16;21)-AML patients and it could be a useful indicator for poor prognosis, failure of complete remission (CR) and extramedullary involvement [7]. Although some prognostic factors have been reported in AML patients with t(16;21) (p11;q22), the underlying mechanism of poor prognosis and high relapse rate in those patients is not yet fully understood. Thus, identification of new biological markers is urgently needed and would be useful to establish a new therapeutic strategy for t(16;21)-AML patients who are at extremely high risk of relapse. A subset of recurrent genetic alterations has been found in AML with potential clinical implications [8–12]; therefore, these genetic mutations are expected to hold prognostic importance for AML patients. More recently, genome-wide analysis using next generation sequencing have suggested two molecular models involved in the relapse pathogenesis of AML. First, the original clone in primary tumor is susceptible to gain new mutations and evolves into the relapse clone. Second, development of a subclone from the original clone, surviving initial therapy, acquires additional mutations and expands at relapse [13]. To investigate the genetic changes associated with primary and relapsed samples, we performed comprehensive genetic, clinical and morphological assessments for three pediatric cases diagnosed as having de novo AML with t(16;21)(p11;q22) to delineate new molecular features and better understand the mechanism of relapse for this unique cytogenetic subtype of AML.

Patients and samples

Three patients satisfying the diagnostic criteria for AML (according to the WHO classification) were included in this study. Morphological diagnosis was made according to the French–American–British (FAB) morphologic classification. Cytogenetic analysis was performed for all patients at diagnosis and after relapse. Peripheral blood (PB) and/or BM samples were collected from all patients at diagnosis, during CR or after relapse and mononuclear cell fractions were isolated using a Ficoll gradient. RNA and cDNA were prepared following the manufacturer's instructions (Roche Diagnostics, Mannheim, Germany) and Genomic DNA was isolated using the QIAmp DNA blood mini kit (Qiagen, Hilden, Germany) according to the manufacturer's protocol. Informed consent was obtained from the guardians of all patients, in accordance with institutional guidelines, and study protocols were approved by the Institutional Review Boards of Nagoya University Graduate School of Medicine.

Cytogenetics analysis

Karyotyping of blood or BM cells from all patients was done by routine G-banding karyotype analysis.

Detection of TLS/FUS-ERG fusion transcript by RT-PCR

Reverse transcriptase polymerase chain reaction (RT-PCR) and real-time PCR were performed to detect *TLS/FUS-ERG* fusion transcript. In addition, sensitivity was evaluated as described previously [6].

Flow cytometric analysis

We performed detailed surface marker analysis including anti-CD13, CD10, CD33, CD34, CD15, CD41, CD38, CD56, cytoplasmic myeloperoxidase (MPO), and HLA-DR. (Positive and negative controls were examined along with samples. Positivity was defined as involving more than 20 % of the cells among the blast gate).

Mutation analysis of FLT3, c-KIT, NRAS, KRAS, RUNX1, TP53, CBL, TET2, ASXL1, IDH1/2 and DNMT3A

We investigated the following candidate genes at known mutational hot spots: *FLT3*, *c-KIT, IDH1/2, DNMT3A, NRAS* (exons 2 and 3), *KRAS* (exons 2 and 3), *TET2* (exons 3–11), *RUNX1* (exons 3–8), *ASXL1* (exon 12), *CBL* (exons 7, 8, 9), and the complete coding region for *TP53* were searched by sequencing analysis after PCR amplification of genomic DNA. PCR amplification and purification were performed in a 25-μl PCR mix containing at least 50 ng of template cDNA using quick Taq PCRTM HS Dye mix (Qiagen) under the following conditions: 94 °C for 2 min (first denaturing step); 94 °C for 30 s; 65 °C for 30 s; 35 cycles of 68 °C for 30 s to 1 min, depending on PCR product length; and 68 °C for 7 min (final extension step). PCR products were purified from the reaction mixture using the QIAquick PCR purification kit (Qiagen), and

were directly sequenced on a DNA sequencer (ABI PRISM 3100 Genetic Analyzer; Applied Biosystems, Japan) using a Big Dye terminator cycle sequencing kit (Applied Biosystems). All DNA sequence abnormalities were confirmed by three independent experiments.

Results

Clinical and hematological features

Three de novo AML patients (two females, one male) with a median age at onset of 2 years (range 2–10 years) were included. The main clinical and hematologic features of all patients are summarized in Table 1. The median white blood cell counts, percent of PB and BM blast, were 2.7×10^9/l (range 1.9–39.2×10^9/l), 53 % (range 23–62 %) and 57 % (range 9.3–73 %), respectively. Karyotypes of patient Nos. 1 and 2 at the onset were t(16;21)(p11;q22) with additional abnormalities observed in patient No. 2 in the form of 46, XY, t(16;21)(p11;q22), add(11)(q13), del(13)(q12q14). Patient No. 3 did not show the t(16;21)(p11;q22) and showed various additional chromosomal abnormalities (Table 2). Histopathologic examination of BM showed leukemic cells with hemophagocytosis (erythrophagocytosis and megakaryophagocytosis) and vacuolation (Fig. 1). Among three AML patients with t(16;21), two showed positivity for CD56, CD13+, 33+, 15+, 34+, MPO+, HLA-DR+, while the other patient expressed only CD13+, 33+, HLA-DR+. CD56-positive cell percentage was 73.3 and 33 % in the diagnostic samples, while at the relapsed one was 66 and 63 % in patient Nos. 2 and 3, respectively.

Table 1 Clinical features of 3 pediatrics patients with *TLS/FUS-ERG* chimera

Patient no.	Sex/ Age (Y)	WBC (x10^9/l)	FAB classification	CD56	DFS (months)	1st HSCT	2nd HSCT	Overall survival (months)	Survival outcome	Cause of death
1	F/2	39.2	M1	−	15	At 2nd CR, from HLA-mismatched mother	–	>121	Alive	–
2	M/2	2.7	M7	+	12	At 1st CR, from unrelated HLA-matched donor	At 1st relapse, from HLA-mismatched mother	27	Death	Relapse
3	F/10	1.9	M1 with MLD	+	10	At 2nd CR, from HLA-matched sibling	At 2nd relapse, from HLA-mismatched mother	45	Death	Hepatitis

MLD multilineage dysplasia, *DFS* disease-free survival, *HSCT* hematopoietic stem cell transplantation, *CR* complete remission

Table 2 Detailed cytogenetic analysis and mutations profile of 3 pediatrics patients with *TLS/FUS-ERG* chimera

ID	Disease stage	Karyotype	*TLS/FUS- ERG* chimera (copies/μgRNA)	Transcript type	Molecular alterations	
					RUNX1	Others
1	At diagnosis	46,XX,t(16;21)(p11;q22)[8]	497,814	B, C	–	–
2		46,XY,t(16;21)(p11;q22)[8]/46, idem, add(11)(q13), del(13)(q12q14) [6]	6,960	B	–	–
3		45,XX,der(1;17), +8[2]	1,237,000	B	–	–
1	At relapse	46,XX,t(16;21)(p11;q22)[14]	28,304	B, C	–	–
2		46,XY,t(16;21)(p11;q22),add(1) (q12), add(2)(p13),add(3)(q21), add(8)(p21), der (8),t(8;11) (q11.2;q11), −11, −15, add(15)(q24)[18]	0	–	+	–
3		47,X,t(X;3)(p22;p12), add(1)(p34),der(1)ad(1)add (1)(q21),add(7)(q32),−8, t(8;11)(q24;q13),add(12) (q24.1),add(17)(q21), +mar1[18]	132,168	B	–	–

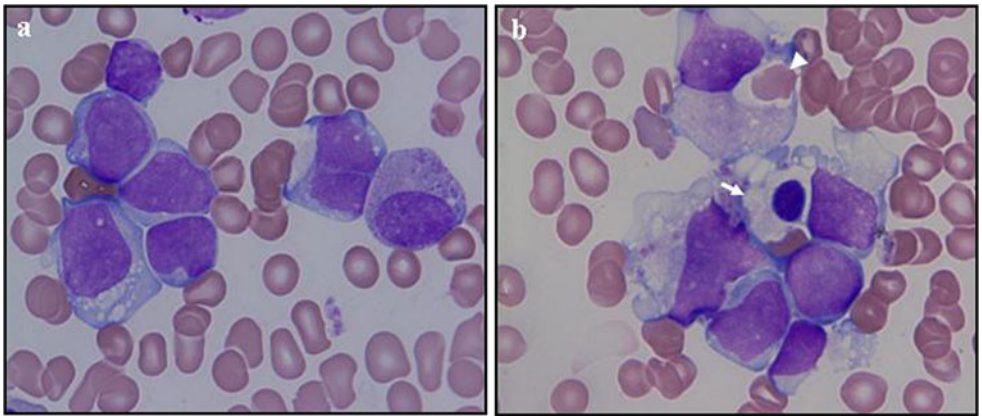

Fig. 1 Morphologic examination of leukemic cells obtained from bone marrow aspirates of t(16;21)-AML-CD56-positive pediatric patients. **a** Leukemic cells with cytoplasmic vacuolation. **b** Leukemic cells with erythrophagocytosis (*white arrow*) and megakaryocyte phagocytosis (*white arrow head*)

TLS/FUS-ERG fusion transcript

We detected the chimeric fusion *TLS/FUS-ERG* transcripts in all cases at the onset of diagnosis (patient 1 had type B and C fusion transcripts, patients 2 and 3 had type B fusion transcript). However, in patient 2, the band of fusion transcripts was absent at the relapse (Table 2). A serial tenfold dilution of cDNA of patients' samples was used to detect the chimeric transcripts; type B and C transcripts were found in very low-diluted solutions (10^{-6}).

Mutation profiling of pediatric patients with t(16;21) AML

We identified 203-bp (149_351) deletion that led to a frameshift mutation at codon 137 in the runt domain of *AML1/RUNX1* at relapse in RNA sample obtained from BM of patient No. 2 (Fig. 2a). Interestingly, missense point mutation in *TET2* (R835C) was detected in a diagnostic, complete remission and relapsed BM samples obtained from patient No. 3 (Fig. 2b), but 3 out of 50 healthy Japanese control were found to harbor this mutation, indicating that *TET2* (R835C) mutation could be encountered as single-nucleotide polymorphism (SNP). All t(16;21)-AML patients were negative for *FLT3, c-KIT*, *NRAS*, *KRAS*, *TP53*, *CBL*, *ASXL1*, *IDH1/2* and *DNMT3A* genetic alterations.

Therapy and clinical outcome

Patient Nos. 1, 2, 3 received AML-oriented chemotherapy (ECM regimen; VP16, AraC and Idarubicin), but they relapsed after 15, 12 and 10 months respectively from the onset of the disease. Patient No. 1 underwent HLA-haploidentical hematopoietic stem cell transplantation

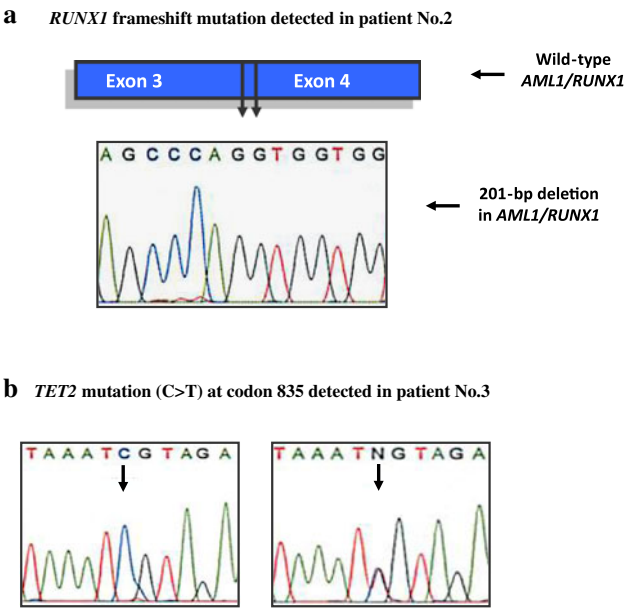

Fig. 2 *RUNX1* and *TET2* alterations detected in pediatric patients with t(16;21)(p11;q22). **a** Sequence data for *AML1/RUNX1* gene in patient No. 2. Nucleotide sequences showing wild-type exon 3 and 4 boundary of *AML1/RUNX1* in cDNA and 201-bp deletion from exon 3 resulting in a frameshift mutation. **b** Sequence traces showing *TET2* exon 3, C to T mutation at codon 835 in patient No. 3

(HSCT) from her mother during the 2nd complete remission (CR) (25 months after the 1st CR) and she is still alive. Patient No. 2 received HSCT from HLA-matched unrelated donor at 5 months after the 1st CR, but he relapsed and received the 2nd HSCT from HLA 3 loci-mismatched mother without induction chemotherapy. He achieved 2nd CR after HSCT but experienced 2nd relapse 12 months later and died soon due to the disease progression. Patient No. 3 received HSCT from HLA-matched related sibling at 6 months after the 2nd CR.

However, she relapsed 4 months after the 1st HSCT and underwent 2nd HSCT from HLA 1 locus-mismatched mother. She developed fulminant hepatitis (Caused by adenovirus) and died 4 months after the 2nd HSCT. Notably, two patients had poor prognosis with over all survival (OS) 27 and 45 months and the other patient is still alive (Table 1).

Discussion

Several studies demonstrated the clinical importance of genetics in prognostification of AML patients and this depends mainly upon the use of cytogenetic to categorize patients into favorable, intermediate, or adverse cytogenetic groups, in addition to identification of new molecular genetic abnormalities. We would like to emphasize the importance of cytogenetic analysis as well as genetic assessment in predicting the clinical outcome of AML patients. Herein, we report three pediatric AML patients with *TLS/FUS-ERG* fusion transcript. Although t(16;21)(p11;q22) karyotype was found in two out of three patients, chimeric fusion *TLS/FUS-ERG* transcript was detected in all cases at the onset of diagnosis and in two cases at the relapse phase, suggesting that detection of *TLS/FUS-ERG* chimeric transcript by RT-PCR has the upper hand in identification and monitoring of t(16;21)-AML patients. On the other hand, it is quite possible that absence of *TLS/FUS*-ERG fusion transcript at relapse phase in patients No. 2 may be attributed to RNA degradation eliminating the *TLS/FUS-ERG* transcripts. In line with our results, Kong et al. [6] demonstrated that RT-PCR analysis for detecting *TLS/FUS-ERG* chimeric fusion transcript is an important monitoring tool for t(16;21)-AML patients during various clinical stages. Remarkably, *RUNX1* mutation was detected in relapsed sample of one patient in whom cytogenetic analysis showed the emergence of a new additional clone, while *TET2* SNP was found at diagnosis, during complete remission (CR) and after relapse. Our study extends the findings of a recent study [13] showed that genetic alterations could contribute to clonal evolution and relapse pathogenesis. It has been shown that *RUNX1* mutations are frequently associated with AML disease [14–16] and particular t(16;21)-AML patients [7]. Auewarakul et al. [16] further demonstrated that a higher frequency of *RUNX1* mutation was found in southeast Asian t(16;21)-AML patients. Accumulated knowledge with strong evidence supports the integral and important role of *TET2* mutations in myeloid diseases [17, 18]. Approximately, 17 % of AML patients have been reported to carry *TET2* mutations [19], however, the prognostic impact of *TET2* mutation in AML remains enigmatic. Fathi et al. showed that there was no association between *TET2* mutations and patients' survival [19]. Conversely, other investigators have documented that *TET2* mutations were associated with low rate of complete remission, decrease overall survival and worse clinical outcome in patients with AML diagnosis [20]. In our study, immunophenotypic analysis of leukemic cells in t(16;21)-AML pediatric patients revealed positive expression for CD13, CD15, CD34, CD33, CD56, MPO, HLA-DR. Specifically, CD56 was strongly expressed in patients with decrease OS, but the small patients' number makes it difficult to draw a firm conclusion of this possible association. These findings are similar to previous reports that showed variable degree of surface markers expression in t(16;21)-AML patients [21]. Jekarl et al. [7] clearly described that high CD56 expression confer an unfavorable prognosis in AML patients with t(16; 21)(p11;q22). In conclusion, our findings lend significant credence for the use of CD56 as a prognostic marker for AML patients with t(16;21)(p11;q22). Further investigations are required to define precisely clonal evolutions and mutational changes that may be relevant for relapse pathogenesis of t(16;21) AML.

Conflict of interest The authors declare no conflict of interest.

References

1. Shing DC, McMullan DJ, Roberts P, Smith K, Chin SF, Nicholson J, Tillman RM, Ramani P, Cullinane C, Coleman N. FUS/ERG gene fusions in Ewing's tumors. Cancer Res. 2003;63:4568–76.
2. Ferro MR, Cabello P, Garcia-Sagredo JM, Resino M, San Roman C, Larana JG. t(16;21) in a Ph positive CML. Cancer Genet Cytogenet. 1992;60:210–1.
3. Mecucci C, Bosly A, Michaux JL, Broeckaert-Van Orshoven A, Van den Berghe H. Acute nonlymphoblastic leukemia with bone marrow eosinophilia and structural anomaly of chromosome 16. Cancer Genet Cytogenet. 1985;17:359–63.
4. Morgan R, Riske CB, Meloni A, Ries CA, Johnson CH, Lemons RS, Sandberg AA. t(16;21)(p11.2;q22): a recurrent primary rearrangement in ANLL. Cancer Genet Cytogenet. 1991;53:83–90.
5. Yao E, Sadamori N, Nakamura H, Sasagawa I, Itoyama T, Ichimaru M, Tagawa M, Nakamura I, Kamei T. Translocation t(16;21) in acute nonlymphocytic leukemia with abnormal eosinophils. Cancer Genet Cytogenet. 1988;36:221–3.
6. Kong XT, Ida K, Ichikawa H, Shimizu K, Ohki M, Maseki N, Kaneko Y, Sako M, Kobayashi Y, Tojou A, Miura I, Kakuda H, Funabiki T, Horibe K, Hamaguchi H, Akiyama Y, Bessho F, Yanagisawa M, Hayashi Y. Consistent detection of TLS/FUS-ERG chimeric transcripts in acute myeloid leukemia with t(16;21)(p11;q22) and identification of a novel transcript. Blood. 1997;90:1192–9.
7. Jekarl DW, Kim M, Lim J, Kim Y, Han K, Lee AW, Kim HJ, Min WS. CD56 antigen expression and hemophagocytosis of leukemic cells in acute myeloid leukemia with t(16;21)(p11;q22). Int J Hematol. 2010;92:306–13.
8. Rocquain J, Carbuccia N, Trouplin V, Raynaud S, Murati A, Nezri M, Tadrist Z, Olschwang S, Vey N, Birnbaum D, Gelsi-Boyer V, Mozziconacci MJ. Combined mutations of ASXL1, CBL, FLT3, IDH1, IDH2, JAK2, KRAS, NPM1, NRAS, RUNX1, TET2 and WT1 genes in myelodysplastic syndromes and acute myeloid leukemias. BMC Cancer. 2010;10:401.

9. Marcucci G, Metzeler KH, Schwind S, Becker H, Maharry K, Mrozek K, Radmacher MD, Kohlschmidt J, Nicolet D, Whitman SP, Wu YZ, Powell BL, Carter TH, Kolitz JE, Wetzler M, Carroll AJ, Baer MR, Moore JO, Caligiuri MA, Larson RA, Bloomfield CD. Age-related prognostic impact of different types of DNMT3A mutations in adults with primary cytogenetically normal acute myeloid leukemia. J Clin Oncol. 2012;30(7): 742–50.
10. Ruan M, Wang YQ, Zhang L, Liu TF, Liu F, Liu XM, Zhang JY, Zou Y, Chen YM. Zhu XF [FLT3 mutations in children with acute myeloid leukemia: a single center study]. Zhongguo Dang Dai Er Ke Za Zhi. 2011;13:863–6.
11. Metzeler KH, Becker H, Maharry K, Radmacher MD, Kohlschmidt J, Mrozek K, Nicolet D, Whitman SP, Wu YZ, Schwind S, Powell BL, Carter TH, Wetzler M, Moore JO, Kolitz JE, Baer MR, Carroll AJ, Larson RA, Caligiuri MA, Marcucci G, Bloomfield CD. ASXL1 mutations identify a high-risk subgroup of older patients with primary cytogenetically normal AML within the ELN Favorable genetic category. Blood. 2011;118:6920–9.
12. Ahmad EI, Gawish HH, Al Azizi NM, Elhefni AM. The prognostic impact of K-RAS mutations in adult acute myeloid leukemia patients treated with high-dose cytarabine. Onco Targets Ther. 2011;4:115–21.
13. Ding L, Ley TJ, Larson DE, Miller CA, Koboldt DC, Welch JS, Ritchey JK, Young MA, Lamprecht T, McLellan MD, McMichael JF, Wallis JW, Lu C, Shen D, Harris CC, Dooling DJ, Fulton RS, Fulton LL, Chen K, Schmidt H, Kalicki-Veizer J, Magrini VJ, Cook L, McGrath SD, Vickery TL, Wendl MC, Heath S, Watson MA, Link DC, Tomasson MH, Shannon WD, Payton JE, Kulkarni S, Westervelt P, Walter MJ, Graubert TA, Mardis ER, Wilson RK, DiPersio JF. Clonal evolution in relapsed acute myeloid leukaemia revealed by whole-genome sequencing. Nature. 2012;481:506–10.
14. Roumier C, Fenaux P, Lafage M, Imbert M, Eclache V, Preudhomme C. New mechanisms of AML1 gene alteration in hematological malignancies. Leukemia. 2003;17:9–16.
15. Tang JL, Hou HA, Chen CY, Liu CY, Chou WC, Tseng MH, Huang CF, Lee FY, Liu MC, Yao M, Huang SY, Ko BS, Hsu SC, Wu SJ, Tsay W, Chen YC, Lin LI, Tien HF. AML1/RUNX1 mutations in 470 adult patients with de novo acute myeloid leukemia: prognostic implication and interaction with other gene alterations. Blood. 2009;114:5352–61.
16. Auewarakul CU, Leecharendkeat A, Tocharoentanaphol C, Promsuwicha O, Sritana N, Thongnoppakhun W. AML1 mutation and its coexistence with different transcription factor gene families in de novo acute myeloid leukemia (AML): redundancy or synergism. Haematologica. 2007;92:861–2.
17. Li Z, Cai X, Cai CL, Wang J, Zhang W, Petersen BE, Yang FC, Xu M. Deletion of Tet2 in mice leads to dysregulated hematopoietic stem cells and subsequent development of myeloid malignancies. Blood. 2011;118:4509–18.
18. Klaus M, Psaraki A, Mastrodemou S, Pyrovolaki K, Mavroudi I, Kalpadakis C, Papadaki HA. Evaluation of TET2 deletions in myeloid disorders: a fluorescence in situ hybridization analysis of 109 cases. Leuk Res. 2011;35:413–5.
19. Fathi AT, Abdel-Wahab O. Mutations in epigenetic modifiers in myeloid malignancies and the prospect of novel epigenetic-targeted therapy. Adv Hematol. 2012;2012:469592.
20. Metzeler KH, Maharry K, Radmacher MD, Mrozek K, Margeson D, Becker H, Curfman J, Holland KB, Schwind S, Whitman SP, Wu YZ, Blum W, Powell BL, Carter TH, Wetzler M, Moore JO, Kolitz JE, Baer MR, Carroll AJ, Larson RA, Caligiuri MA, Marcucci G, Bloomfield CD. TET2 mutations improve the new European LeukemiaNet risk classification of acute myeloid leukemia: a Cancer and Leukemia Group B study. J Clin Oncol. 2011;29:1373–81.
21. Shikami M, Miwa H, Nishii K, Takahashi T, Shiku H, Tsutani H, Oka K, Hamaguchi H, Kyo T, Tanaka K, Kamada N, Kita K. Myeloid differentiation antigen and cytokine receptor expression on acute myelocytic leukaemia cells with t(16;21)(p11;q22): frequent expression of CD56 and interleukin-2 receptor alpha chain. Br J Haematol. 1999;105:711–9.